INL/EXT-20-59614
Revision 0

Light Water Reactor Sustainability Program

RISA Plant Reload Process Optimization: Development of design basis accident methods for plant reload license optimization

August 2020

U.S. Department of Energy

Office of Nuclear Energy

INL/EXT-20-59614
Revision 0

RISA Plant Reload Process Optimization: Development of design basis accident methods for plant reload license optimization

Andrea Alfonsi
Mohammad Abdo
Jarrett Valeri
Chris Gosdin
Diego Mandelli
Paul Talbot
Cesare Frepoli
Curtis Smith

August 2020

Prepared for the
U.S. Department of Energy
Office of Nuclear Energy

EXECUTIVE SUMMARY

The United States nuclear industry is facing a strong challenge to ensure maximum safety while enhancing economic benefit. Safety is a key parameter to all aspects related to light water reactor (LWR) nuclear power plants (NPPs), especially cost savings. Since the goal is to extend the lifetimes of these NPPs, the traditional deterministic safety concept may not guarantee a current economic asset. The Light Water Reactor Sustainability (LWRS) Program has been promoting a wide range of research and development (R&D) in this field to maximize the safety, economics, and performance of these NPPs through improved scientific understanding.

One of the best practices to achieve this goal is to identify and optimize safety margin, which can in turn lead to cost reduction. To do this, among different other projects, the Risk-Informed Systems Analysis (RISA) Pathway (LWRS) has proposed a new activity named "Plant Reload Process Optimization".

Optimization of plant reloading reactor core thermal limit is one of the highest requests from U.S. nuclear plant utilities, which can help reduce significant amounts of fuel cost. The optimization of safety margins could be proposed by developing independent methods for design basis accident analysis, including LOCA and non-LOCA events that will be compliant with the new proposed 10 CFR 50.46c regulations and thermal conductivity degradation (TCD) evaluations. This will also include peak cladding temperature (PCT) during LOCA analysis and departure of nucleate boiling (DNB) analysis associated with non-LOCA events. The Plant Reload Process Optimization scope includes an analysis of core design, safety margins, fuel performance, and modern data management. The project will focus on customizing the thermal limits for the NPPs based on the core physics at certain reload cycles by applying the risk-informed method to optimizing safety margin.

Since cost reduction from plant reloading is an immediate demand from utilities, the outcome of this research will give high impact on the current fuel market, as well as the utility cost reduction plan. Though regulation issues still need to be solved, positive changes are foreseen in the future fuel supply chain.

This report is aimed to summarize the outcomes and findings of the Phase I of the RISA "Plant Reload Process Optimization" project, whose activities have effectively begun in FY2020.

CONTENTS

FIGURES

TABLES

ACRONYMS

1D	one-dimensional
2D	two-dimensional
3D	three-dimensional
ALWR	Advanced Light Water Reactor
API	Application Programming Interface
ATWS	Anticipated Transients without Scram
BDBA	Beyond Design Basis Accident
BOP	Balance Of Plant
DBA	Design Basis Accident
DNB	Departure of Nucleate Boiling
DOE	U.S. Department of Energy
GA	Genetic Algorithm
INL	Idaho National Laboratory
LOCA	Loss Of Coolant Accident
LWR	Light Water Reactor
LWRS	Light Water Reactor Sustainability
MAAP	Modular Accident Analysis Program
MOOSE	Multiphysics Object-Oriented Simulation Environment
MP-BEPU	Multi-Physics Best Estimate Plus Uncertainty
NEA	Nuclear Energy Agency
NEAMS	Nuclear Energy Advanced Modeling and Simulation
NIST	National Institute of Standards and Technology
NPP	Nuclear Power Plant
NRC	U.S. Nuclear Regulatory Commission
OECD	Organization for Economic Co-operation and Development
PCT	Peak Cladding Temperature
PRA	Probabilistic Risk Assessment
PSF	Performance-Shaping Factor
PSM	Plant “Super” Model
PWR	Pressurized Water Reactor
R&D	Research and Development
RAVEN	Risk Analysis and Virtual Environment
RD&D	Research, Development, and Demonstration

RELAP-5 Reactor Excursion and Leak Analysis Program-5

RHR Residual Heat Removal

RIA Reactivity Initiated Accident

RIMM Risk-Informed Margin Management

RI-MP-BEPU Risk-Informed Multi-Physics Best Estimate Plus Uncertainty

RISA Risk-Informed Systems Analysis

RISC Risk-Informed Safety Categorization

RISMC Risk-Informed Safety Margins Characterization

RPS Reactor Protection System

RPV Reactor Pressure Vessel

SA Simulating Annealing

SSC System, Structure, and Component

SVVP Software Verification and Validation Plan

TCD Thermal Conductivity Degradation

V&V Verification and Validation

Risk-Informed Systems Analysis (RISA) Plant Reload Process Optimization Technical Plan

1. INTRODUCTION

Safety is central to the design, licensing, operation, and economics of the United States light water reactor (LWR) nuclear power plant (NPP) fleet. Plant designers commonly "over-design" portions of NPPs and provide robustness in the form of redundant and diverse-engineered safety features to ensure that, even in the case of well-beyond design basis accident (BDBA) scenarios, public health and safety will be protected with a very high degree of assurance. This form of defense-in-depth concept is a reasoned response to uncertainties and is often referred to generically as a "safety margin." Historically, specific safety margin provisions have been formulated primarily based on "engineering judgment." Further, these historical safety margins have been set conservatively (for example in design and operational limits) in order to compensate for uncertainties.

The Light Water Reactor Sustainability (LWRS) Program [1] is focused on ensuring the safety and performance of the nuclear fleet to enhance operational efficiencies of existing NPPs, support long-term operation, and provide confidence for subsequent license renewals. Within this program, the Risk-Informed Systems Analysis (RISA) Pathway [2] is solving technical issues for several of the "sustainability" dimensions that exist.

One of the best practices to achieve this goal is to identify and optimize safety margin, which can in turn lead to cost reduction. To do this, among different other projects, the Risk-Informed Systems Analysis (RISA) Pathway (LWRS) has proposed a new activity named "Plant Reload Process Optimization".

Optimization of plant reloading reactor core thermal limit is one of the highest requests from U.S. nuclear plant utilities, which can help reduce significant amounts of fuel cost. The optimization of safety margins could be proposed by developing independent methods for design basis accident analysis, including LOCA and non-LOCA events that will be compliant with the new proposed 10 CFR 50.46c regulations and thermal conductivity degradation (TCD) evaluations. This will also include peak cladding temperature (PCT) during LOCA analysis and departure of nucleate boiling (DNB) analysis associated with non-LOCA events. The Plant Reload Process Optimization scope includes an analysis of core design, safety margins, fuel performance, and modern data management.

Since cost reduction from plant reloading is an immediate demand from utilities, the outcome of this research will have high impact in the current fuel market, as well as the utility cost reduction plan. Though regulation issues still need to be solved, positive changes are foreseen in the future fuel supply chain.

In FY2019, a project plan [3] has been carried out and the deployment of this RISA WP has been organized in three phases (one per year). This report is aimed to summarize the outcomes and findings of the Phase I of the RISA "Plant Reload Process Optimization" project, whose activities have effectively begun in FY2020.

The document is organized in 6 Chapters (including this one):

1) Project background and motivations (In this section)

2) Project phases: outlining how the project has been organized in three sub-sequential phases
3) Description of the Phase I: brief description of the phase I and FY 2020 deployment
4) DBA M&S: description and report of the modeling and execution of the DBAs simulation using the RELAP5-3D Super model
5) Fuel pattern optimization algorithm deployment: description of the optimization algorithms that have been prototyped for the thermal limits and fuel pattern optimization
6) Conclusions and future work

2. PROJECT PHASES

The "Plant Reload Process Optimization" project is chartered with the development and deployment of technologies that can have an immediate impact in the nuclear power plant industry. In order to aim for an immediate impact:

1. All tools should (if possible) be mature enough to accurately reflect the physics, plus have sufficient validation present for implementation;
2. The simulation models should (if possible) have enough level of detail to accurately represent the physics, the scenario results must be credible, and be representative of the models that would be submitted to the US NRC and approved.

A successful execution of the project could act as accelerator to risk informed commercial initiatives for the deployment of vendor independent safety analysis capabilities to the utilities in the US, enabling the following advancements:

1. Create a workable framework for realistic scenarios and analysis methodology that will demonstrate the feasibility and readiness for licensing applications
2. Enable commercialization of INL analytical tools in the market (e.g. regulator review of RELAP5-3D [4])

The main goals (See Figure 1) of the projects can be summarized as follows:

1. Optimization of fuel thermal limits to reduce the feed fuel batch size;
2. In-dependent methods/tools from the vendor, which can be used in-house to reduce reload costs;
3. A complete set of methods/tools for reload analysis that will commoditize the nuclear fuel market.

The project is organized in three basic phases (See Figure 2):

DBA Methods Phase (Phase-I): focuses on studying, from a deterministic perspective, the limiting events in Chapter 15 (NUREG-0800) for a prototypical PWR and on the investigation of optimization algorithms for the fuel pattern and thermal limits optimization.

RISA Methods Development Phase (Phase-II): will develop the methods to optimize the thermal limit;

RISA Benefit Quantification Phase (Phase-III): will conclude with plant reloading using a management method developed using optimized safety limits.

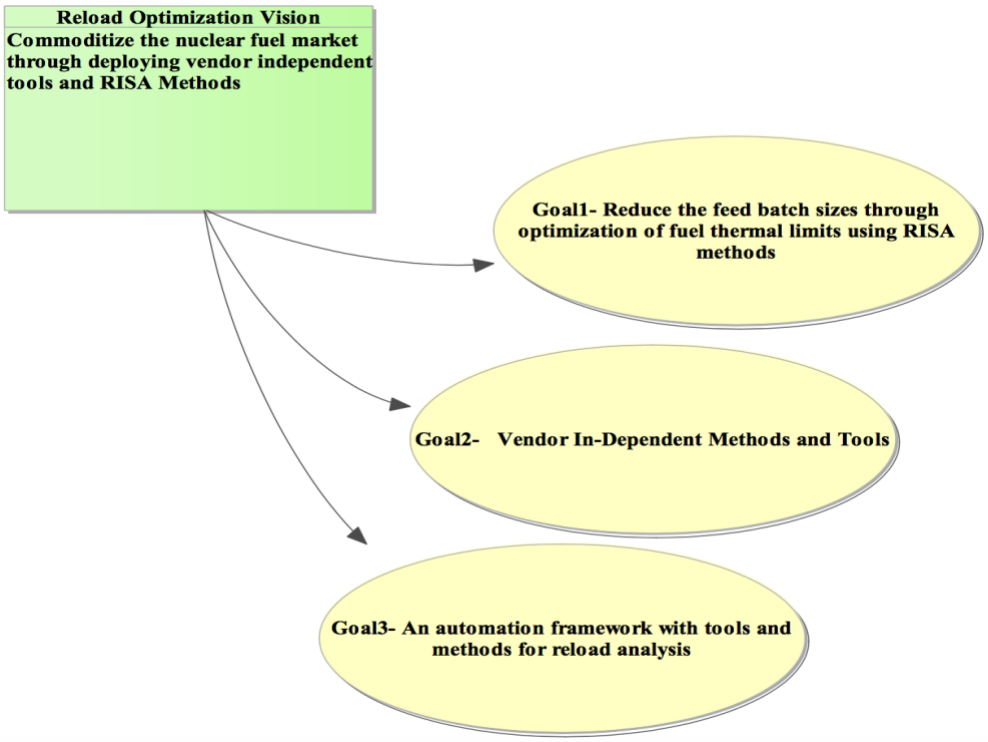

Figure 1 - Project Goals

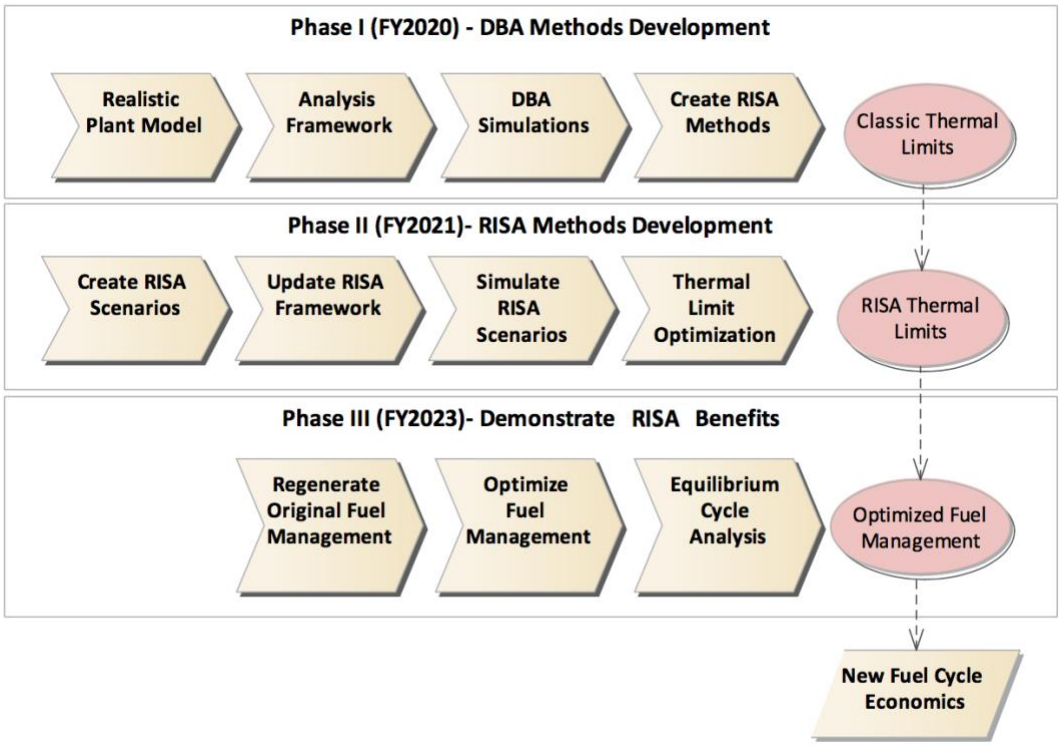

Figure 2 - Project plan.

3. PHASE I - DBA METHODS DEVELOPMENT

The main idea resolves around the demonstration of the gains of the RISA program and enticing a US nuclear utility to implement and license risk informed scenarios. For this reason, this project needed to build a confident foundation of trust that the outcomes generated as part of this task would reflect operating plants. The first stage of the Phase I was about a carful and deep analysis of the NUREG-0800 [5] and the representative plant's licensing basis documentation (UFSAR) to determine which key thermal limit setting scenarios should be simulated with the RISA framework, using deterministic methods for benchmarking to the plant's licensing Design Basis Accidents (DBAs). This benchmarking is aimed to provide confidence to the utilities that the toolkit and models can be representative of the current licensing basis. Phase I thereby focused on demonstration of current DBAs to investigate the possible procedures to move from classic NUREG-0800 Chapter 15 to risk informed space in NUREG-0800 Chapter 19. Throughout Phase I, the team reviewed the ~10 limiting events (see Table 1) in Chapter 15 (NUREG-0800).

Table 1 - Identified Limiting Events in Chapter 15

Limiting Events in Chapter 15 (NUREG-0800)	
EVENT	SECTION
Steam System Piping Failure	15.1.5
Turbine Trip	15.2.3
Loss of Nonemergency Ac Power to The Plant Auxiliaries	15.2.6
Reactor Coolant Pump Shaft Seizure (Locked Rotor)	15.3.3
Chemical and Volume Control System Malfunction That Results in A Decrease in The Boron Concentration in The Reactor Coolant	15.4.6
Spectrum of Rod Cluster Control Assembly Ejection Accidents	15.4.8
Inadvertent Operation of the Emergency Core Cooling System During Power Operation	15.5.1
Steam Generator Tube Failure	15.6.3
Loss-Of-Coolant Accidents	15.6.5
Feedwater System Malfunctions that Result in an Increase in Feedwater Flow	15.3.2

In the following sub sections, some of the Phase I activities are reported and detailed.

3.1 RELAP5-3D Plant Model Reference Model

This activity is focused on developing the key components/items for constructing the RELAP5-3D Plant Model. The starting point of the model construction is based on a generic 4-loop PWR model.

Significant industry credibility is envisioned to be gained by using a PWR RELAP5-3D model that has high fidelity nodalization of the important components (steam generator, pressurizer, reactor vessel, etc.). This activity focuses on the development of the components of that model, as well as making it reflective of a real US Nuclear Power Plant (NPP). A

RELAP5-3D plant model with high fidelity in the vessel or other important components will enable a more robust uncertainty analysis for RISA as well a gain US utility perspective.[a]

3.2 DBA Simulations

This activity focused on modeling and executing the design basis simulations and comparison to the existing plant's licensing basis. The resulting outcomes are aimed to build credibility with the utilities that RELAP5-3D (driven, when necessary, by RAVEN [6] [7] [8]) can generate simulation results similar to what is licensed as well as provide a benchmark to RELAP5-3D results against a known standard.

3.3 Optimization algorithm

In preparation of Phase II, the team deployed an initial version of the optimization workflow for thermal limits and, consequentially, fuel patter optimization. Details of such algorithms are reported in section 0.

4. DBA MODELING AND SIMULATION

4.1 Plant Model

In order to model and execute the limiting events listed in previous sections, a RELAP5-3D PWR model has been deployed. The reference plant model is a refined version of the preliminary plant model developed in Phase 0 (FY19). The preliminary plant model used for Phase 0 was the 4-loop Westinghouse PWR Zion. The plant choice was discussed between FPoliSolutions and INL, resulting in both groups deciding to use a different plant's operating conditions. This decision was made due to the lack of information pertaining to the Zion plant model, and that using a newer plant would appeal more to the

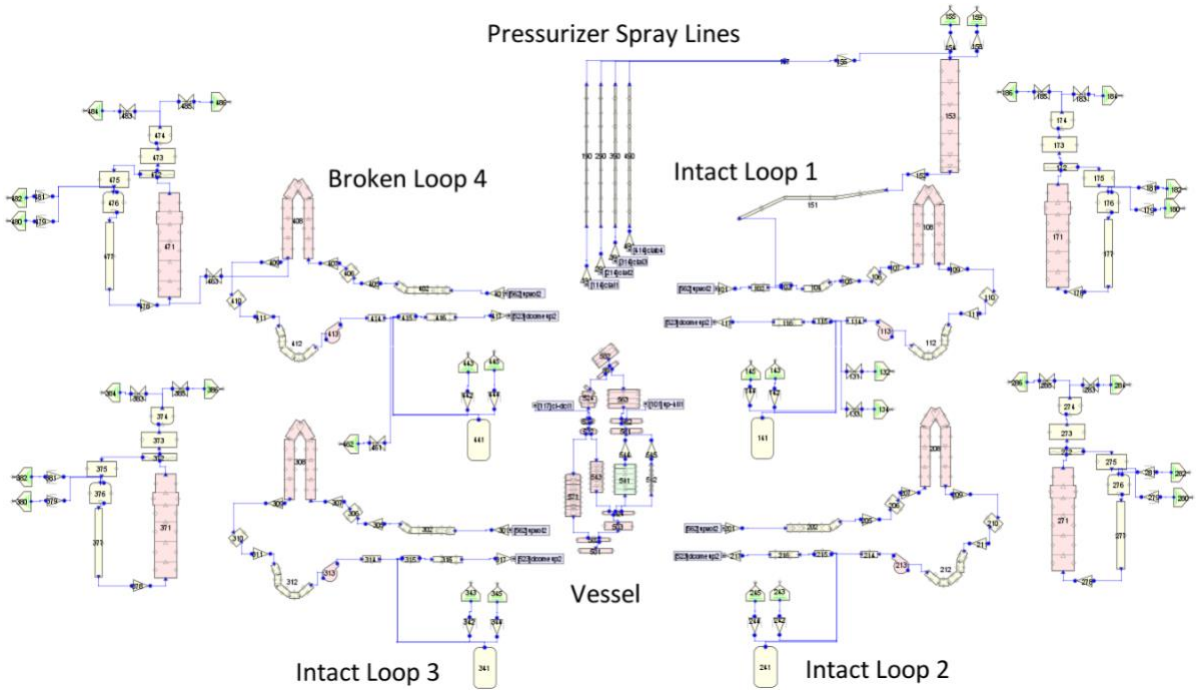

Figure 3 - Reference Plant SNAP Model Layout

industry.

4.1.1 Component Numbering and Layout

The model layout of the reference plant is shown in Figure 3. The Reference plant model is intended to have a component naming and numbering scheme that makes identification of components as easy as possible. The numbering scheme is characterized as follows:

- Loops:
  - The intact loops are assigned numbers 1 through 3, and the "broken" loop is 4. The "broken" loop will generally be used to impose any asymmetric condition which affects 1 loop. In the description below, X is the loop number.
  - The pressurizer is connected to loop 1.

- The primary coolant loop components are numbered X01 through X17. There is room for component numbering up to X30.
- The SS charging and letdown components are numbered 131 through 134. There is room for component numbering up to X40.
- The SI components are numbered X41 through X45. There is room for component numbering up to X50.
- The pressurizer components are numbered 151 through 159. There is room for component numbering up to X60.
- The break-related components are numbered 461, 462, and 463. There is room for component numbering up to X70.
- The secondary components are numbered X71 through X86. There is room for component numbering up to X89.
- The pressurizer spray line components are numbered X90.

o Vessel:

- The lower plenum components are numbered 501 through 504. There is room for component numbering up to 520.
- The downcomer components are numbered 521 through 524. There is room for component numbering up to 540.
- The core components are numbered 541 through 545. There is room for component numbering up to 560.
- The upper plenum components are numbered 561 through 563. There is room for component numbering up to 580.
- The upper head components are numbered 581 through 582. There is room for component numbering up to 599.

o Heat Structures:

- The numbering convention is CCCN, where CCC is the lowest component number among the connected fluid channels, and N is 0 for the first connection to a component number and it is increased by 1 for each additional heat structure attached.

The naming convention for the fluid components is that there is an acronym which represents the identity of the component, and then at the end, there is i1, i2, or i3, for intact loops 1 through 3, and b4 for broken loop 4. The acronyms should be consistent across all 4 loops, and the names only differentiated by the i1, i2, i3, or b4.

The naming convention for heat structures is to use a descriptive name to the extent possible. When "vess" is in the name, this indicates it is part of the vessel wall (and thus uses an outside "symmetry" condition, while "inthts" in the name indicates an internal heat structure (thus the inside connection is either symmetry or a copy of the outside connection (for two-sided heat transfer)).

4.1.2 Plant specific inputs

To enhance the capabilities of the reference model, the geometry (which was based on the Zion model) was updated for the reference plant design, for some key parameters.

One of these enhancements was the steam generator tube geometry. The SG tube geometry was revised to more accurately reflect the radii and HT surface area of the reference model plant.

Another change was the core modeling. In order to model Chapter 15 safety analyses, it is necessary to have a model with different power shapes. In order to implement this, the existing core pipe was split into 2 pipes, and the existing rods heat structure was split into 2 heat structures. The first pipe is the hot assembly pipe, which means that it models a single assembly connected to the hot assembly heat structure. The second pipe is the average assembly pipe, which means that it models a single assembly connected to the average assembly heat structure. The following information from the reference plant was used to calculate the required information for the model:

- FQ – Ratio of the maximum local power to the core average power: This is set to a value of 2.55.
- FΔH – Ratio of the power generated in the hot rod to the power generated in an average rod: This is set to a value of 1.65. Note that this is implemented as the ratio of the power generated in the hot assembly (rather than rod) to the power generated in an average rod, for simplicity.
- Number of Assemblies: This is set to a value of 193.
- Power Deposition: The fraction of power which is generated within the fuel rod, as opposed to that which is deposited directly into the moderator, generally by gamma rays. The value of 0.974 is consistent with the typical PWR model input, and that used in most safety analyses.
- Core Length: The fueled length of the reactor core is 12 ft. This is the length of most PWR cores.
- Number of Core Cells: Based on the base model, 6 cells are used to represent the core.

The linear power fraction is shown in Figure 4. This shows that a top skewed cosine type power shape is modeled, as desired.

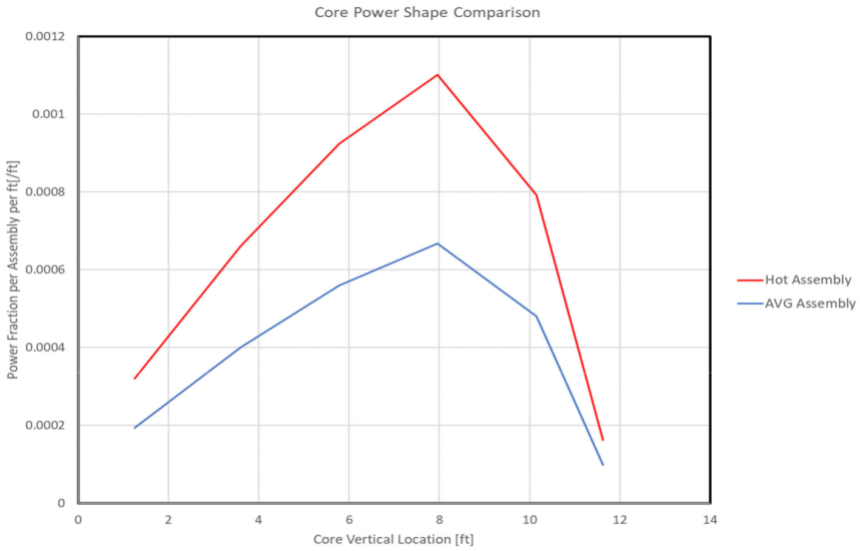

Figure 4 - Core Power Shape

4.2 DBA Simulations

The limiting DBA cases previously identified have been modeled and executed. In the following sections, details about the models and results are reported.

4.2.1 Reactor Coolant Pump Shaft Seizure (Locked Rotor)

Reactor coolant pump shaft seizure is an ANS Condition IV incident and is commonly referred to as a locked rotor incident.

The reactor coolant pump (RCP) rotor has an instantaneous seizure causing rapidly reduced flow through its associated coolant loop. This leads to a reactor trip on low flow signal. The fuel rods continue to heat the coolant, causing expansion of the water. At the same time, heat transfer from the primary side to the secondary side through the steam generator (SG) tubes decreases. This happens for two reasons:

1. The reduced primary flow results in a decreased film coefficient inside the tubes

2. The reactor coolant in the tubes cools while the secondary side temperature increases, because the turbine steam flow is reduced to zero upon plant trip.

The coolant expansion in the core, combined with the reduced heat transfer through the SG, causes a surge into the pressurizer, resulting in a pressure increase throughout the reactor coolant system. Prior to insertion of the control rods, the pellet and clad temperatures of the fuel rods increase rapidly as a result of the degradation of heat transfer from fuel rods to the coolant due to the reduced flow. The pressurizer pressure increase should activate the automatic pressurizer spray system, open the power-operated relief valves, and open the pressurizer safety valves. The FSAR states that “The power-operated relief valves are safety grade and would be expected to function properly during an accident; however, for conservatism, the analysis does not use the pressure-reducing effect of the power-operated relief valves and the pressure-reducing effect of the spray.”

The locked rotor scenario presents two cases in the FSAR:

1. Loss-of-offsite power (LOOP)
2. Offsite power available (OPA)

4.2.1.1 Results

The RELAP results are compared to the locked rotor runs from the FSAR in the paragraphs below. Note that the figures labeled with -A are for LOOP and the figures labeled with -B are for OPA.

The transient vessel mass flow as a fraction of the nominal flow is shown in Figures 5-A and 5-B. From Figure 5-A, the LOOP RELAP run initially decreases slightly more slowly than the FSAR run, but the brief plateau encountered by the FSAR run does not happen for the RELAP LOOP run. As such, the RELAP LOOP run drops significantly below the FSAR run starting at about 2 seconds, and they slowly converge by the end of the transient. From Figure 5-B, the OPA RELAP run initially decreases a bit more slowly, but the curves mostly converge by about 4 seconds. These figures also illustrate the difference between LOOP and OPA most clearly. The vessel flow in the LOOP case drops significantly further and faster than that in the OPA case, and the OPA case stabilizes at around 70% of the nominal flow.

The transient locked rotor loop (loop 4) mass flow as a fraction of the nominal flow is shown in Figures 6-A and 6-B. From Figures 6-A and 5.5-2-B, the LOOP and OPA RELAP runs decrease more slowly than the FSAR run and ends up with reverse flow of a significantly smaller magnitude. These figures show a small difference between LOOP and OPA. The reverse flow in the LOOP case is of slightly lower magnitude than in the OPA case.

The transient average rod heat flux is shown in Figures 7-A and 7-B. From Figures 7-A and 7-B, the RELAP runs have a slightly lower peak heat flux than the FSAR runs, and the heat flux decreases more quickly throughout the RELAP transients. These figures show no appreciable difference between LOOP and OPA.

The transient hot rod heat flux is shown in Figures 8-A and 8-B. From Figures 8-A and 8-B, at about 1 second, the RELAP runs suddenly drop significantly, and then have a smooth increase for a bit before decreasing throughout the rest of the transient. In both cases, they are nothing like the FSAR runs. It is theorized that RELAP is switching to a heat transfer mode with significantly decreased heat transfer coefficient. These figures show no appreciable difference between LOOP and OPA.

The transient core power as a fraction of the nominal power is shown in Figures 9-A and 9-B. From Figures 9-A and 9-B, the RELAP runs have a similar core power transient to the FSAR runs, but with a lower peak. These figures show no appreciable difference between LOOP and OPA.

The transient maximum clad temperature is shown in Figures 10-A and 10-B. From Figures 10-A and 10-B, the RELAP runs have significantly lower peak temperature than the FSAR runs. It is unclear why this is the case, but it is theorized that the fuel rod geometry or material properties could be contributing. These figures show no appreciable difference between LOOP and OPA.

The transient departure from nucleate boiling ratio (DNBR) at the peak power location of the hot rod is shown in Figures 11-A and 11-B. There are no FSAR plots for comparison, but this value is listed as an acceptance criterion in the FSAR section. From Figures 11-A and 11-B, the RELAP runs both experience similar progression of DNBR, which show that after a small initial

decrease, the DNBR shoots very high, then quickly drops back down, then gradually increases for the remainder of the transient. It is noted that the large, sudden changes in DNBR occur at a similar time to the large, sudden changes in heat flux, lending further credibility to the possibility that a change in HT mode is causing the heat flux change.

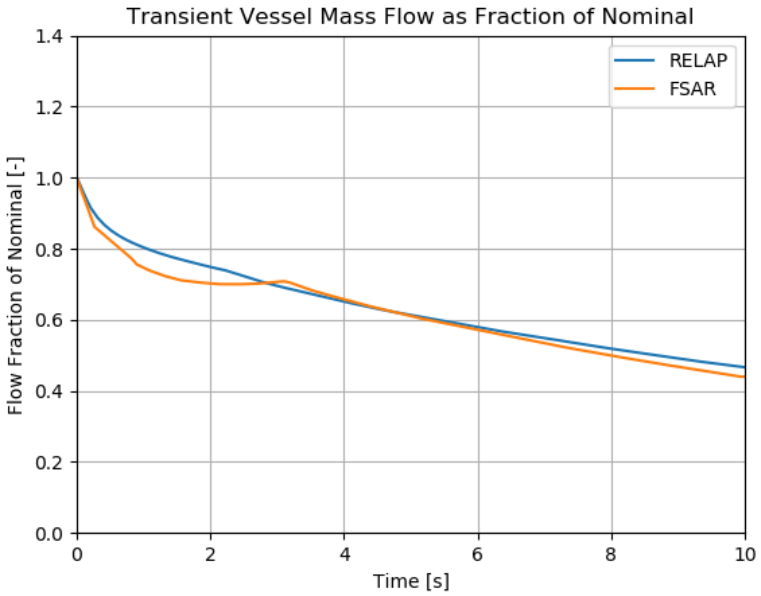

(A)

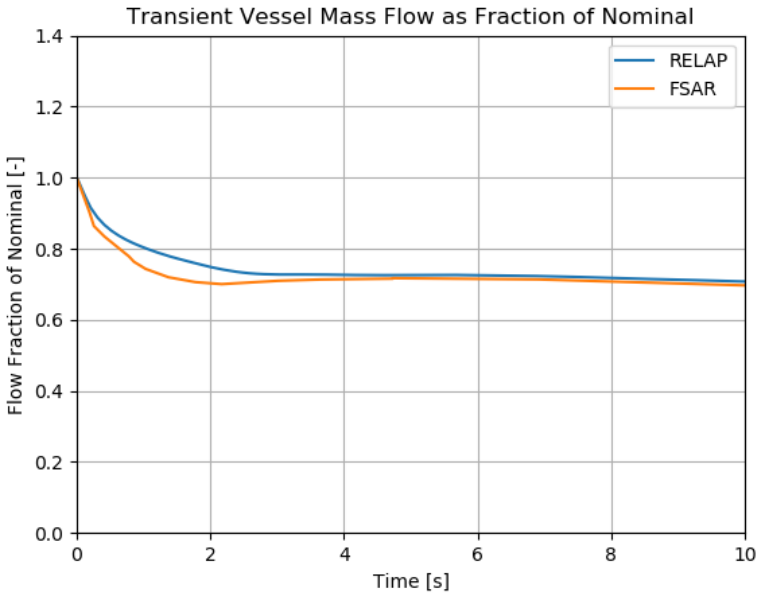

(B)

Figure 5 - Transient Vessel Mass Flow as a Fraction of Nominal for the Locked Rotor Scenario (both LOOP and OPA)

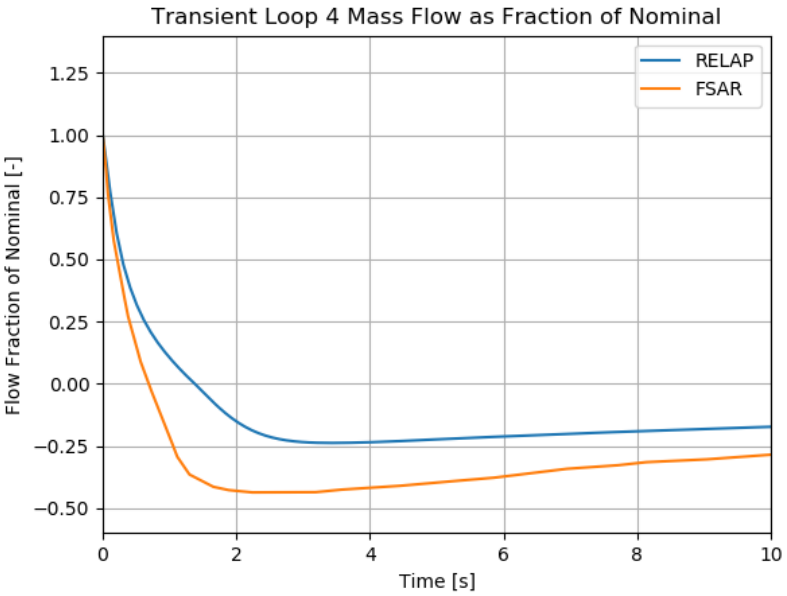

(A)

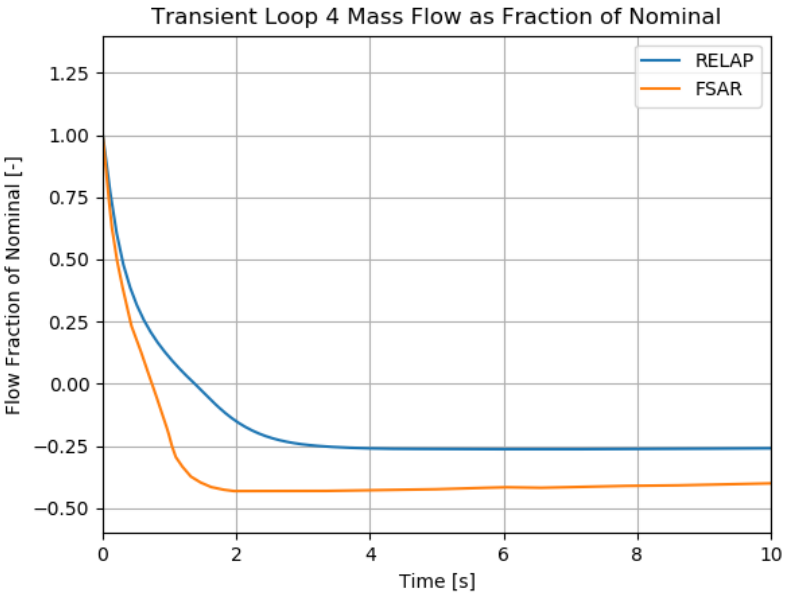

(B)

Figure 6 - Transient Loop 4 Mass Flow as a Fraction of Nominal for the Locked Rotor Scenario (both LOOP and OPA)

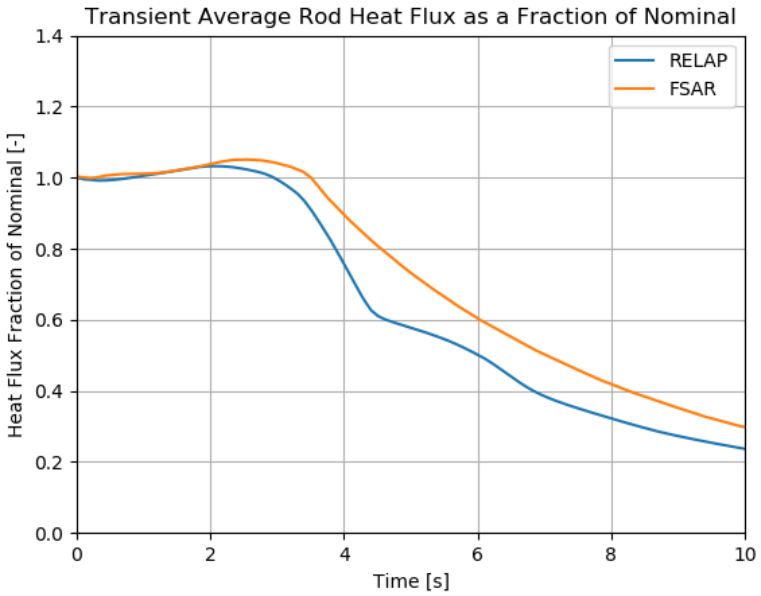

(A)

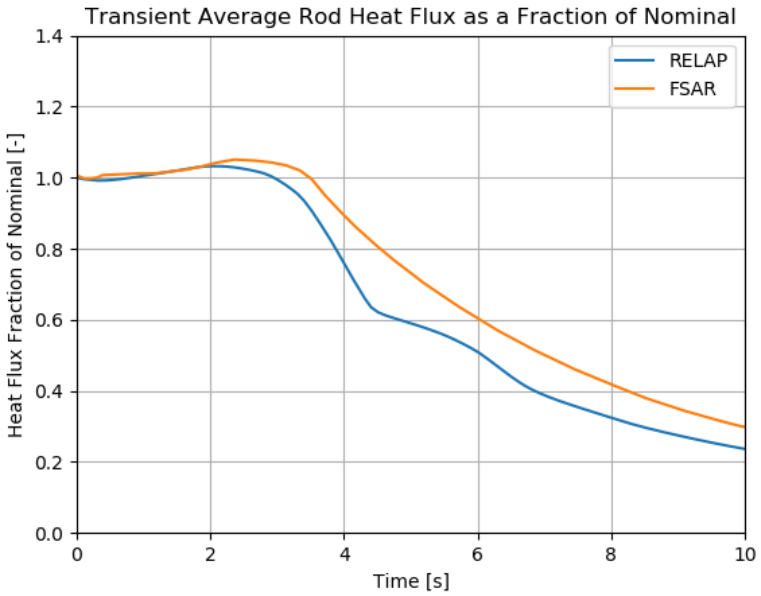

(B)

Figure 7 - Transient Average Rod Heat Flux as a Fraction of Nominal for the Locked Rotor Scenario (both LOOP and OPA)

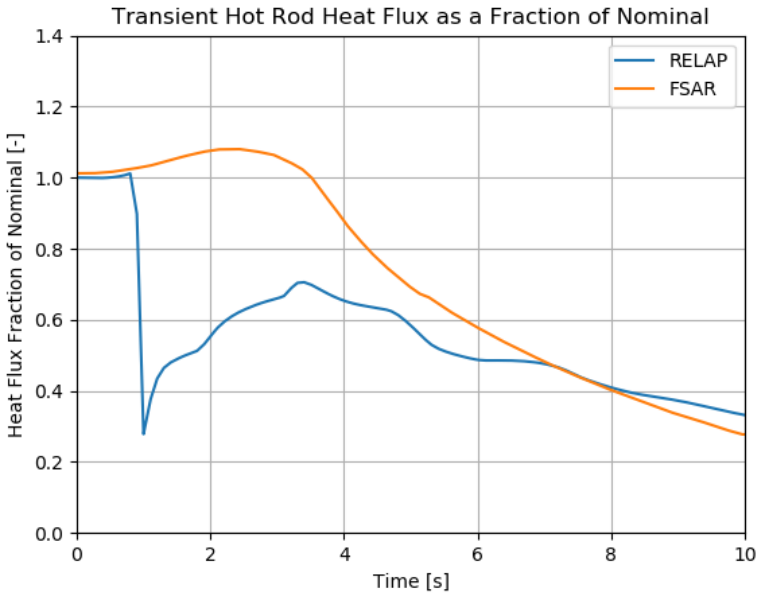

(A)

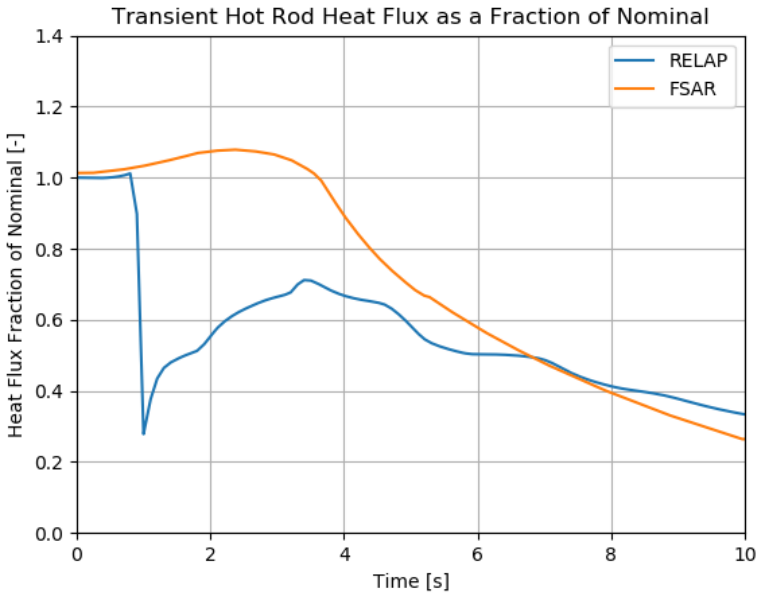

(B)

Figure 8 - Transient Hot Rod Heat Flux as a Fraction of Nominal for the Locked Rotor Scenario (both LOOP and OPA)

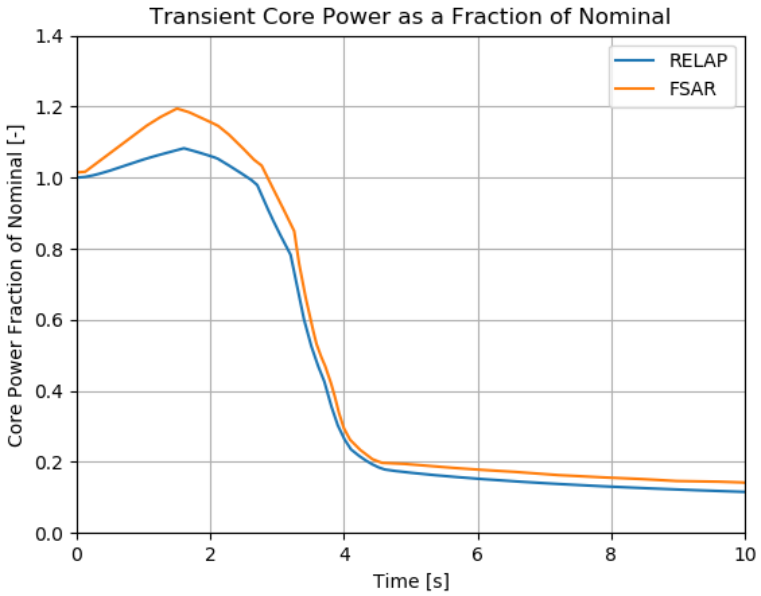

(A)

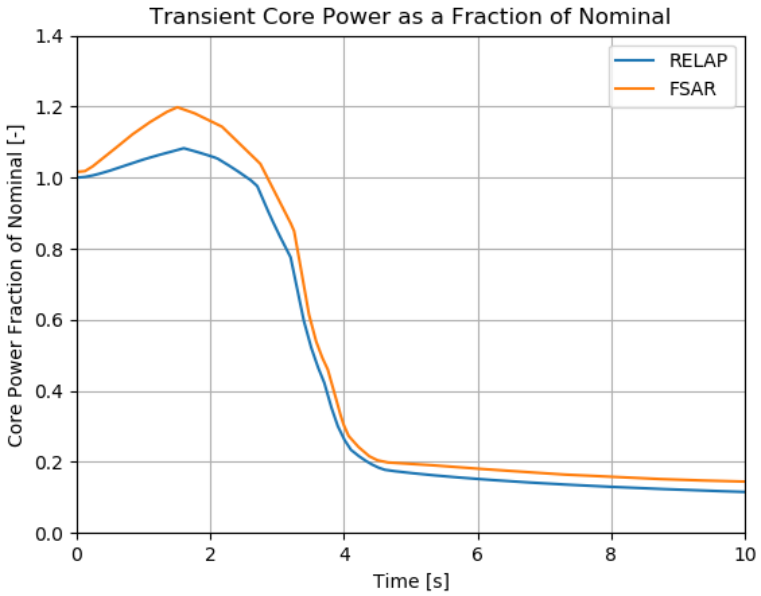

(B)

Figure 9 - Transient Core Power as a Fraction of Nominal for the Locked Rotor Scenario (both LOOP and OPA)

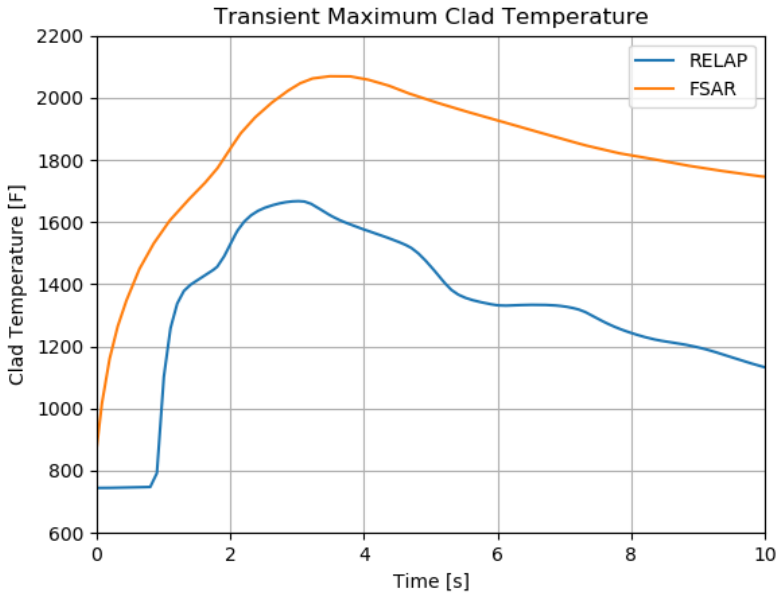

(A)

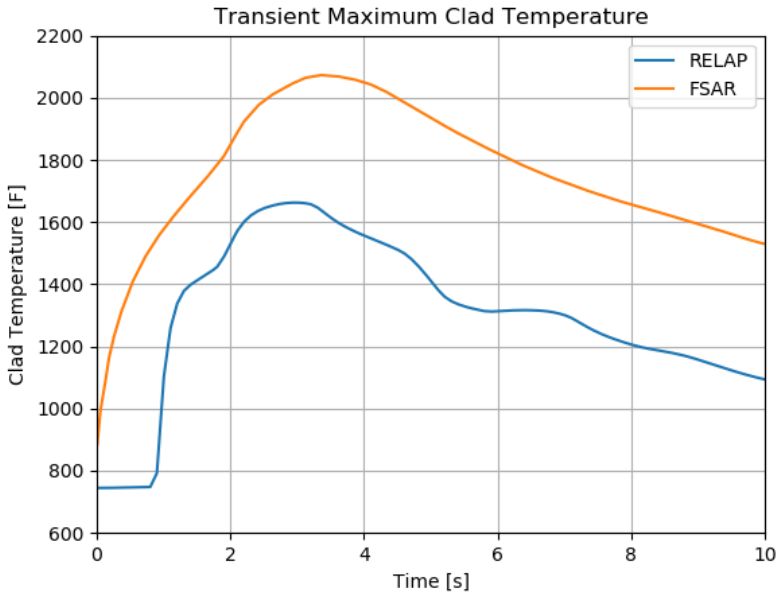

(B)

Figure 10 - Transient Maximum Clad Temperature for the Locked Rotor Scenario (both LOOP and OPA)

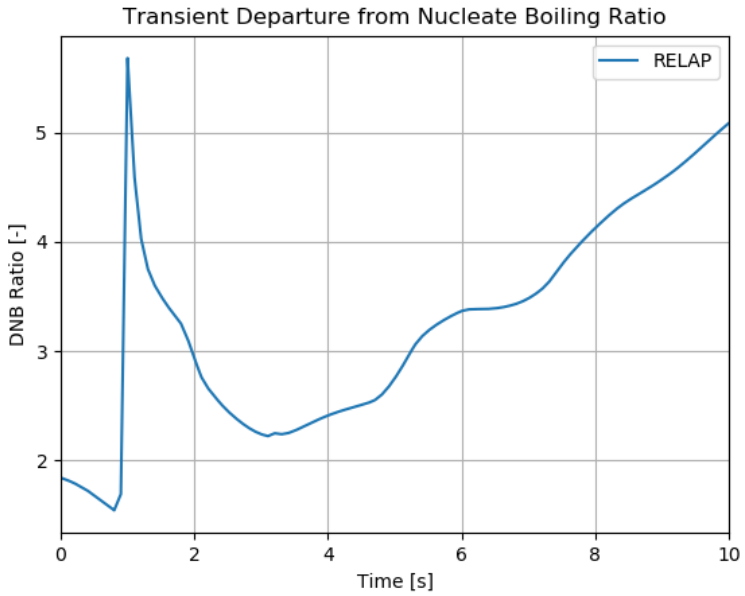

(A)

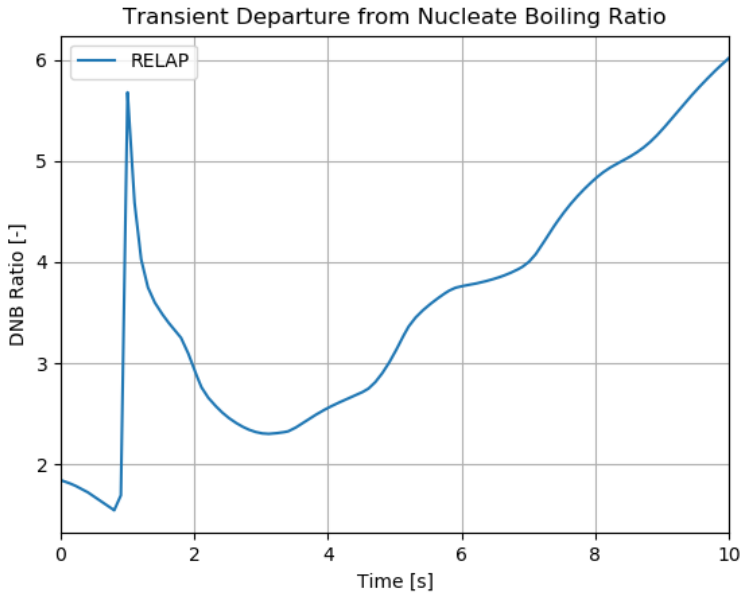

(B)

Figure 11 - Transient DNBR for the Locked Rotor Scenario (both LOOP and OPA)

4.2.2 Steam System Piping Failure (Main Steam-line Break)

Steam system piping failure is an ANS Condition IV incident and is commonly referred to as a main steam line break/rupture (MSLB).

The steam release resulting from a MSLB will produce an initially-large increase in steam flow that decreases during the accident as the steam pressure falls. The increased energy removal from the reactor coolant system (RCS) causes a reduction of coolant temperature and pressure. In the presence of a negative moderator temperature coefficient, the cooldown results in an increase in reactivity. If the most reactive rod cluster control assembly (RCCA) is assumed stuck in its fully withdrawn position after reactor trip, it is more likely that the core will become critical and return to power. A return to power following a steam line rupture is a potential problem mainly because of the high-power peaking factors which exist, assuming the most reactive RCCA to be stuck in its fully withdrawn position. The core is ultimately shut down by the boric acid solution delivered by the safety injection (SI) system and accumulators.

According to the FSAR, numerous combinations of break sizes and power level were run to determine the limiting cases. For the purposes of this work, the limiting cases presented in the FSAR section are re-created. This includes:

- Hot zero power (HZP) operation assuming LOOP
- Hot zero power (HZP) operation assuming OPA
- Hot full power (HFP) operation (no information is provided on LOOP vs. OPA)

The HZP cases have identical input, except for pump behavior, and the SI delay.

The HFP case has substantially different input. LOOP is arbitrarily assumed.

4.2.2.1 Results

The RELAP results are compared to the MSLB runs from the FSAR in the paragraphs below. Note that the figures labeled with -A are for LOOP and the figures labeled with -B are for OPA. The HZP and HFP cases are discussed separately.

Hot Zero Power Cases

The transient vessel mass flow as a fraction of the nominal flow is shown in Figures 12-A and 12-B. From Figure 12-A, the LOOP RELAP run matches the FSAR run closely. From Figure 12-B, the OPA RELAP run initially increases similar to the FSAR run for the first ~50 seconds, but the FSAR run then increases significantly more. This timing seems to coincide with the much more significant re-criticality observed in RELAP, discussed below.

The transient pressurizer pressure is shown in Figures 13-A and 13-B. From Figures 13-A and -B, both RELAP runs de-pressurize significantly more slowly than the FSAR run. At approximately the time of re-criticality, the pressure begins to increase significantly in the RELAP runs, while it continues to decrease in the FSAR runs. Note that the pressure increase in the LOOP run is a little slower than the OPA run due to the slower increase in power. These differences suggest that the significantly higher power excursion in the RELAP run drives a major difference in RCS conditions.

The transient average rod heat flux is shown in Figures 14-A and 14-B, and the core power as a fraction of nominal is shown in Figures 15-A and 15-B. From these figures, in both cases, the

power excursion is significantly higher in the RELAP runs than the FSAR runs. In the LOOP cases, both the FSAR and RELAP runs have a power excursion that is lower in peak, but longer in duration than the OPA case. As the kinetics model is sensitive to small changes, and the FSAR inputs were simplified a bit for entry into RELAP, it is not surprising that there are significant differences between the RELAP power results and the FSAR results.

The transient maximum clad temperature is shown in Figures 16-A and 16-B. There are no equivalent figures in the FSAR, but these results are still of interest. Neither the LOOP nor OPA case experience any significant heatup.

The transient feedwater flow is shown in Figures 17-A and 17-B. From Figures 17-A and -B, both RELAP runs start with no MFW flow, then the AFW comes on and goes to a level consistent with that in the FSAR run. The FSAR runs start with normal MFW flow, but as discussed in the SS sections, this is due to the difficulties in obtaining a good HZP SS with this model.

The transient steam flow is shown in Figures 18-A and 18-B. From Figures 17-A and -B, the RELAP steam flow values are very similar initially. In the LOOP case, the RELAP steam flow continues to be very similar to the FSAR run until about 250 seconds. In the OPA case, there is a significant deviation starting at about 50 seconds, and then the RELAP run steam flow ceases by about 100 seconds. All things considered, the differences between the RELAP runs and the FSAR runs are fairly minimal.

The transient SG pressure is shown in Figures 19-A and 19-B. From Figures 19-A and -B, the broken SG pressure follows nearly identical trends to the steam flow. The intact SGs appear to initialize from substantially lower pressure in the FSAR run, but they converge to similar pressures with the RELAP runs.

The transient average core temperature is shown in Figures 20-A and 20-B. From Figures 20-A and -B, both RELAP runs decrease in temperature significantly more slowly than the FSAR run. At approximately the time of re-criticality, the temperature begins to increase in the RELAP runs, while it continues to decrease in the FSAR runs. These differences suggest that the significantly higher power excursion in the RELAP run drives a major difference in RCS conditions.

The transient vessel inlet temperature is shown in Figures 21-A and 21-B. From Figure 21-A, the intact loops have a fairly similar transient between the RELAP run and the FSAR run, and the faulted loop is very similar until about 80 seconds for OPA and 150 seconds for LOOP. At that point, the RELAP run experiences a rapid increase in temperature. This is likely due to the larger power excursion in RELAP. Both RELAP runs decrease in temperature significantly more slowly than the FSAR run. From Figure 21-B, in all 4 RELAP loops, the temperature barely decreases, then stays nearly the same for the last 500 seconds. The FSAR runs have a sustained, significant decrease in temperature in all loops. This is likely due to the larger power excursion in RELAP.

The transient pressurizer water volume is shown in Figures 22-A and 22-B. From Figures 22-A and -B, both RELAP runs decrease in pressurizer water volume significantly more slowly than the FSAR run. At approximately the time of re-criticality, the temperature begins to increase in the RELAP runs, while it continues to decrease in the FSAR runs. These differences suggest that the significantly higher power excursion in the RELAP run drives a major difference in RCS conditions.

The transient reactivity is shown in Figures 23-A and 23-B. From Figures 23-A and -B, both RELAP runs have an initial increase in reactivity, which results in the large re-criticality of the

run. Once this decreases, the FSAR runs decrease more quickly, which explains the much lower power.

The transient core boron concentration is shown in Figures 24-A and 24-B. From Figures 24-A and -B, both RELAP runs experience a very similar increase in core boron concentration. This is strange, since the RCPs continued operation would be expected to promote the movement of boron to the core more rapidly. This is reflected in the FSAR run.

The transient DNBR is shown in Figures 25-A and 25-B. From Figures 25-A and -B, both RELAP runs show a value of 0 for the entire transient. In RELAP, this indicates that the heat structure is in a HT mode which does not even calculate CHF (i.e., single phase liquid). This is thus interpreted as a very high DNBR value.

Hot Full Power Cases

The transient pressurizer pressure is shown in Figure 26. From Figure 26, the RELAP run de-pressurizes a bit initially. At approximately the time of re-criticality, the pressure begins to increase again, and then at the time of scram, it drops significantly. Note that this plot should have an FSAR curve to compare to, however, there is an error in the FSAR, where these figures are instead replaced with the figures from the previous page (so there are two pages in a row with identical figures, when the second page should have 3 new figures on it).

The transient average rod heat flux is shown in Figure 27 and the core power as a fraction of nominal is shown in Figure 28. From these figures, it is apparent that RELAP does have a power excursion, but it is very small compared to that in the FSAR analysis. As the kinetics model is sensitive to small changes, and the FSAR inputs were simplified a bit for entry into RELAP, it is not surprising that there are significant differences between the RELAP power results and the FSAR results. Note that Figure 28 should have an FSAR curve to compare to, however, there is an error in the FSAR, where these figures are instead replaced with the figures from the previous page.

The transient maximum clad temperature is shown in Figure 29. There are no equivalent figures in the FSAR, but these results are still of interest. The RELAP run experiences a significant heatup which terminates shortly after the reactor scrams.

The transient SG pressure is shown in Figure 30. From Figure 30, the broken SG pressure in RELAP follows a very similar trend to that from the FSAR, other than the last 5 seconds, or so. The intact SG pressures in RELAP stay about the same, until a sudden pressurization after scram, while in the FSAR, they decrease very similar to the broken SG prior to the pressurization after scram.

The transient average core temperature is shown in Figure 31. From Figure 31, the temperature stays fairly consistent through the RELAP transient, while the FSAR run decreases significantly.

The transient vessel inlet temperature is shown in Figure 32. From Figure 32, the intact loops stay more or less the same until a decrease after reactor scram. The broken loop shows a cooldown fairly similar to the FSAR results.

The transient pressurizer water volume is shown in Figure 33. From Figure 33, the RELAP run shows a fairly slow and steady decrease in pressurizer water volume for the first 15 seconds or so. It then begins a very gradual increase until reactor scram causes it to start deceasing very quickly.

Note that this figure should have an FSAR curve to compare to, however, there is an error in the FSAR, where these figures are instead replaced with the figures from the previous page.

The transient steam flow as a fraction of nominal is shown in Figure 34. From Figure 34, the RELAP steam flow initially increases to almost 20% higher than nominal, then rapidly drops to about 10% higher than nominal, and slowly drops after that. Once the reactor trips, it drops very quickly. This trend is very similar to the FSAR run, except that the FSAR run ends up with a much higher sustained flow rate.

The transient DNBR is shown in Figure 35. From Figure 35, the RELAP run shows significant margin in the beginning, and then around 14 seconds, the DNBR drops sharply and goes to 0. In RELAP, a value of 0 may indicate that the heat structure is in a HT mode which does not even calculate CHF (i.e., single phase liquid) or it may be in CHF. Since this time period is approximately when the clad temperature excursion occurs, it is presumed that this plot is showing that DNBR is below 1 starting at around 16 seconds.

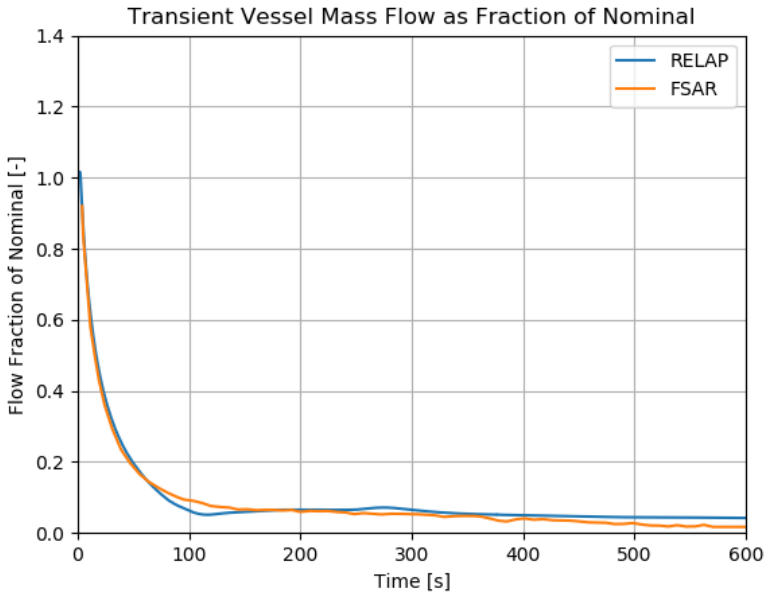

(A)

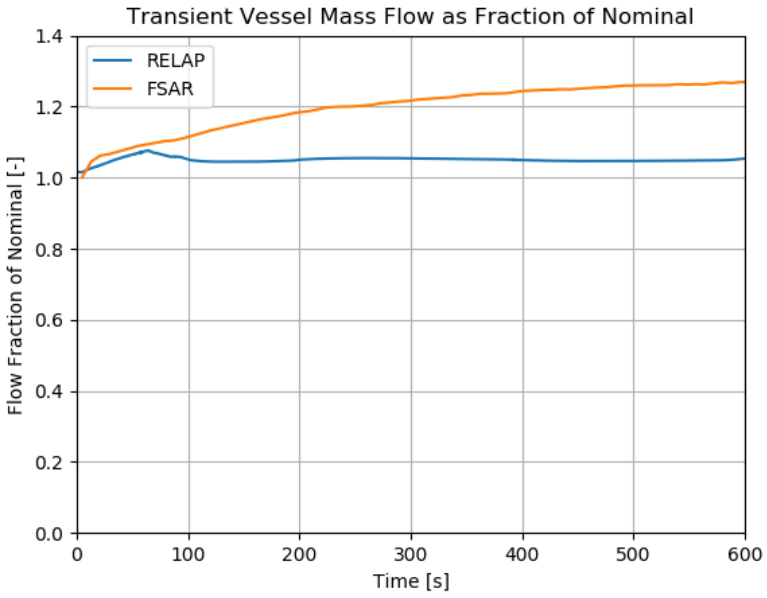

(B)

Figure 12 – Transient Vessel Mass Flow as a Fraction of Nominal for the MSLB Scenario (HZP, both LOOP and OPA)

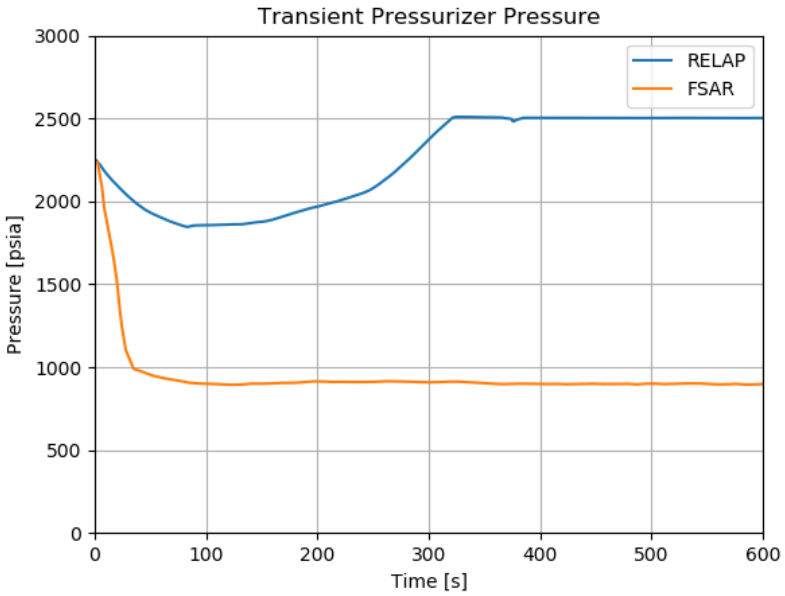

(A)

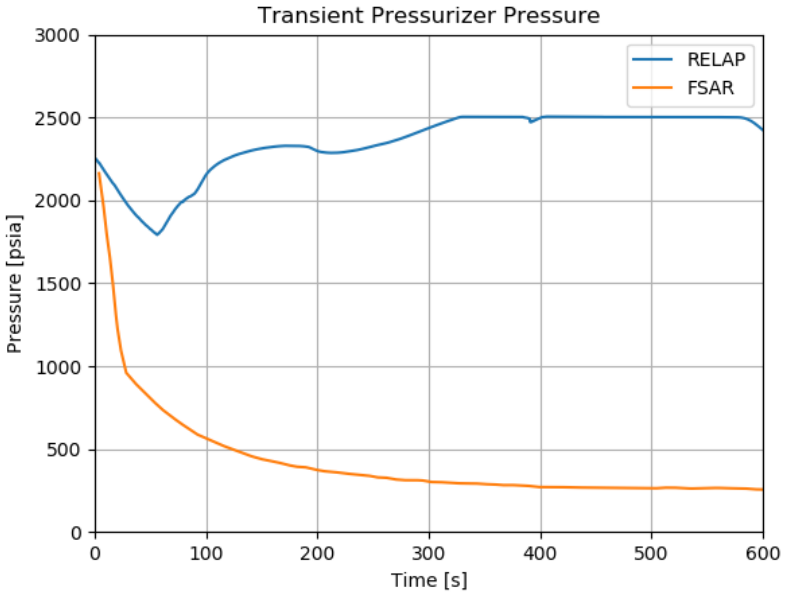

(B)

Figure 13 – Transient Pressurizer Pressure for the MSLB Scenario (HZP, both LOOP and OPA)

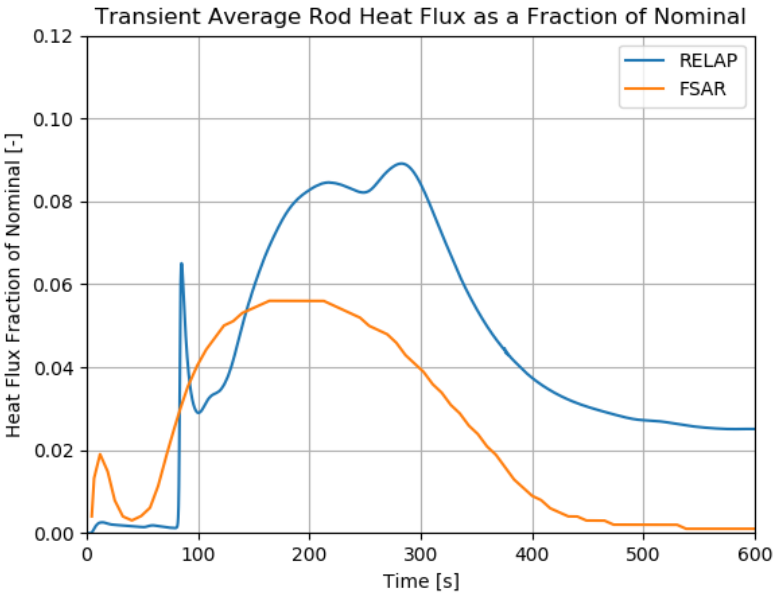

(A)

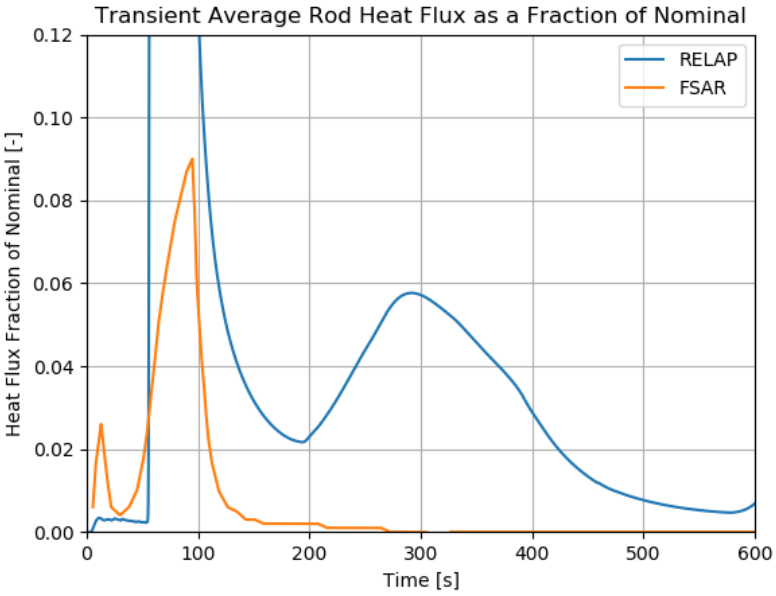

(B)

Figure 14 – Transient Average Rod Heat Flux as a Fraction of Nominal for the MSLB Scenario (HZP, both LOOP and OPA)

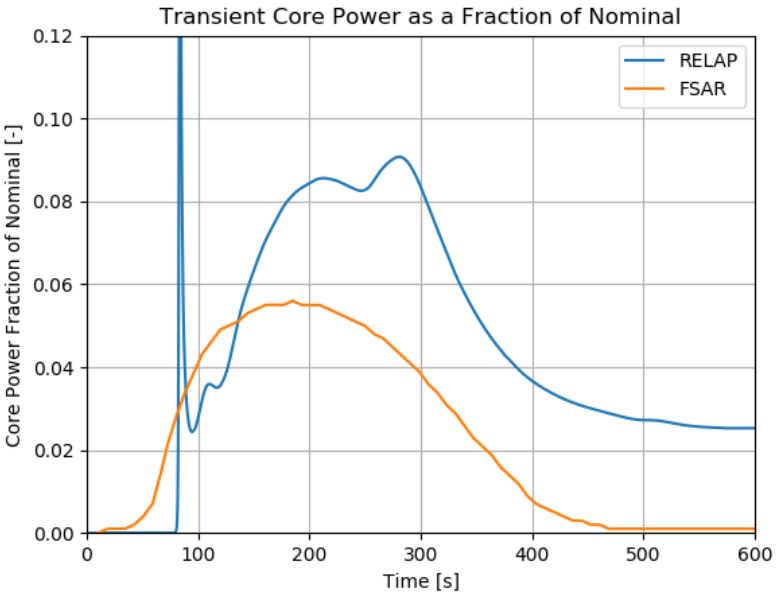

(A)

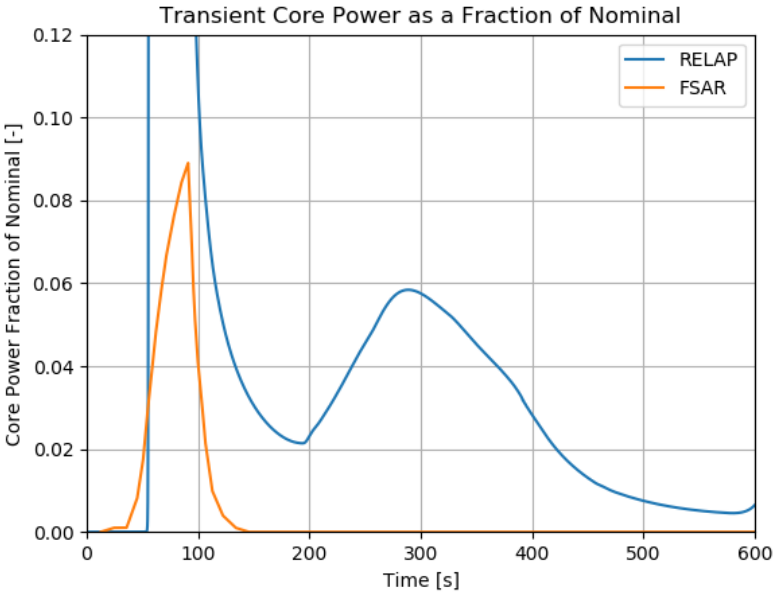

(B)

Figure 15 – Transient Core Power as a Fraction of Nominal for the MSLB Scenario (HZP, both LOOP and OPA)

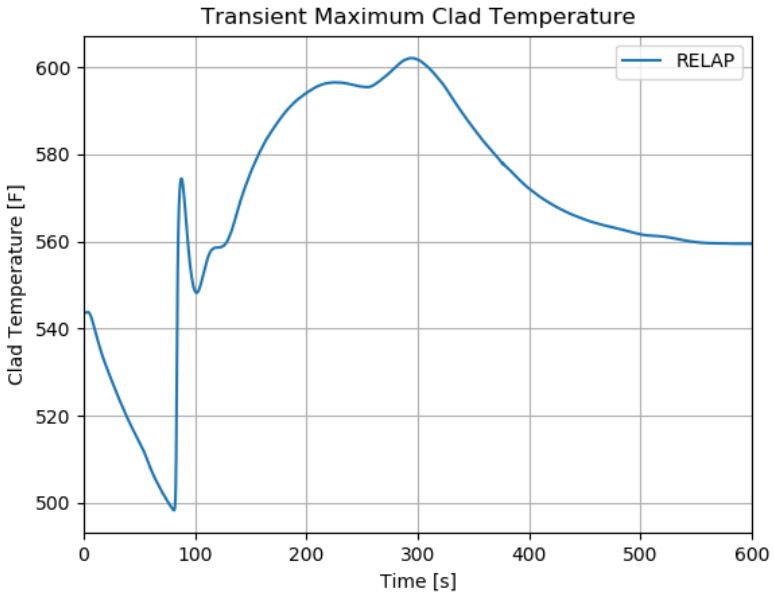

(A)

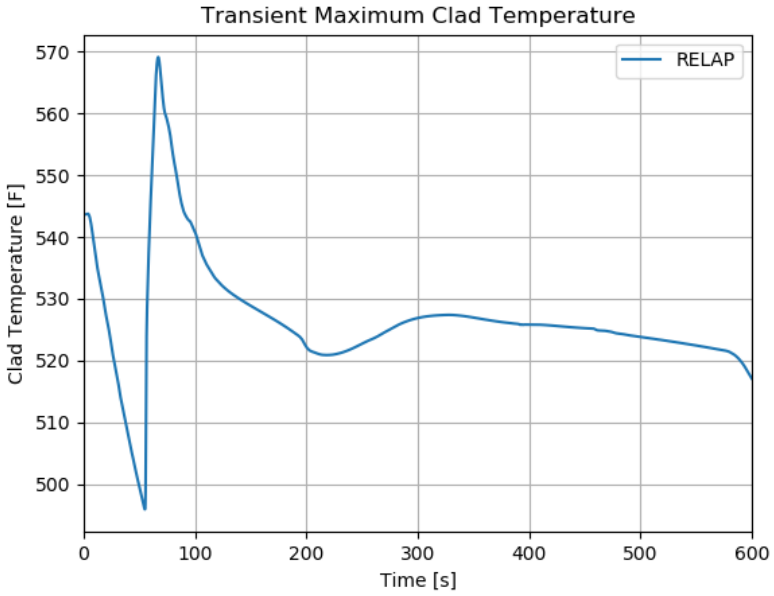

(B)

Figure 16 – Transient Maximum Clad Temperature for the MSLB Scenario (HZP, both LOOP and OPA)

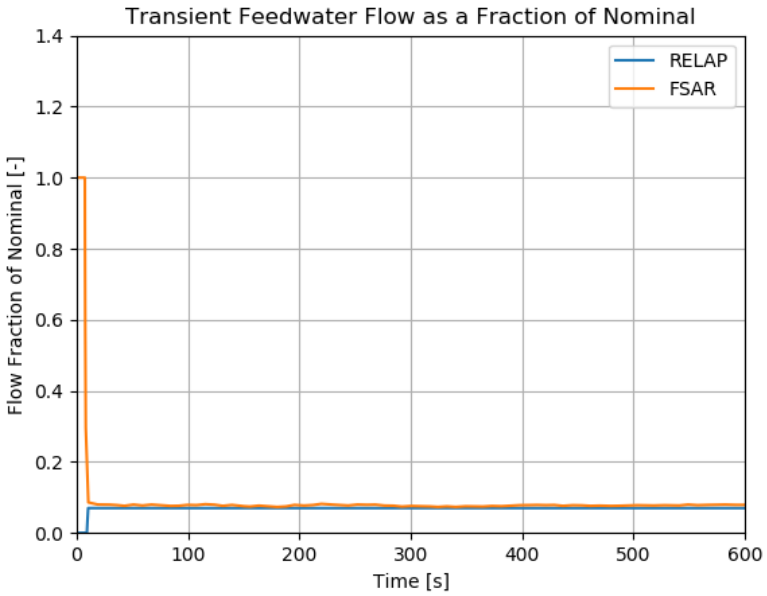

(A)

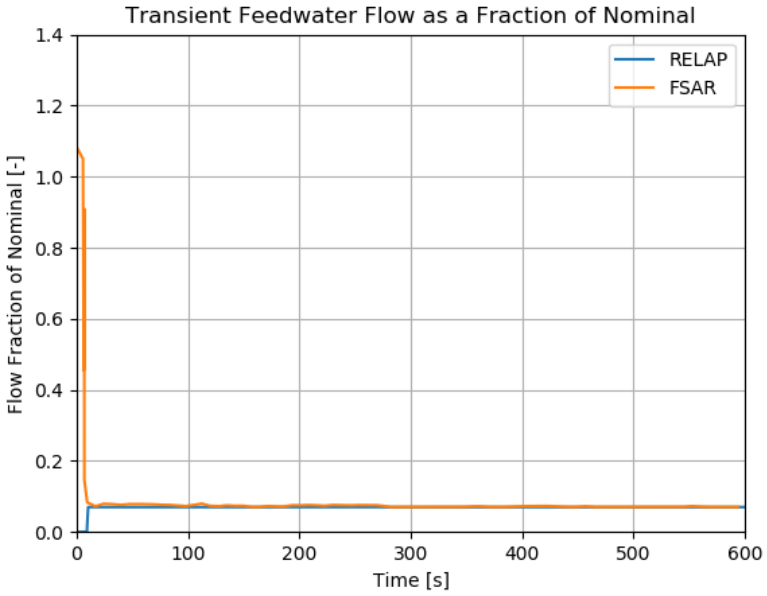

(B)

Figure 17 – Transient Feedwater Flow for the MSLB Scenario (HZP, both LOOP and OPA)

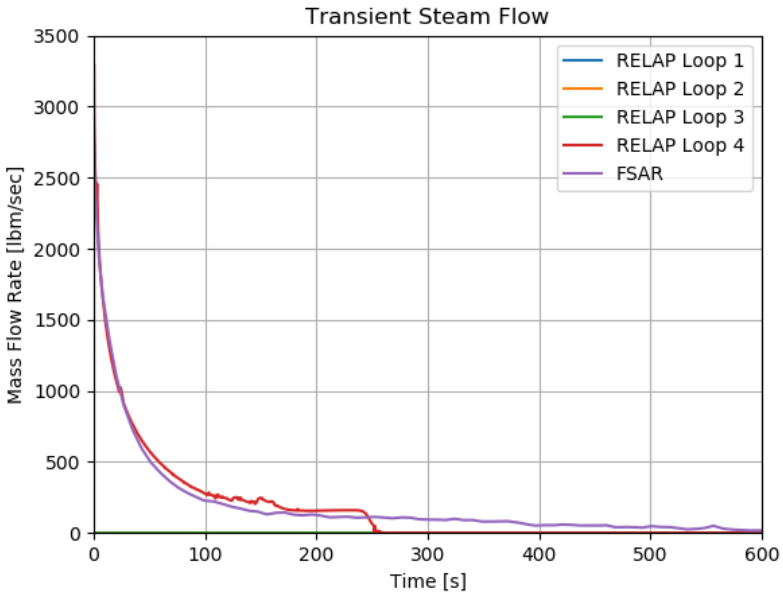

(A)

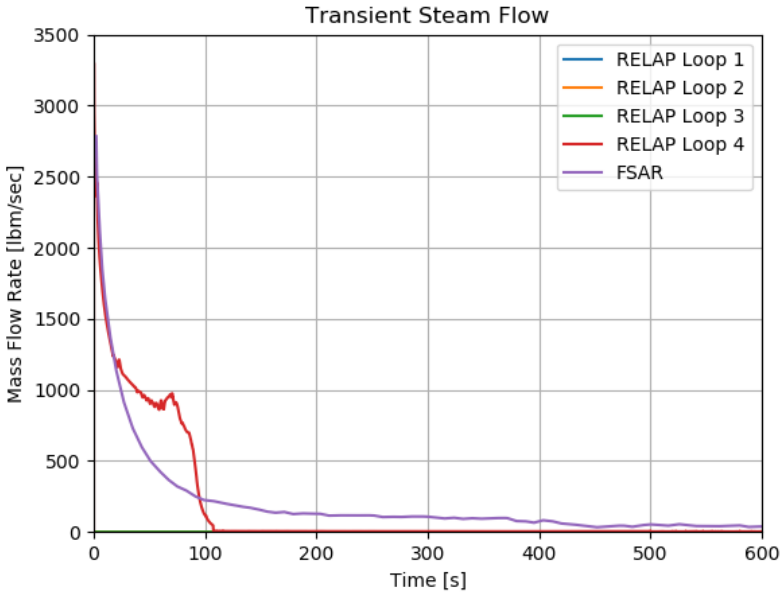

(B)

Figure 18 – Transient Steam Flow for the MSLB Scenario (HZP, both LOOP and OPA)

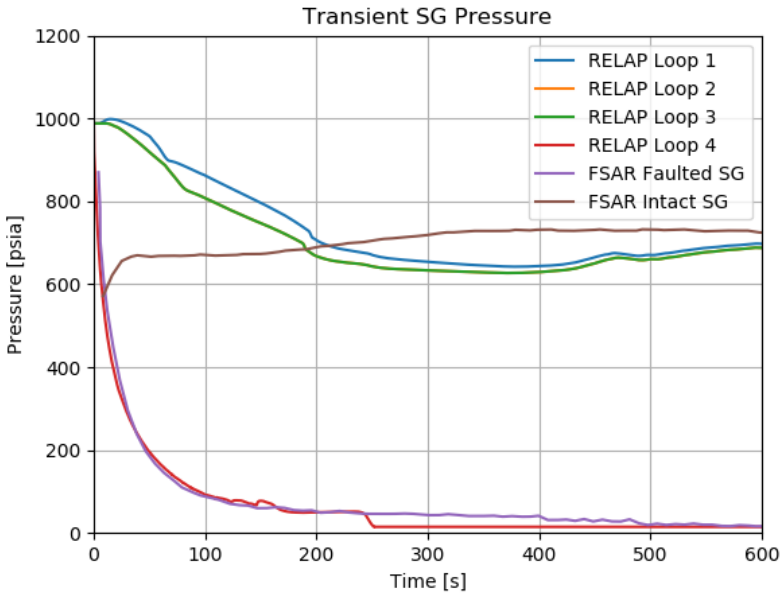

(A)

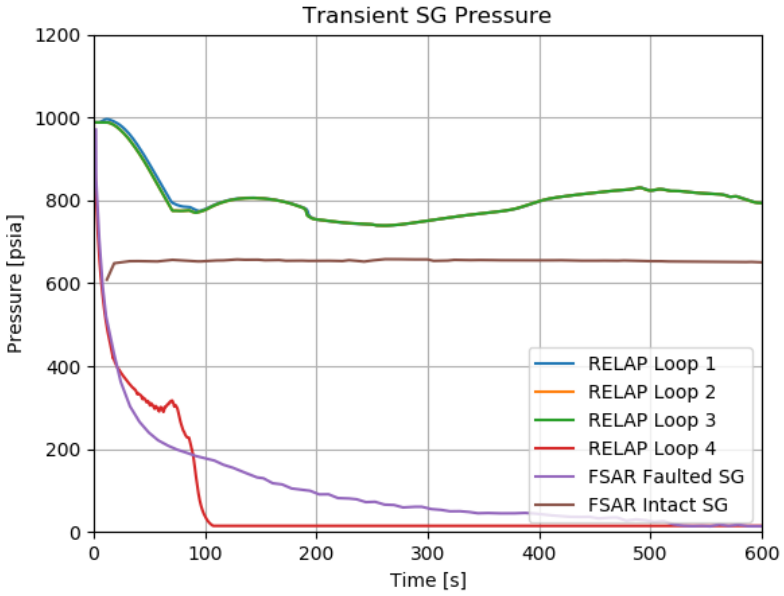

(B)

Figure 19 – Transient SG Pressure for the MSLB Scenario (HZP, both LOOP and OPA)

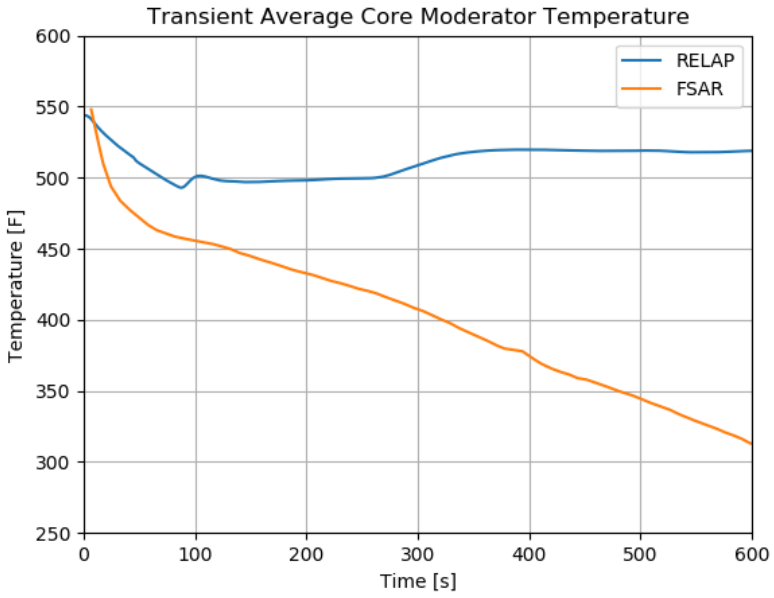

(A)

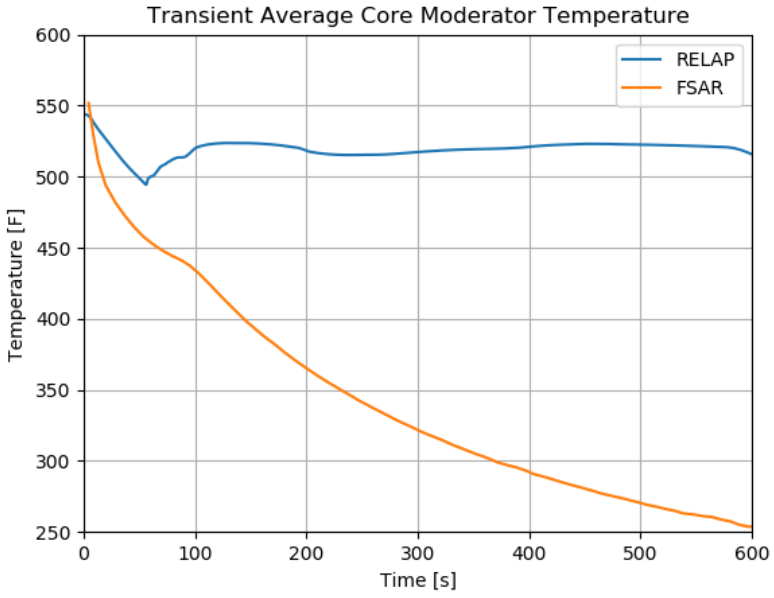

(B)

Figure 20 – Transient Core Average Temperature for the MSLB Scenario (HZP, both LOOP and OPA)

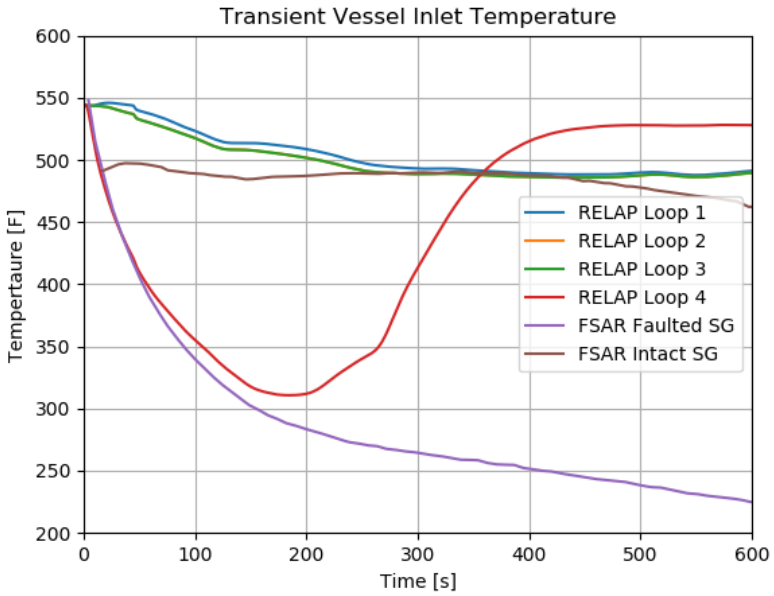

(A)

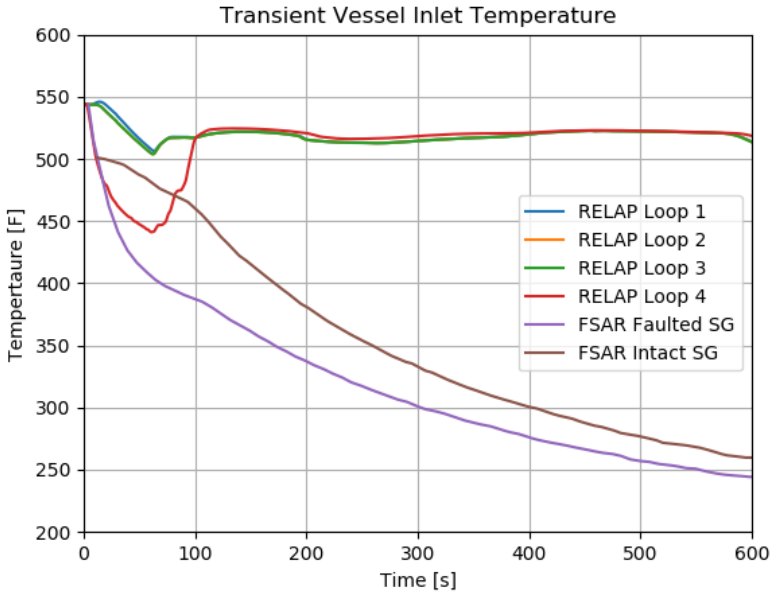

(B)

Figure 21 – Transient Vessel Inlet Temperature for the MSLB Scenario (HZP, both LOOP and OPA)

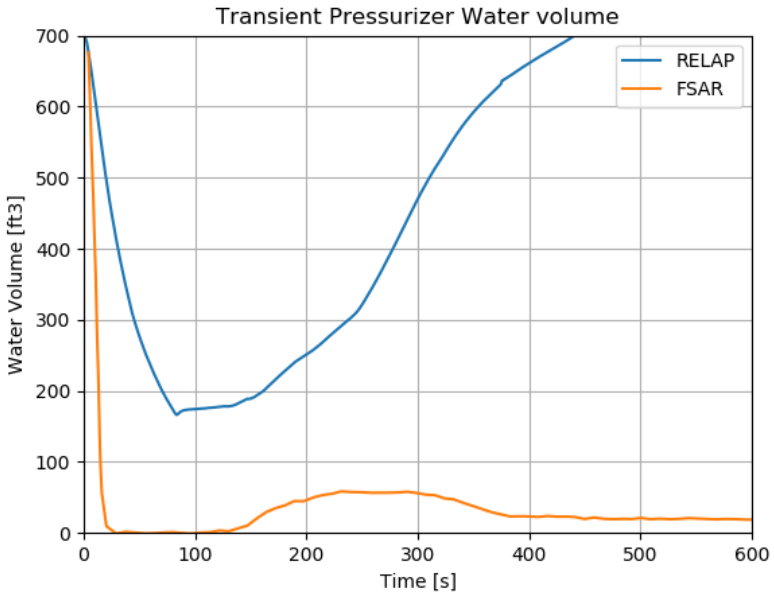

(A)

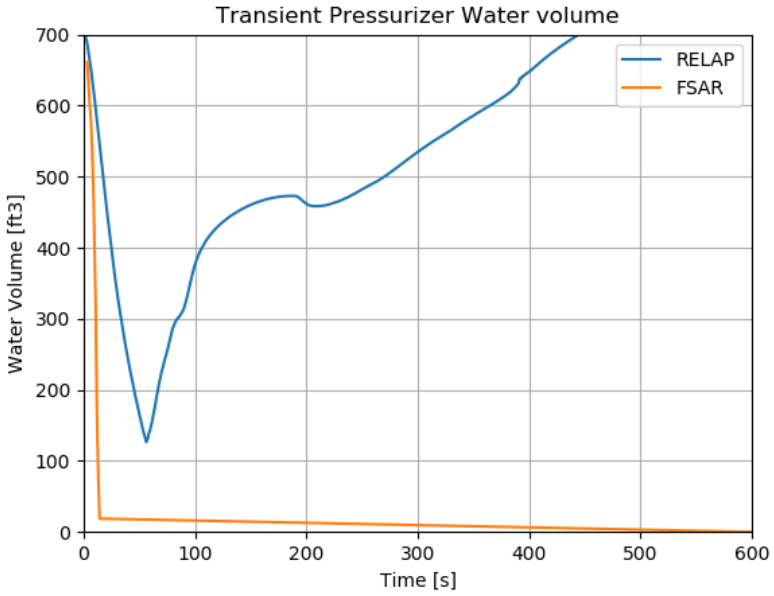

(B)

Figure 22 – Transient Pressurizer Water Volume for the MSLB Scenario (HZP, both LOOP and OPA)

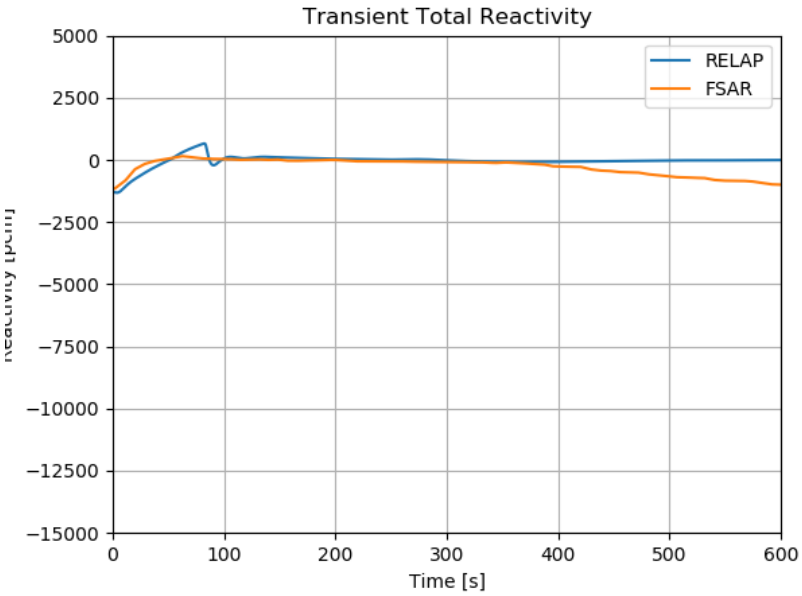

(A)

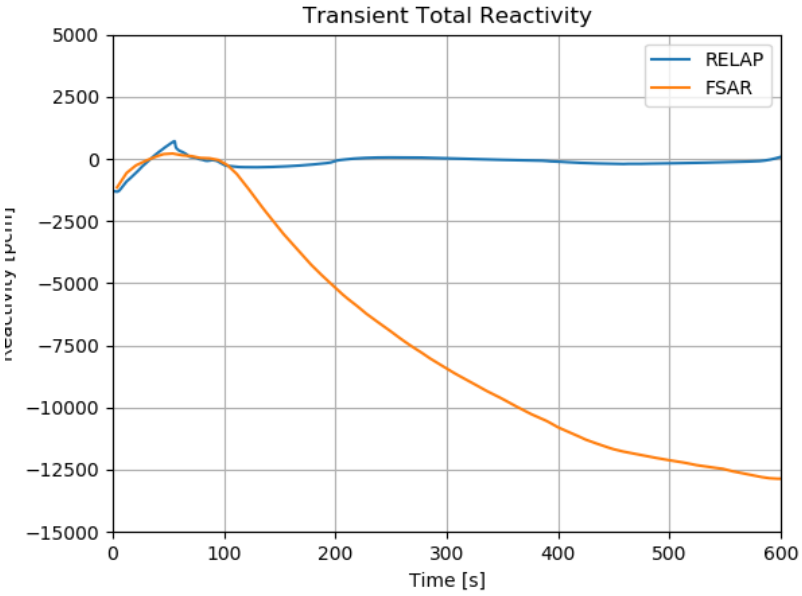

(B)

Figure 23 – Transient Reactivity for the MSLB Scenario (HZP, both LOOP and OPA)

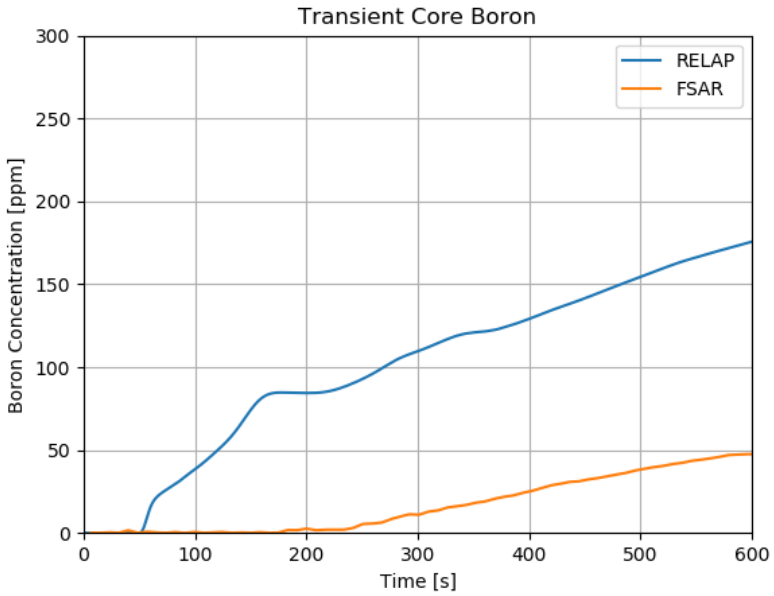

(A)

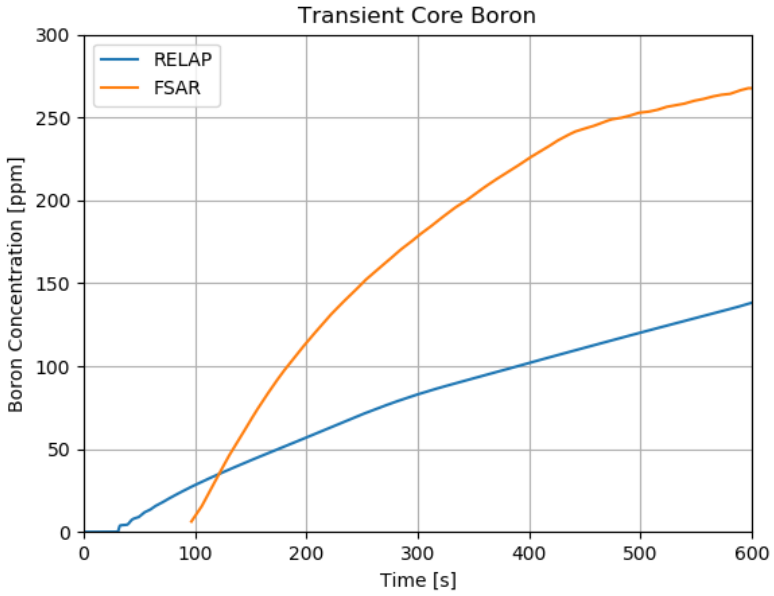

(B)

Figure 24 – Transient Core Boron Concentration for the MSLB Scenario (HZP, both LOOP and OPA)

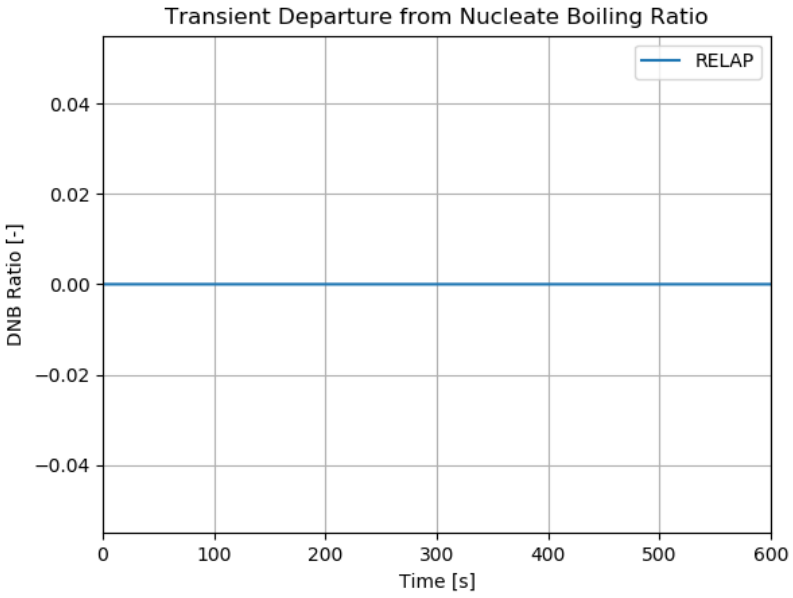

(A)

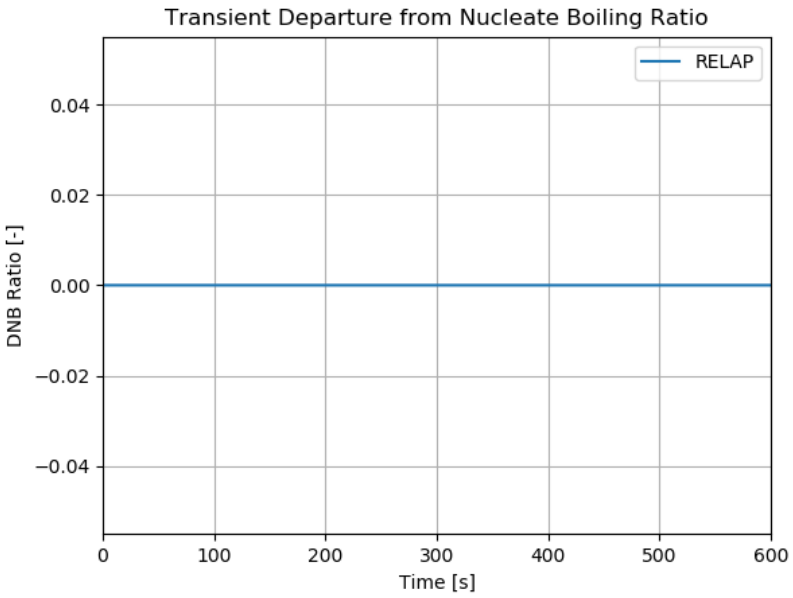

(B)

Figure 25 – Transient DNBR for the MSLB Scenario (HZP, both LOOP and OPA)

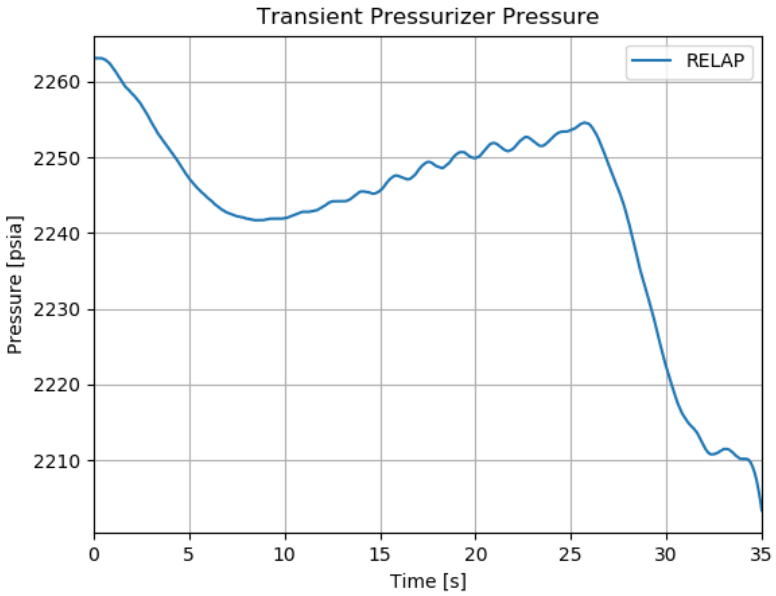

Figure 26 – Transient Pressurizer Pressure for the MSLB Scenario (HFP)

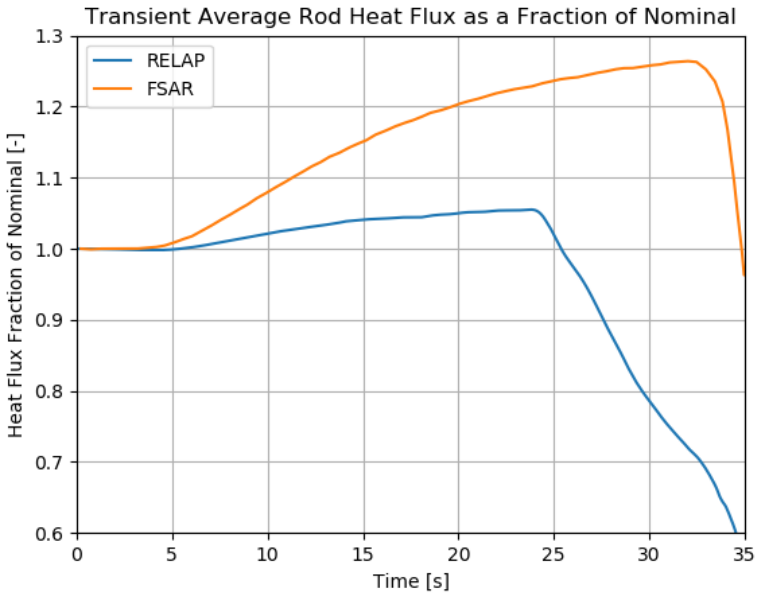

(B)

Figure 27 – Transient Average Rod Heat Flux for the MSLB Scenario (HFP)

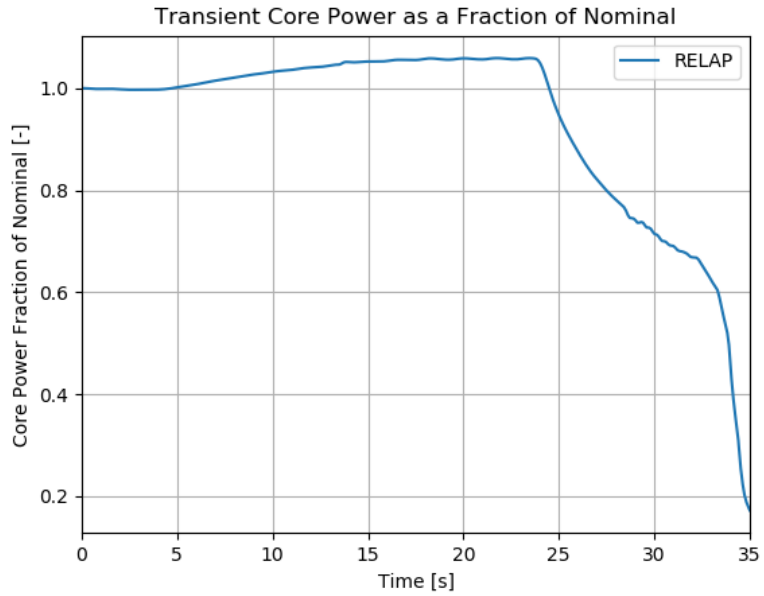

Figure 28 – Transient Core Power as a Fraction of Nominal for the MSLB Scenario (HFP)

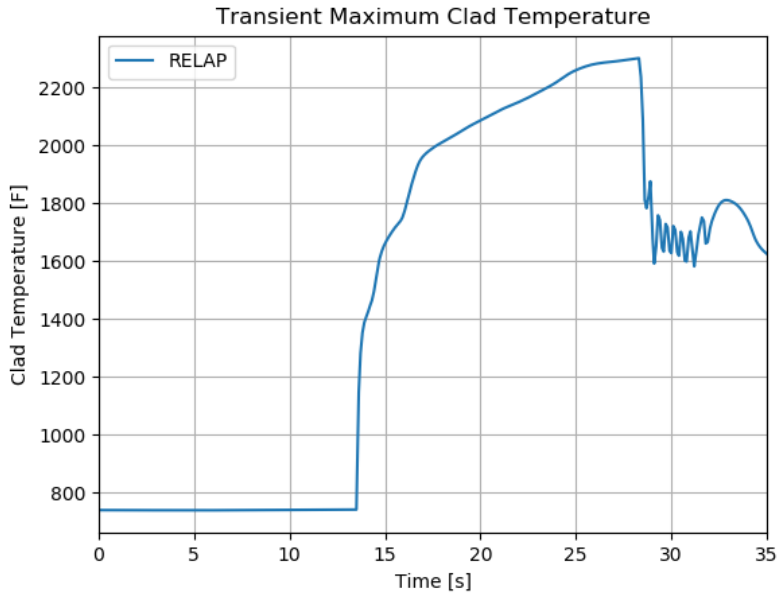

(B)

Figure 29 – Transient Maximum Clad Temperature for the MSLB Scenario (HFP)

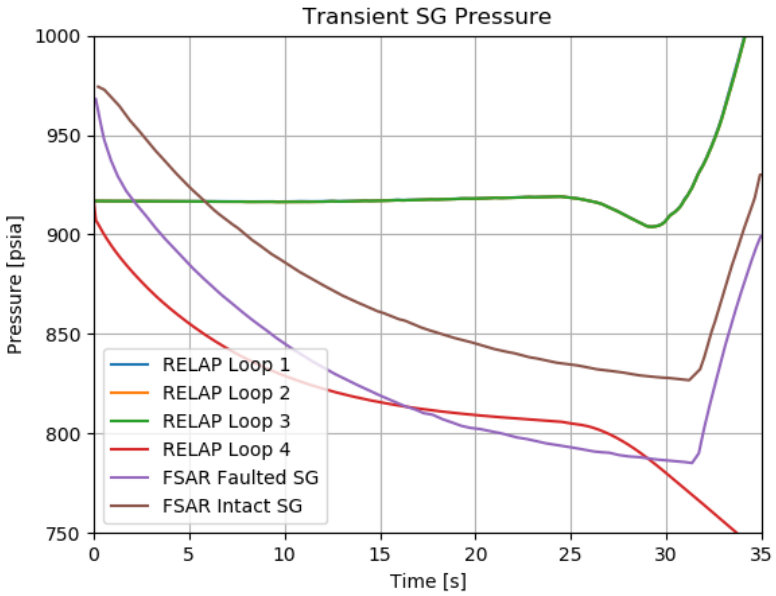

Figure 30 – Transient SG Pressure for the MSLB Scenario (HFP)

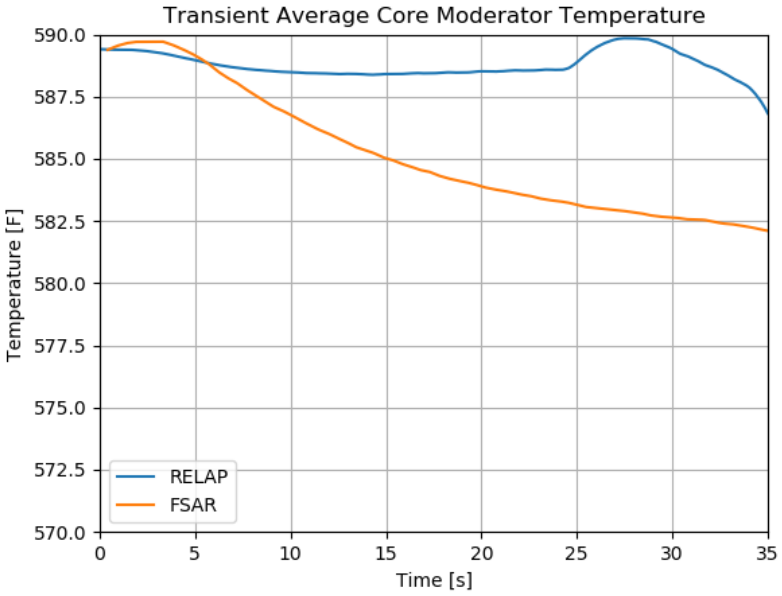

(B)

Figure 31 – Transient Average Core Temperature for the MSLB Scenario (HFP)

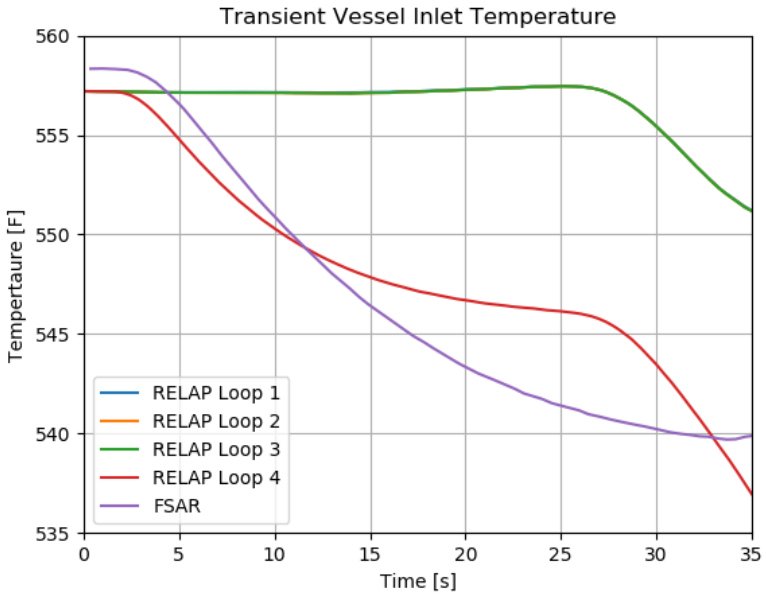

Figure 32 – Transient Vessel Inlet Temperature for the MSLB Scenario (HFP)

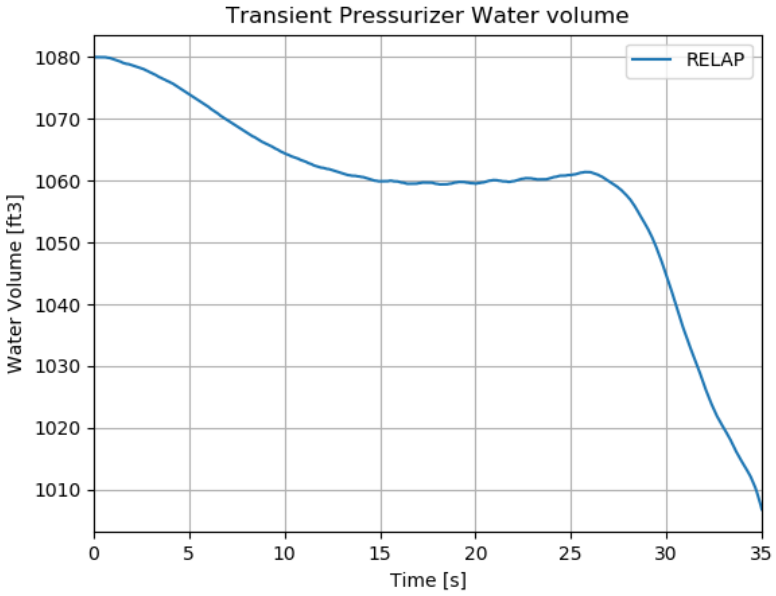

(B)

Figure 33 – Transient Pressurizer Water Volume for the MSLB Scenario (HFP)

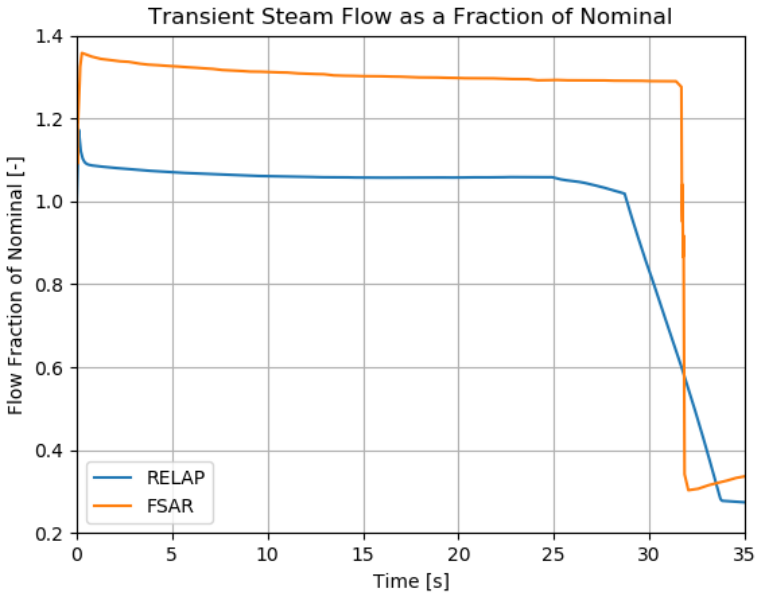

Figure 34 – Transient Steam Flow for the MSLB Scenario (HFP)

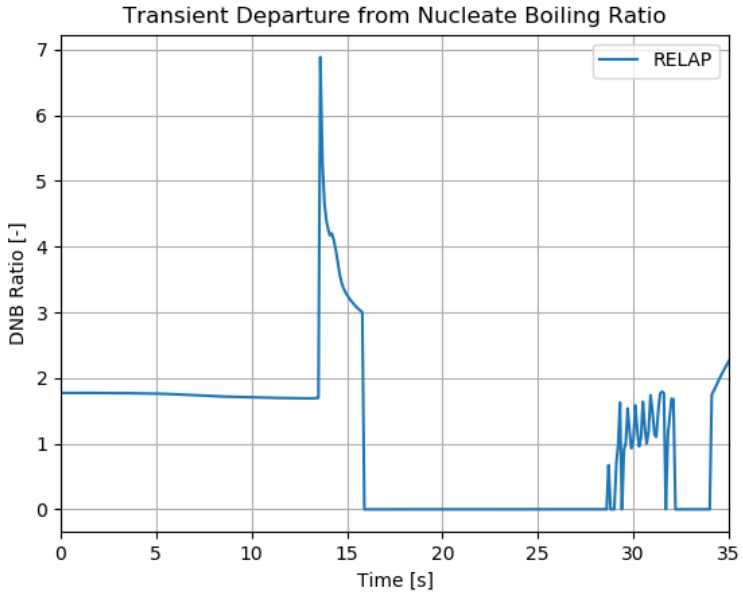

(B)

Figure 35 – Transient DNBR for the MSLB Scenario (HFP)

4.2.3 Turbine Trip

A turbine trip is classified as an American Nuclear Society Condition II event, fault of moderate frequency.

For a turbine trip event, the reactor trips directly (unless below a given power threshold) from a signal derived from the turbine stop signals. Upon initiation closure of the stop valve, steam flow

to the turbine abruptly ceases. Sensors on the stop valve detect the turbine trip and begin turbine bypass through steam dump valves and, if above the power threshold, a reactor trip. The loss of steam flow results in a nearly immediate rise in secondary system temperature and pressure with a resultant increase in primary system temperature and pressure.

The automatic turbine bypass system would accommodate up to 40 percent of rated steam flow. Reactor coolant temperatures and pressure do not increase significantly if the turbine bypass system and pressurizer pressure control system are functioning properly. If the condenser is not available, the excess steam generation is relieved to the atmosphere, and main feedwater flow is lost. For this situation, feedwater flow is maintained by the auxiliary feedwater system to ensure adequate decay heat removal capability.

The turbine trip scenario presents four cases in the FSAR:

1. Maximum moderator feedback without pressurizer spray and PORV.
2. Maximum moderator feedback with pressurizer spray and PORV.
3. Minimum moderator feedback without pressurizer spray and PORV.
4. Minimum moderator feedback with pressurizer spray and PORV.

4.2.3.1 Results

The RELAP results are compared to the turbine trip runs from the FSAR in the subsections below.

Maximum Moderator Feedback without Pressurizer Controls

The transient pressurizer pressure is shown in Figure 36. From Figure 36 the RELAP response is extremely similar to the FSAR run.

The transient core power as a fraction of the nominal power is shown in Figure 37. From Figure 37, RELAP predicts a slightly higher power excursion, and very similar behavior after scram to the FSAR run.

The transient clad temperature is shown in Figure 38. From Figure 38, there is a significant heatup around the time of the power excursion.

The transient oxidation at the hot rod peak power location is shown in Figure 39. From Figure 39, the oxidation increases coincident with the significant heatup from Figure 38, and then flattens out once the clad temperature drops back down.

The transient core average moderator temperature is shown in Figure 40. From Figure 40, the RELAP response is extremely similar to the FSAR run.

The transient vessel inlet temperature is shown in Figure 41. From Figure 41, the RELAP response is extremely similar to the FSAR run.

The transient pressurizer water volume is shown in Figure 42. From Figure 42, the RELAP response is similar to the FSAR run, but has more exaggerated changes.

The transient DNBR is shown in Figure 43. From Figure 43, the RELAP response is very different from the FSAR run, though they indicate a similar trend. The RELAP run shows an increasing DNBR which suddenly drops to 0. In RELAP, this can indicate that the heat structure is in a HT

mode which does not even calculate CHF (i.e., single phase liquid). This is thus interpreted as a very high DNBR value. The FSAR shows a consistent increase in DNBR.

Maximum Moderator Feedback with Pressurizer Controls

The transient pressurizer pressure is shown in Figure 44. From Figure 44, the RELAP response shows a similar trend to the FSAR run, but the initial pressurization is much higher. This indicates that the modeled spray flow and PORV flow may be inadequate.

The transient core power as a fraction of the nominal power is shown in Figure 45. From Figure 45, RELAP predicts a slightly higher initial power excursion, and very similar behavior after scram to the FSAR run. The power plateau between ~10-40 seconds is a bit lower for RELAP, but still fairly close.

The transient clad temperature is shown in Figure 46. From Figure 46, there is a significant heatup around the time of the power excursion.

The transient oxidation at the hot rod peak power location is shown in Figure 47. From Figure 47, the oxidation increases coincident with the significant heatup from Figure 46, and then flattens out once the clad temperature drops back down.

The transient core average moderator temperature is shown in Figure 48. From Figure 48, the RELAP response is similar to the FSAR run. There is a major difference that RELAP is lower during the period when the power plateau is lower, which is consistent.

The transient vessel inlet temperature is shown in Figure 49. From Figure 49, the RELAP response is similar to the FSAR run. There is a major difference that RELAP is lower during the period when the power plateau is lower, which is consistent.

The transient pressurizer water volume is shown in Figure 50. From Figure 50, the RELAP response is similar to the FSAR run for the first 20 seconds, but is then fairly significantly lower for the remainder of the transient.

The transient DNBR is shown in Figure 51. From Figure 51, the RELAP response is very different from the FSAR run, though they indicate a similar trend. The RELAP run shows an increasing DNBR which suddenly drops to 0. In RELAP, this can indicate that the heat structure is in a HT mode which does not even calculate CHF (i.e., single phase liquid). This is thus interpreted as a very high DNBR value. The FSAR shows a consistent increase in DNBR.

Minimum Moderator Feedback without Pressurizer Controls

The transient pressurizer pressure is shown in Figure 52. From Figure 52, the RELAP response is extremely similar to the FSAR run.

The transient core power as a fraction of the nominal power is shown in Figure 53. From Figure 53, RELAP predicts a slightly higher power excursion, and very similar behavior after scram to the FSAR run.

The transient clad temperature is shown in Figure 54. From Figure 54, there is a significant heatup around the time of the power excursion.

The transient oxidation at the hot rod peak power location is shown in Figure 55. From Figure 55, the oxidation increases coincident with the significant heatup from Figure 54, and then flattens out once the clad temperature drops back down.

The transient core average moderator temperature is shown in Figure 56. From Figure 56, the RELAP response is extremely similar to the FSAR run.

The transient vessel inlet temperature is shown in Figure 57. From Figure 57, the RELAP response is extremely similar to the FSAR run.

The transient pressurizer water volume is shown in Figure 58. From Figure 58, the RELAP response is similar to the FSAR run, but is drops more quickly after reactor trip, although the converge on a similar value by the end of the transient.

The transient DNBR is shown in Figure 59. From Figure 59, the RELAP response is very different from the FSAR run, though they indicate a similar trend. The RELAP run shows an increasing DNBR which suddenly drops to 0. In RELAP, this can indicate that the heat structure is in a HT mode which does not even calculate CHF (i.e., single phase liquid). This is thus interpreted as a very high DNBR value. The FSAR shows a consistent increase in DNBR.

Minimum Moderator Feedback with Pressurizer Controls

The transient pressurizer pressure is shown in Figure 60. From Figure 60, the RELAP response shows a similar trend to the FSAR run, but the initial pressurization is much higher. This indicates that the modeled spray flow and PORV flow may be inadequate.

The transient core power as a fraction of the nominal power is shown in Figure 61. From Figure 61, RELAP predicts a large initial power excursion, and very similar behavior after scram to the FSAR run.

The transient clad temperature is shown in Figure 62. From Figure 62, there is a significant heatup around the time of the power excursion.

The transient oxidation at the hot rod peak power location is shown in Figure 63. From Figure 63, the oxidation increases coincident with the significant heatup from Figure 62, and then flattens out once the clad temperature drops back down.

The transient core average moderator temperature is shown in Figure 64. From Figure 64, the RELAP response is very similar to the FSAR run.

The transient vessel inlet temperature is shown in Figure 65. From Figure 65, the RELAP response is similar to the FSAR run.

The transient pressurizer water volume is shown in Figure 66. From Figure 66, the RELAP response is similar to the FSAR run, but it both increases and decreases much faster.

The transient DNBR is shown in Figure 67. From Figure 67, the RELAP response is very different from the FSAR run, though they indicate a somewhat similar trend. Initially, the RELAP run shows an increase in DNBR, which then rapidly drops around the power excursion. When the RELAP run goes to zero at this point, this is interpreted to mean that DNB occurs. The FSAR run shows a slight decrease in DNBR at this time. After the power excursion, the RELAP run shows an increasing DNBR which suddenly drops to 0. In RELAP, this can indicate that the heat structure is in a HT mode which does not even calculate CHF (i.e., single phase liquid). This is thus interpreted as a very high DNBR value. The FSAR shows a consistent increase in DNBR.

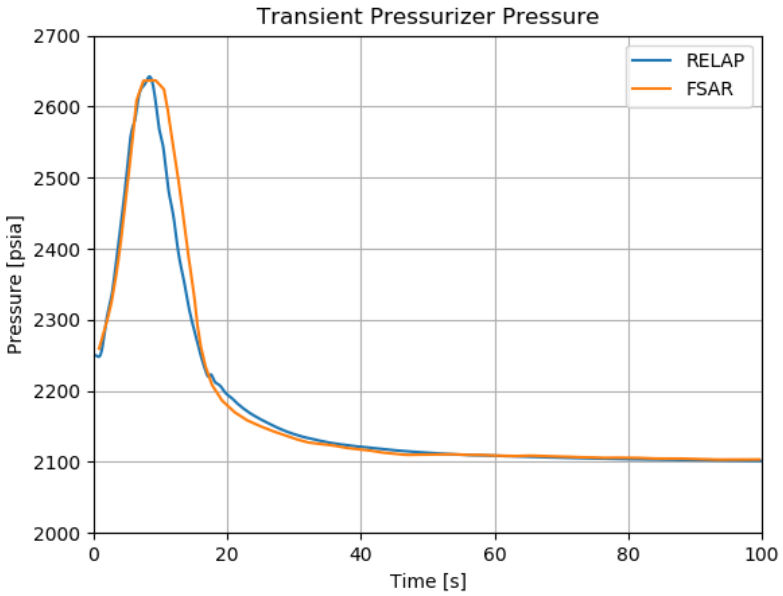

Figure 36 - Transient Pressurizer Pressure for the Turbine Trip Scenario (Max Moderator Feedback without Pressurizer Controls)

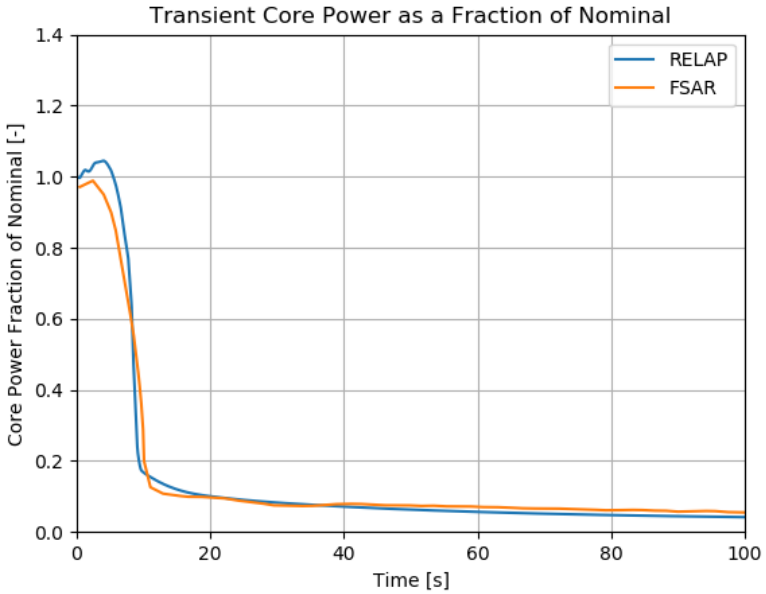

(B)

Figure 37 - Transient Core Power as a Fraction of the Nominal Power for the Turbine Trip Scenario (Maximum Moderator Feedback without Pressurizer Controls)

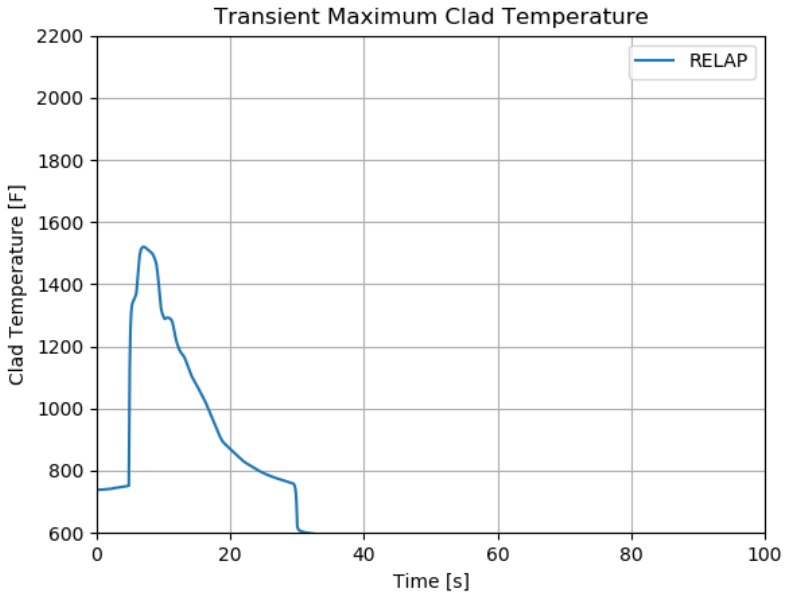

Figure 38 - Transient Maximum Clad Temperature for the Turbine Trip Scenario (Maximum Moderator Feedback without Pressurizer Controls)

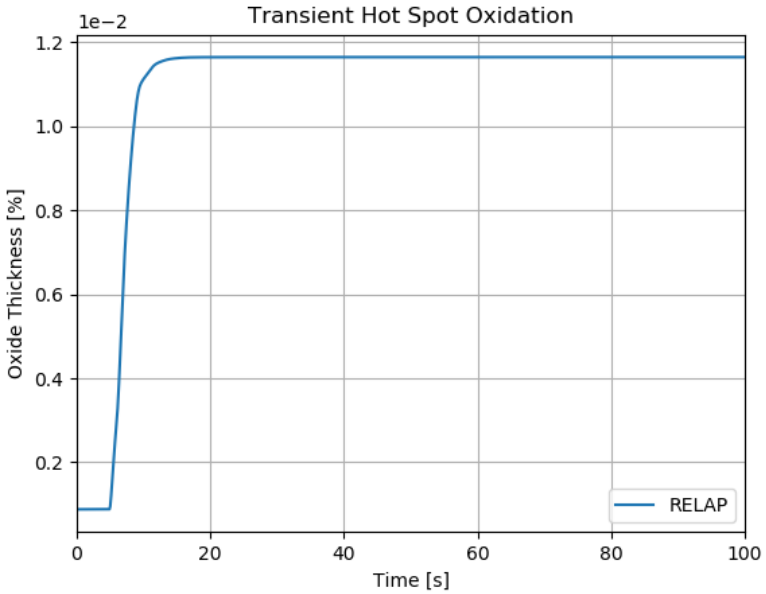

Figure 39 - Transient Oxidation at the Hot Rod Peak Power Location for the Turbine Trip Scenario (Maximum Moderator Feedback without Pressurizer Controls)

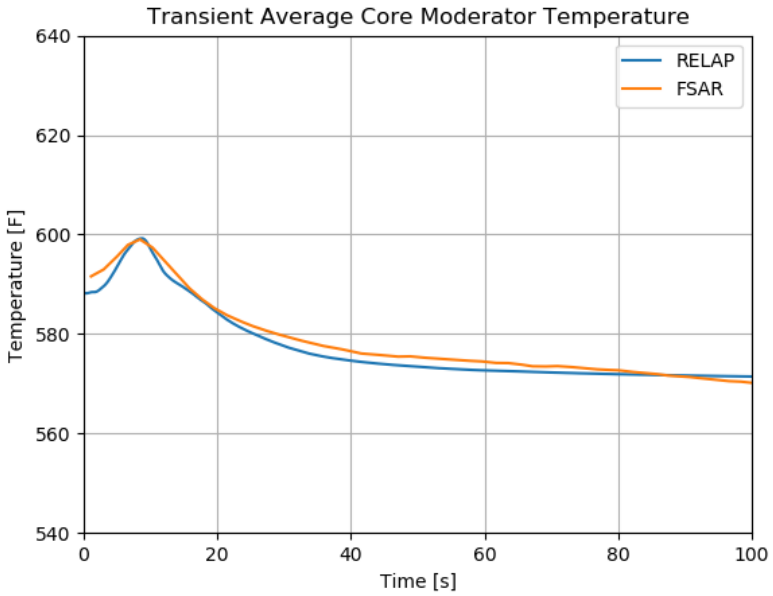

Figure 40 - Transient Core Average Moderator Temperature for the Turbine Trip Scenario (Maximum Moderator Feedback without Pressurizer Controls)

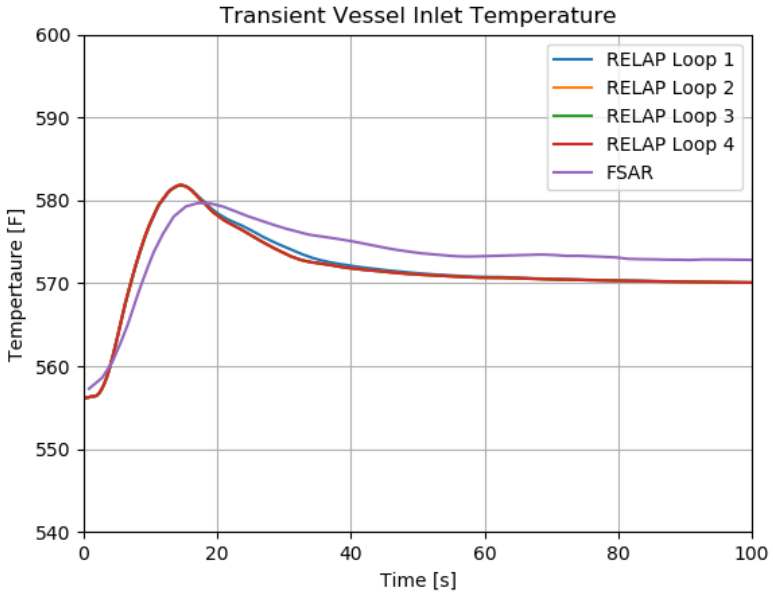

(B)

Figure 41 - Transient Vessel Inlet Temperature for the Turbine Trip Scenario (Maximum Moderator Feedback without Pressurizer Controls)

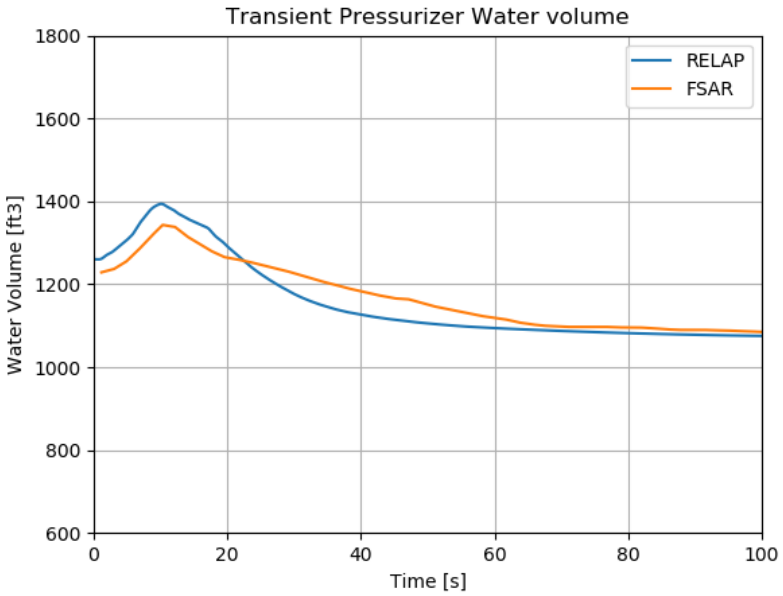

Figure 42 - Transient Pressurizer Water Volume for the Turbine Trip Scenario (Maximum Moderator Feedback without Pressurizer Controls)

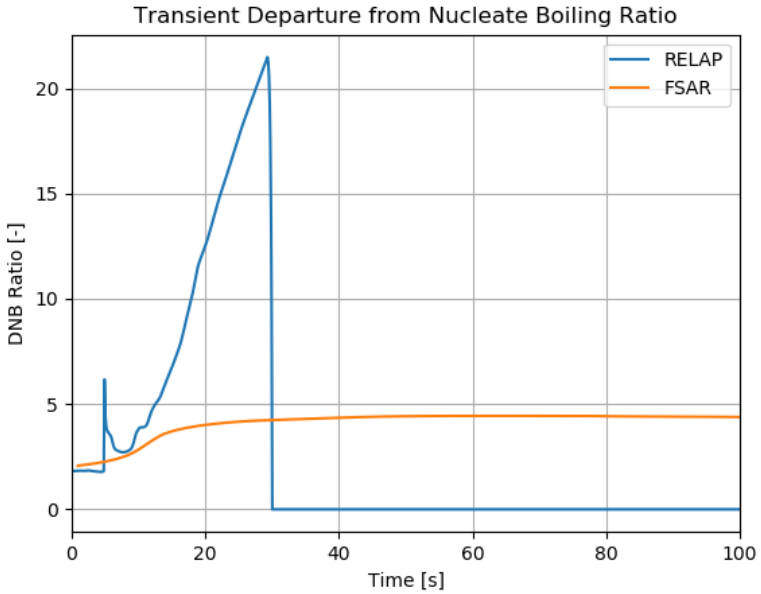

Figure 43 - Transient DNBR for the Turbine Trip Scenario (Maximum Moderator Feedback without Pressurizer Controls)

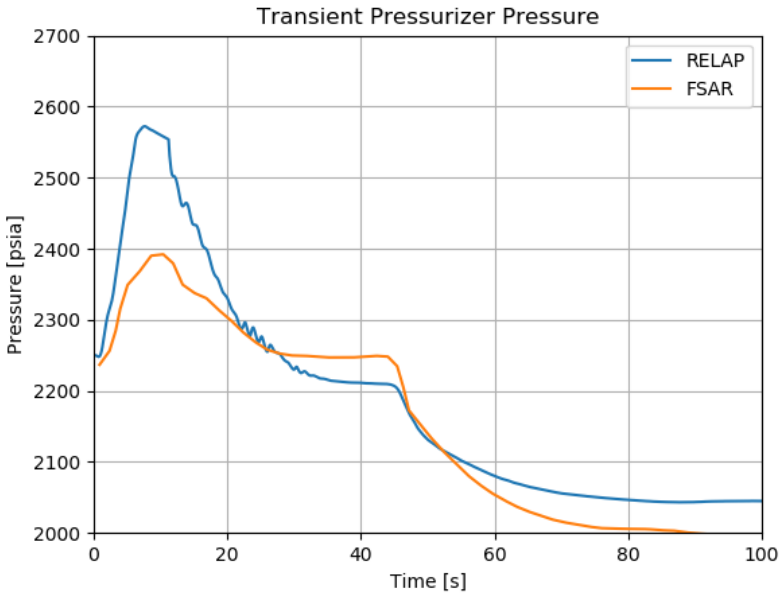

Figure 44 - Transient Pressurizer Pressure for the Turbine Trip Scenario (Maximum Moderator Feedback with Pressurizer Controls)

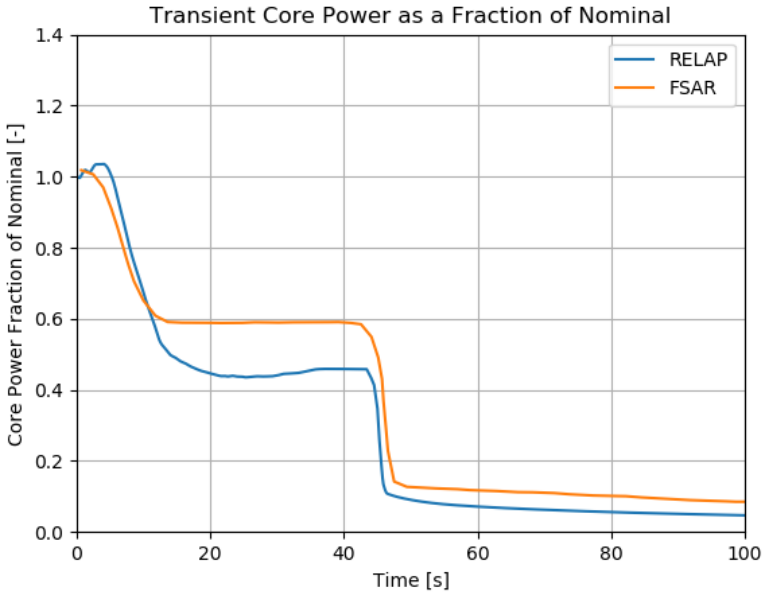

Figure 45 - Transient Core Power as a Fraction of the Nominal Power for the Turbine Trip Scenario (Maximum Moderator Feedback with Pressurizer Controls)

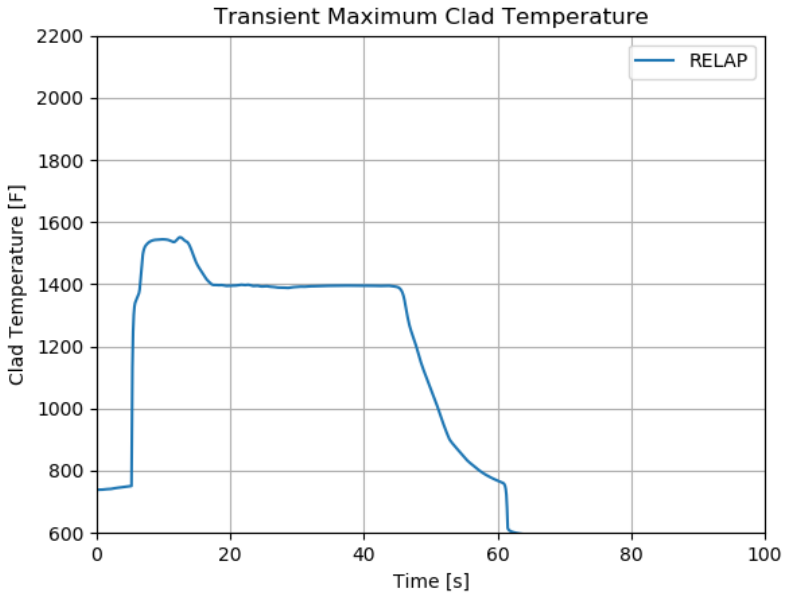

Figure 46 - Transient Maximum Clad Temperature for the Turbine Trip Scenario (Maximum Moderator Feedback with Pressurizer Controls)

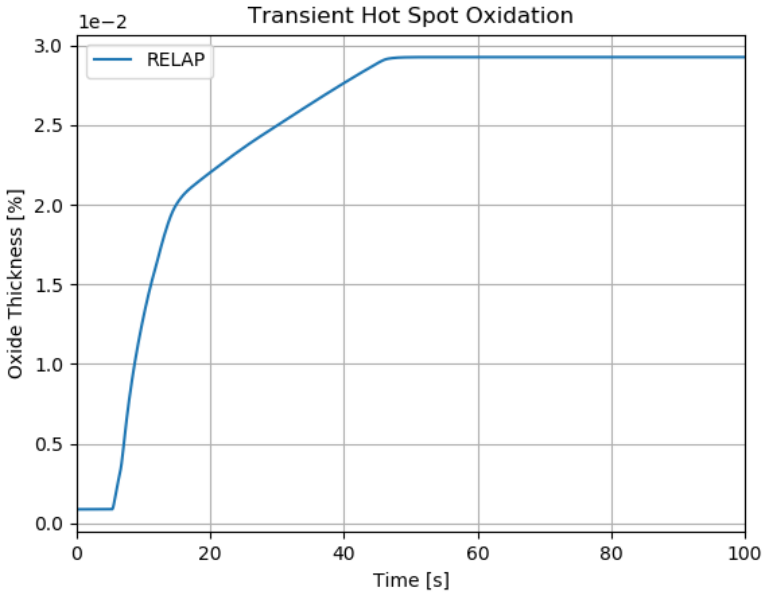

Figure 47 - Transient Oxidation at the Hot Rod Peak Power Location for the Turbine Trip Scenario (Maximum Moderator Feedback with Pressurizer Controls)

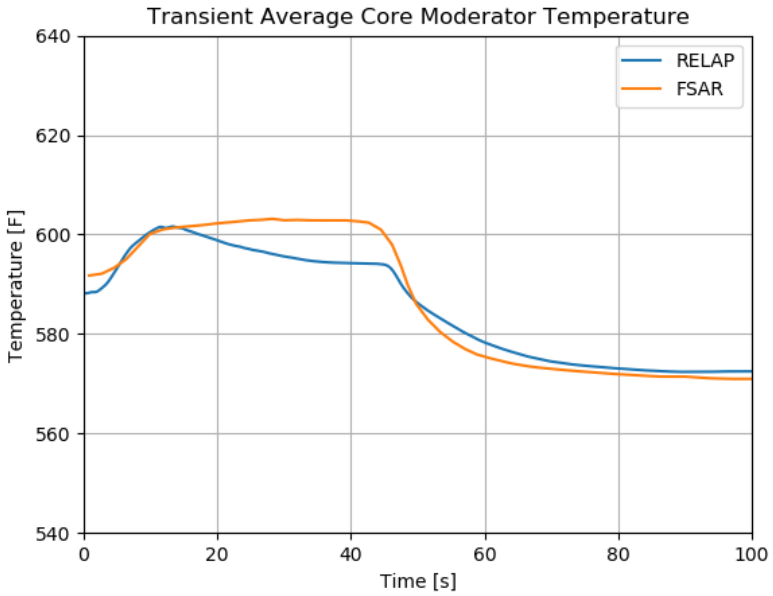

Figure 48 - Transient Core Average Moderator Temperature for the Turbine Trip Scenario (Maximum Moderator Feedback with Pressurizer Controls)

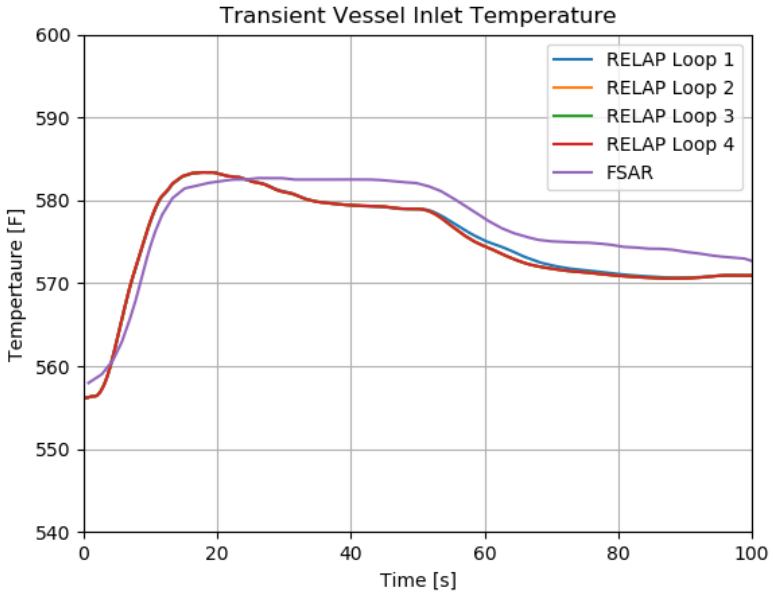

Figure 49 - Transient Vessel Inlet Temperature for the Turbine Trip Scenario (Maximum Moderator Feedback with Pressurizer Controls)

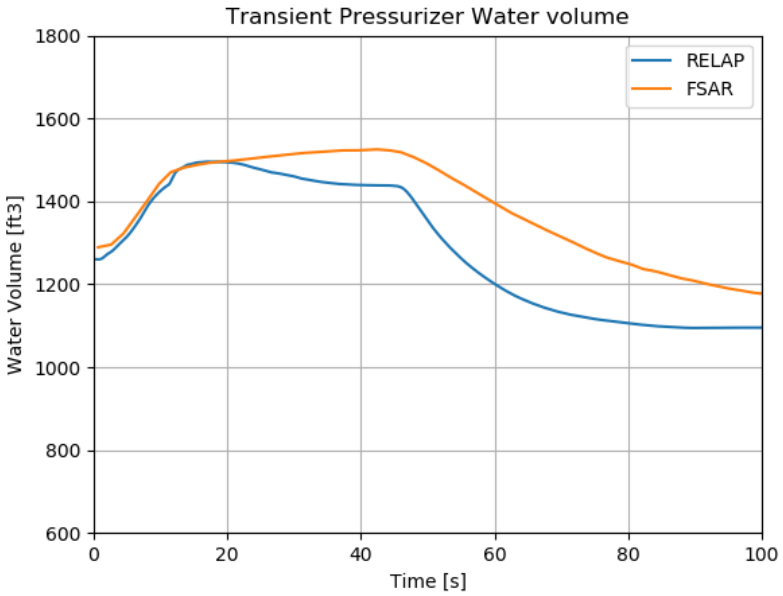

Figure 50 - Transient Pressurizer Water Volume for the Turbine Trip Scenario (Maximum Moderator Feedback with Pressurizer Controls)

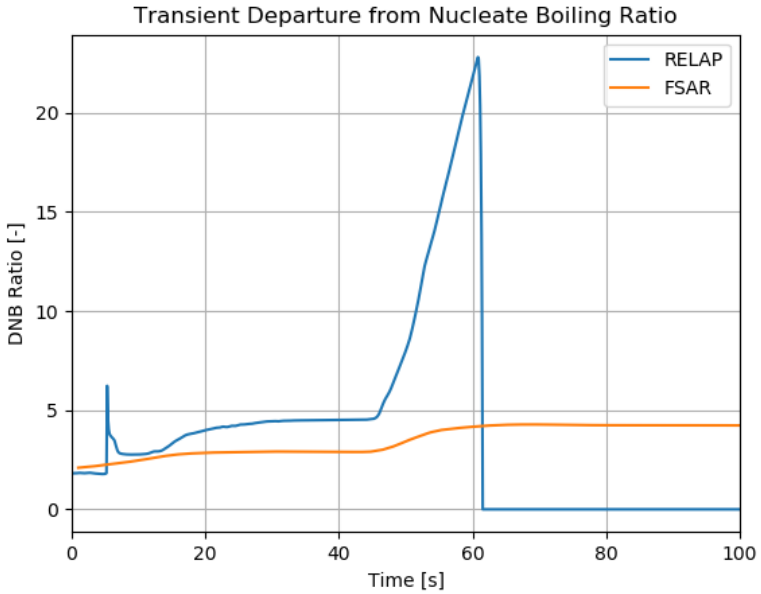

Figure 51 - Transient DNBR for the Turbine Trip Scenario (Maximum Moderator Feedback with Pressurizer Controls)

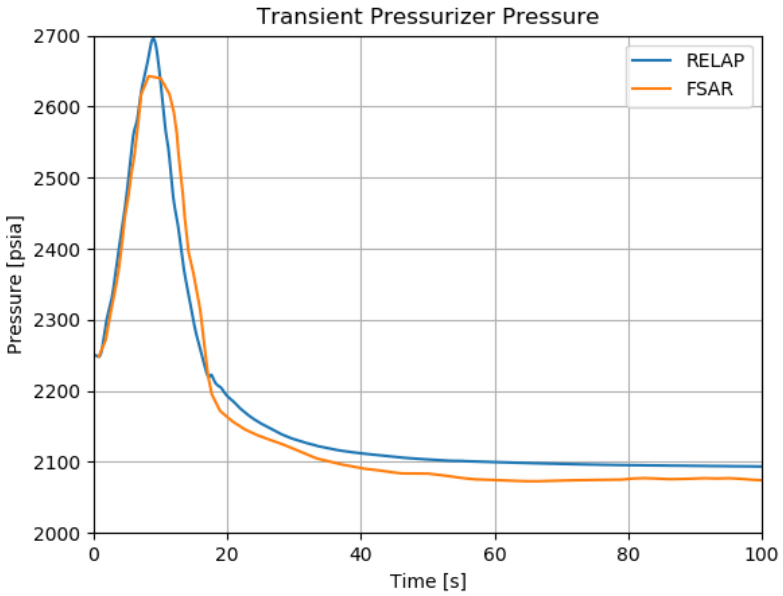

Figure 52 - Transient Pressurizer Pressure for the Turbine Trip Scenario (Minimum Moderator Feedback without Pressurizer Controls)

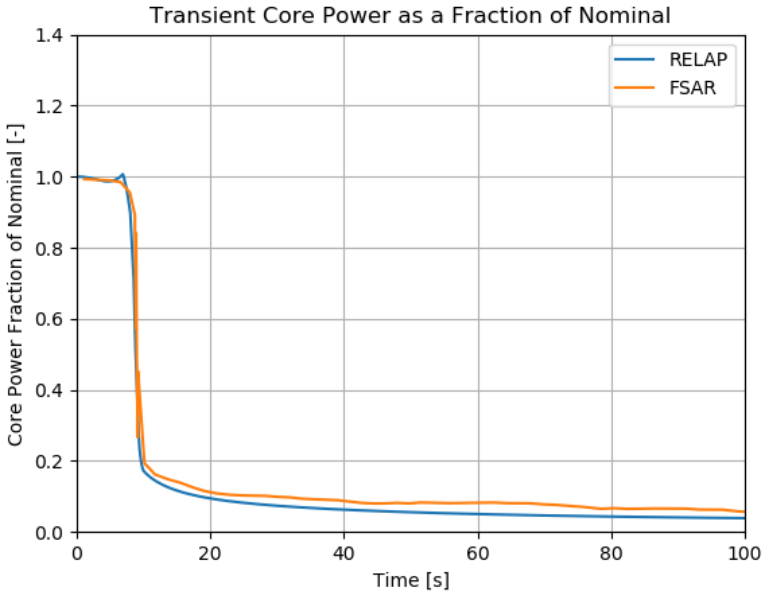

Figure 53 - Transient Core Power as a Fraction of the Nominal Power for the Turbine Trip Scenario (Minimum Moderator Feedback without Pressurizer Controls)

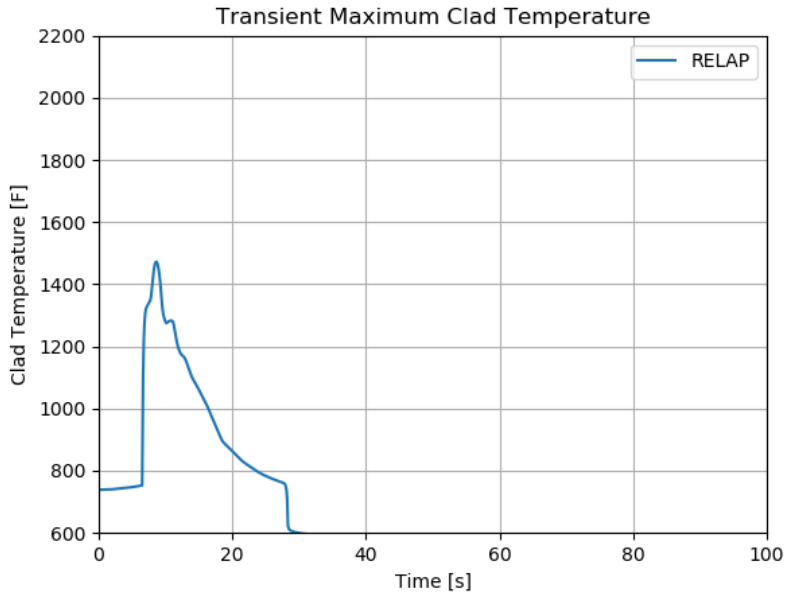

Figure 54 - Transient Maximum Clad Temperature for the Turbine Trip Scenario (Minimum Moderator Feedback without Pressurizer Controls)

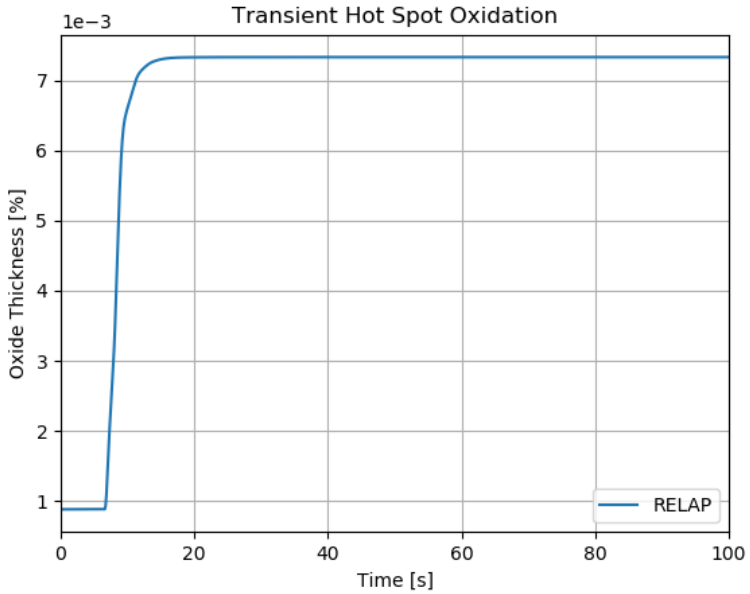

Figure 55 - Transient Oxidation at the Hot Rod Peak Power Location for the Turbine Trip Scenario (Minimum Moderator Feedback without Pressurizer Controls)

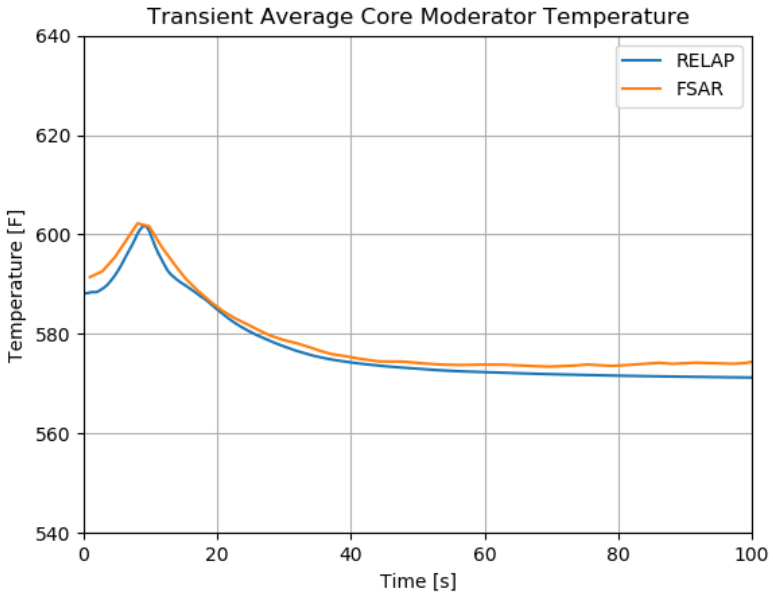

Figure 56 - Transient Core Average Moderator Temperature for the Turbine Trip Scenario (Minimum Moderator Feedback without Pressurizer Controls)

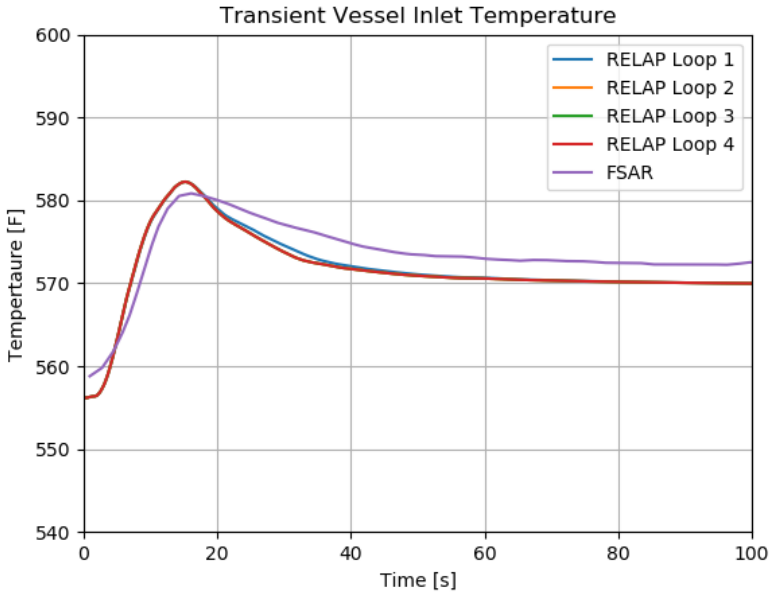

Figure 57 - Transient Vessel Inlet Temperature for the Turbine Trip Scenario (Minimum Moderator Feedback without Pressurizer Controls)

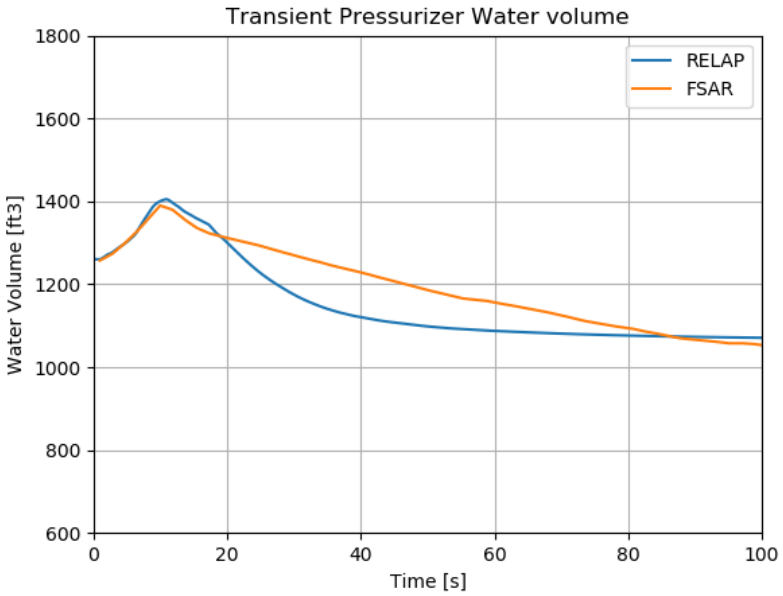

Figure 58 - Transient Pressurizer Water Volume for the Turbine Trip Scenario (Minimum Moderator Feedback without Pressurizer Controls)

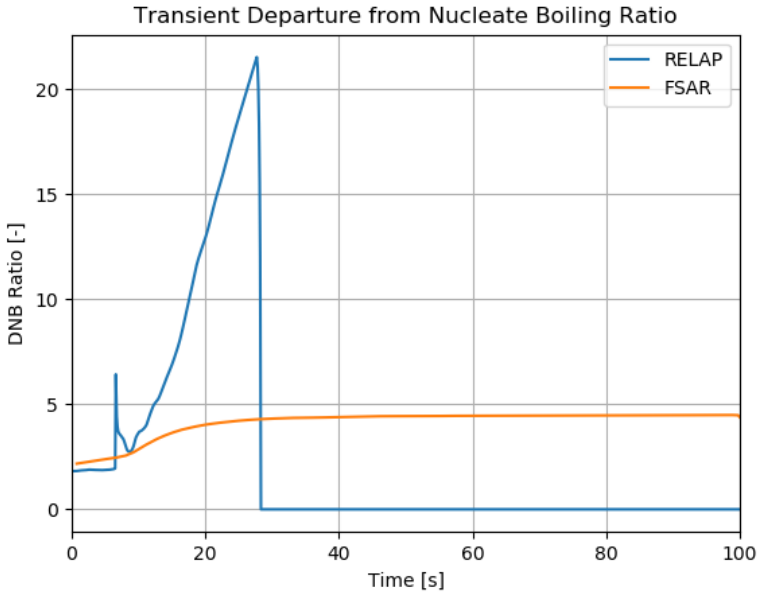

Figure 59 - Transient DNBR for the Turbine Trip Scenario (Minimum Moderator Feedback without Pressurizer Controls)

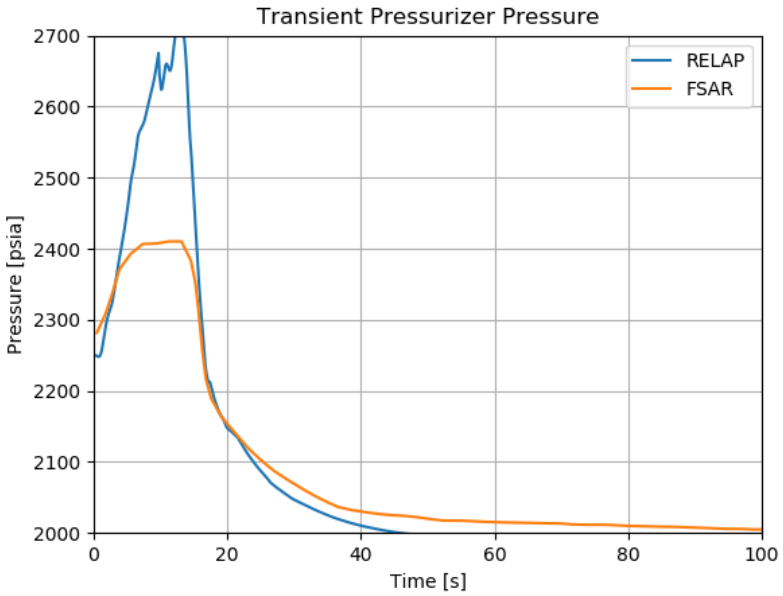

Figure 60 - Transient Pressurizer Pressure for the Turbine Trip Scenario (Minimum Moderator Feedback with Pressurizer Controls)

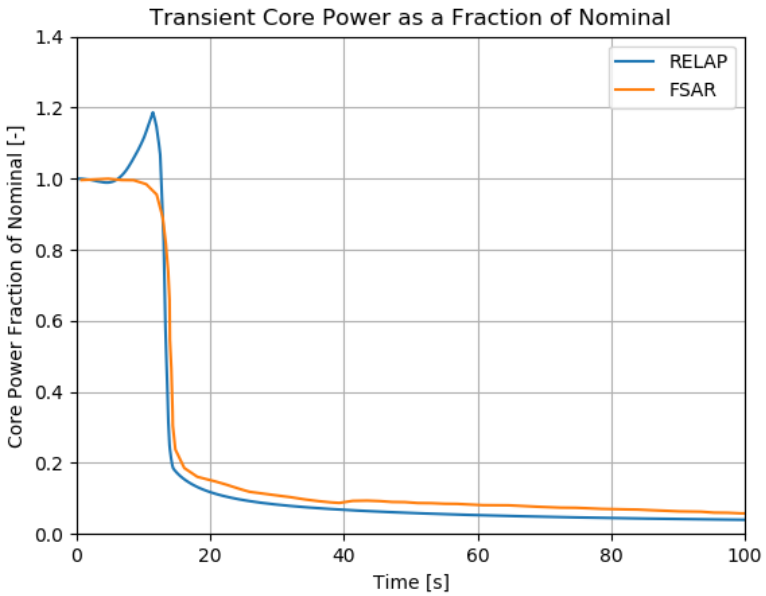

(B)

Figure 61 - Transient Core Power as a Fraction of the Nominal Power for the Turbine Trip Scenario (Minimum Moderator Feedback with Pressurizer Controls)

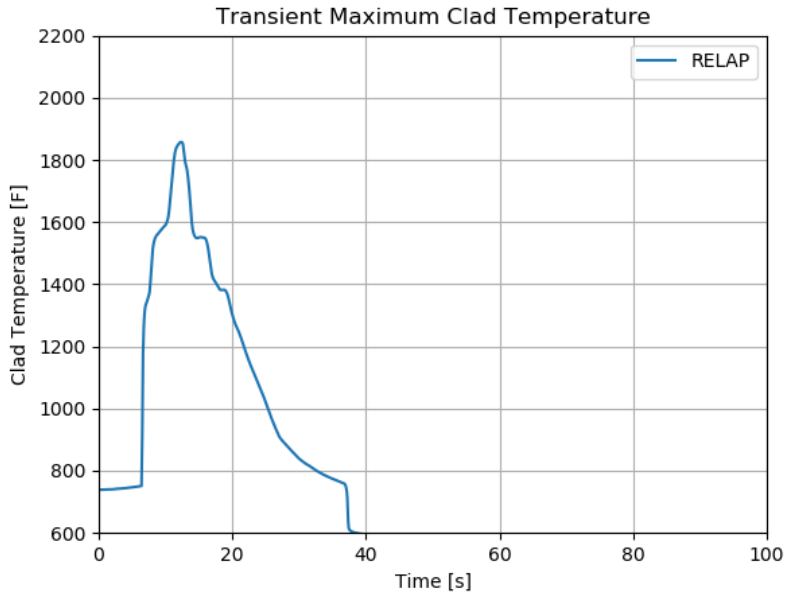

Figure 62 - Transient Maximum Clad Temperature for the Turbine Trip Scenario (Minimum Moderator Feedback with Pressurizer Controls)

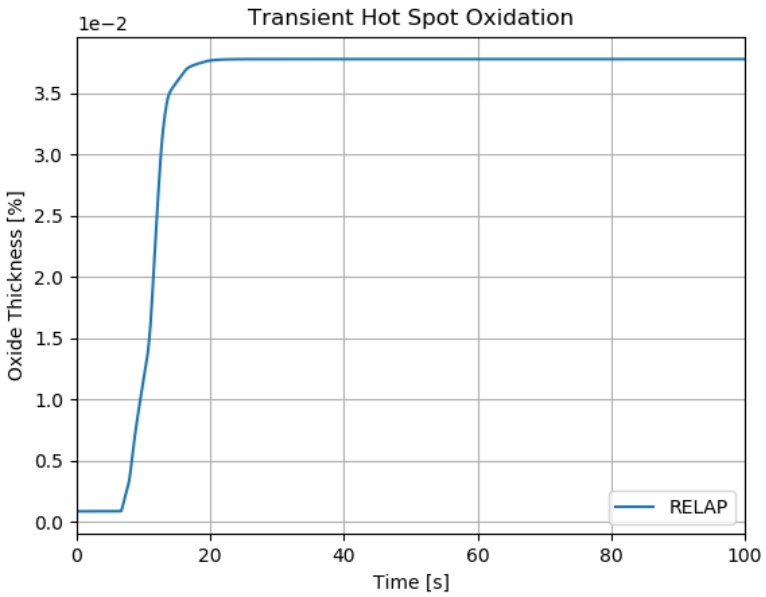

Figure 63 - Transient Oxidation at the Hot Rod Peak Power Location for the Turbine Trip Scenario (Minimum Moderator Feedback with Pressurizer Controls)

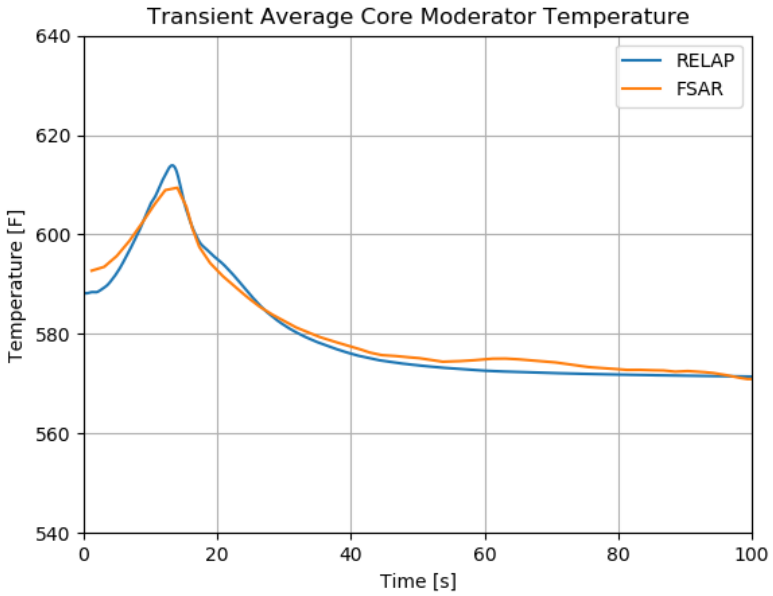

Figure 64 - Transient Core Average Moderator Temperature for the Turbine Trip Scenario (Minimum Moderator Feedback with Pressurizer Controls)

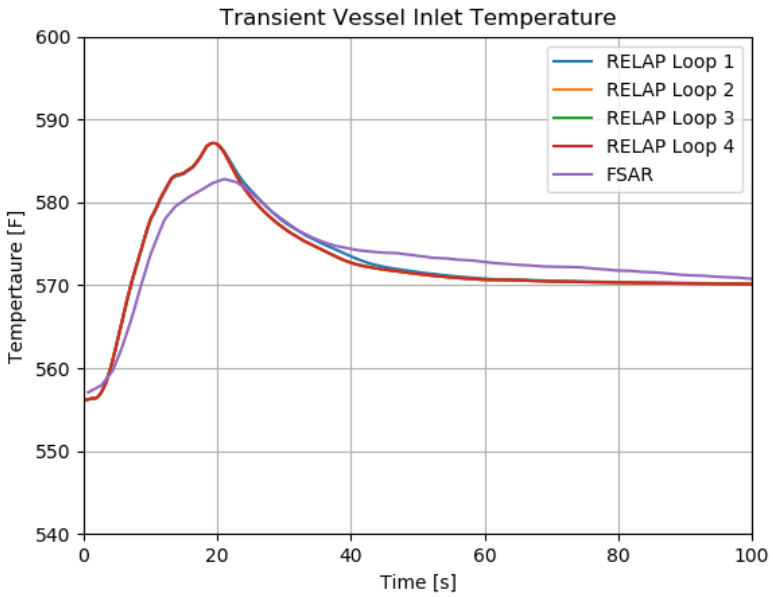

(B)

Figure 65 - Transient Vessel Inlet Temperature for the Turbine Trip Scenario (Minimum Moderator Feedback with Pressurizer Controls)

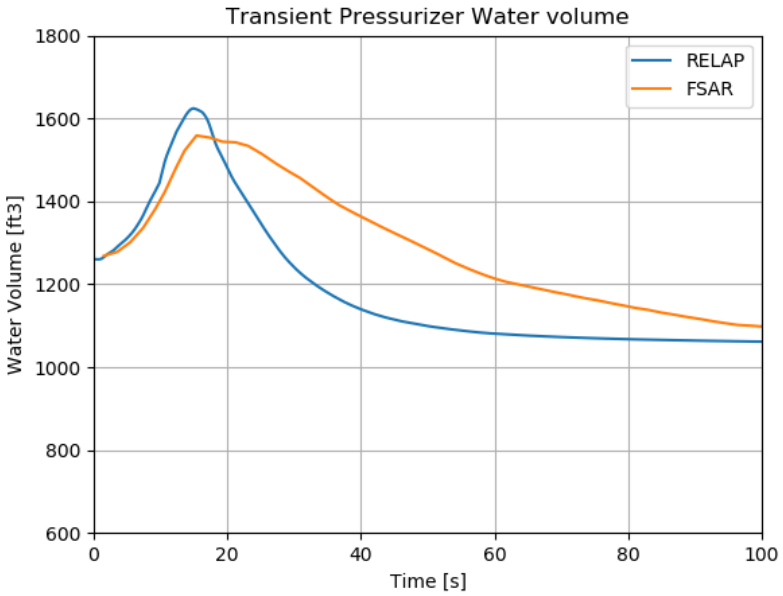

Figure 66 - Transient Pressurizer Water Volume for the Turbine Trip Scenario (Minimum Moderator Feedback with Pressurizer Controls)

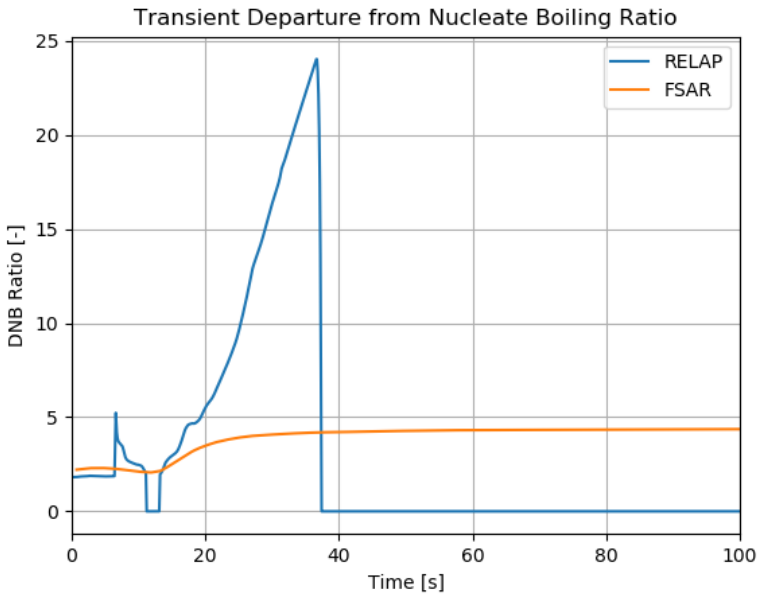

(B)

Figure 67 - Transient DNBR for the Turbine Trip Scenario (Minimum Moderator Feedback with Pressurizer Controls)

4.2.4 Loss of Nonemergency AC Power to the Plant Auxiliaries

A complete loss of nonemergency ac power (also called a loss of offsite power (LOOP)) may result in the loss of all power to the plant auxiliaries (such as the reactor coolant pumps, condensate pumps, etc.). The LOOP may be caused by a complete loss of the offsite grid accompanied by a turbine-generator trip at the plant or by a loss of the onsite DC distribution system. A LOOP is classified as an American Nuclear Society Condition II event, fault of moderate frequency.
This transient is more severe than the turbine trip event because for this case the decrease in heat removal by the secondary system is accompanied by a flow coastdown which further reduces the capacity of the primary coolant to remove heat from the core.
Following a loss of ac power with turbine and reactor trips, the sequence described below will occur:

A. Vital plant instruments are supplied from emergency DC power sources.
B. As the secondary side pressure rises following the trip, the steam generator power-operated relief valves may be automatically opened. The condenser is assumed not to be available for turbine bypass. If the steam flowrate through the power-operated relief valves is not available, the steam generator safety valves may lift to dissipate the sensible heat of the fuel and coolant plus the decay heat produced in the reactor.
C. As the no-load temperature is approached, the steam generator power-operated relief valves (or safety valves, if the power-operated relief valves are not available) are used to dissipate the decay heat and to maintain the plant at the hot shutdown condition.
D. The standby diesel generators, started on loss of voltage on the plant emergency buses, begin to supply plant vital loads.
E. The auxiliary feedwater system is started automatically, and is designed to supply rated flow within 1 min of the initiating signal, even if a loss of all nonemergency AC power occurs simultaneously with loss of normal feedwater

Following the reactor coolant pump coastdown caused by the loss of AC power, the natural circulation capability of the reactor coolant system (RCS) will remove residual and decay heat from the core, aided by auxiliary feedwater in the secondary system.
The LOOP scenario presents three cases in the FSAR:

1. Base LOOP
2. LOOP with the AFW assumption changed due to a Three Mile Island (TMI) concern related to pressurizer overfill. This assumption is to have no AFW delivered to 2 SGs.
3. LOOP with charging flow on to check for pressurizer overfill.

4.2.4.1 Results

The RELAP results are examined in the subsections below.

LOOP Base Case

The transient pressurizer pressure is shown in Figure 68. From Figure 68, the trends in the RELAP response are fairly similar to the FSAR run. The RELAP run has much more subdued changes.
The transient core power as a fraction of the nominal power is shown in Figure 69. From Figure 69, RELAP the base case predicts a small power excursion prior to reactor trip, followed by normal decay heat.
The transient clad temperature is shown in Figure 70. From Figure 70, there is a significant heatup around the time of the power excursion.

The transient oxidation at the hot rod peak power location is shown in Figure 71. From Figure 71, the oxidation increases coincident with the significant heatup from Figure 70, and then flattens out once the clad temperature drops back down.
The transient SG pressures are shown in Figure 72. From Figure 72, the trends in the RELAP response are fairly similar to the FSAR run. The FSAR run has much more subdued changes.
The transient pressurizer water volume is shown in Figure 73. From Figure 73, the trends in the RELAP response are fairly similar to the FSAR run. The FSAR run has much more subdued changes.
The transient DNBR is shown in Figure 74. From Figure 74, the RELAP DNBR is 0 for a vast majority of the transient, other than right around the power excursion. Because of the extremely fast cladding heatup, it is presumed that the DNBR is under 1 at this point.
The transient hot leg, cold leg, and saturation temperatures are shown in Figure 75. The saturation temperatures are very close throughout the transient. The hot leg and cold leg temperature are fairly close through about 3000 seconds. After that point, the RELAP temperatures continue down, while the FSAR temperatures plateau.

LOOP Case with Charging SI Flows

This case is run specifically to check the pressurizer water volume. The pressure is also examined for relevance to the boundary conditions.
The transient pressurizer pressure is shown in Figure 76. This response is fairly different, as the large de-pressurization observed in the base case does not occur, and a large pressurization occurs at the end of the charging case (presumably due to the pressurizer becoming water solid). Note that the PORV and pressurizer safety valve are set to have steam flow and not liquid flow, so this pressurization is non-physical. However, the purpose of this run is to determine if the pressurizer becomes water solid, which it does, so the run can be considered to not meet the acceptance criteria at that point.
The transient pressurizer water volume is shown in Figure 77. From Figure 77, the pressurizer water volume increases significantly throughout the transient, and does become water solid at about 450 seconds.

LOOP Case with Altered AFW Flows for TMI Concerns

This case is run specifically to check the pressurizer water volume. The pressure is also examined for relevance to the boundary conditions.
The transient pressurizer pressure is shown in Figure 78. This response is very similar to the base case.
The transient pressurizer water volume is shown in Figure 79. From Figure 79, the pressurizer water volume is increased significantly above the base case, but it does not go over 1800 ft3.

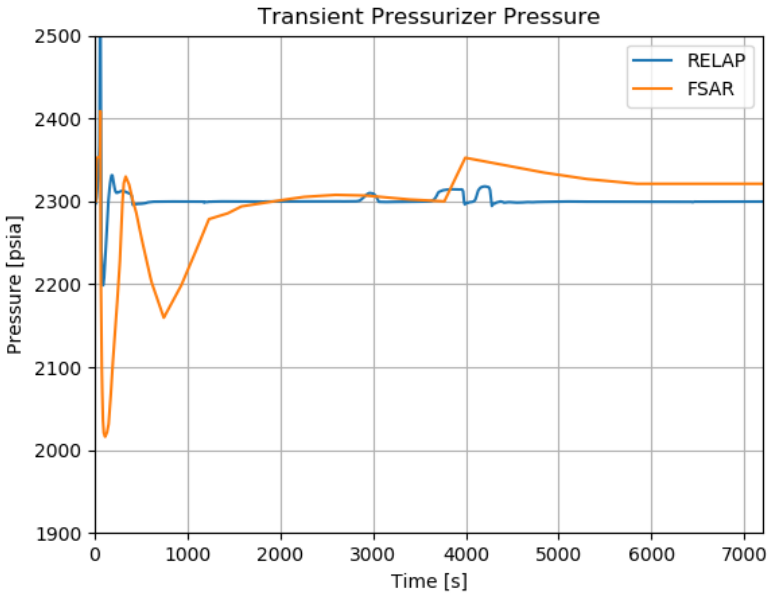

Figure 68 - Transient Pressurizer Pressure for the LOOP Scenario (Base Case)

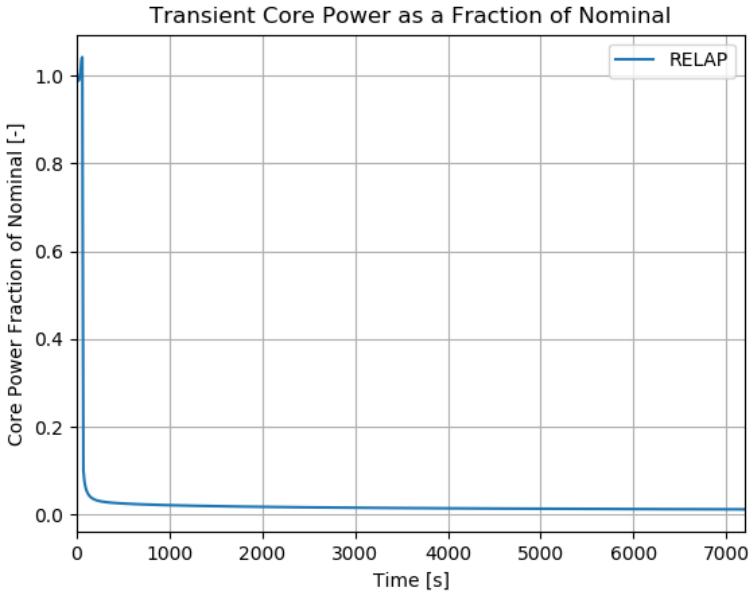

(B)

Figure 69 - Transient Core Power as a Fraction of Nominal Power for the LOOP Scenario (Base Case)

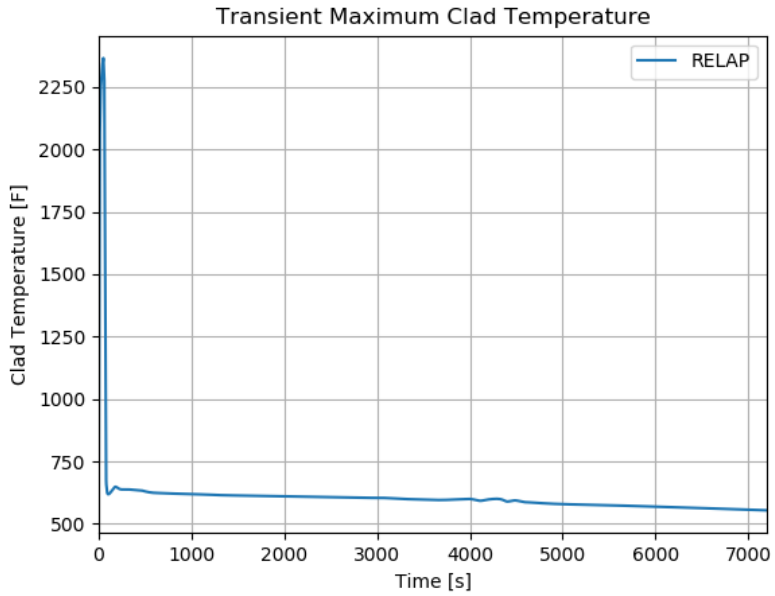

Figure 70 - Transient Maximum Clad Temperature for the LOOP Scenario (Base Case)

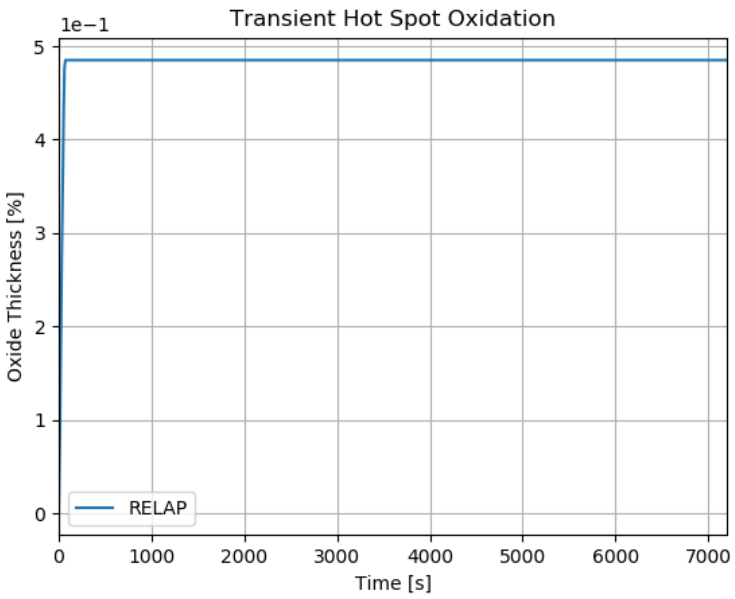

(B)

Figure 71 - Transient Oxidation at the Hot Rod Peak Power Location for the LOOP Scenario (Base Case)

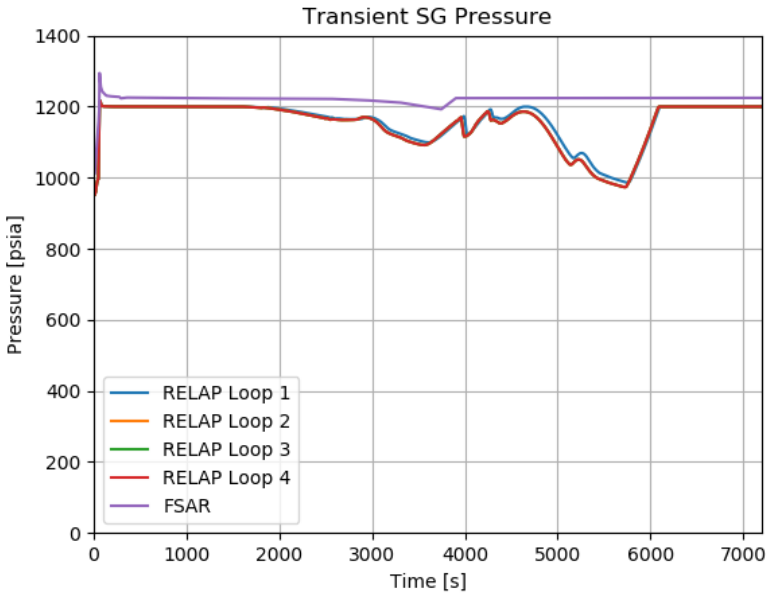

Figure 72 - Transient SG Pressure for the LOOP Scenario (Base Case)

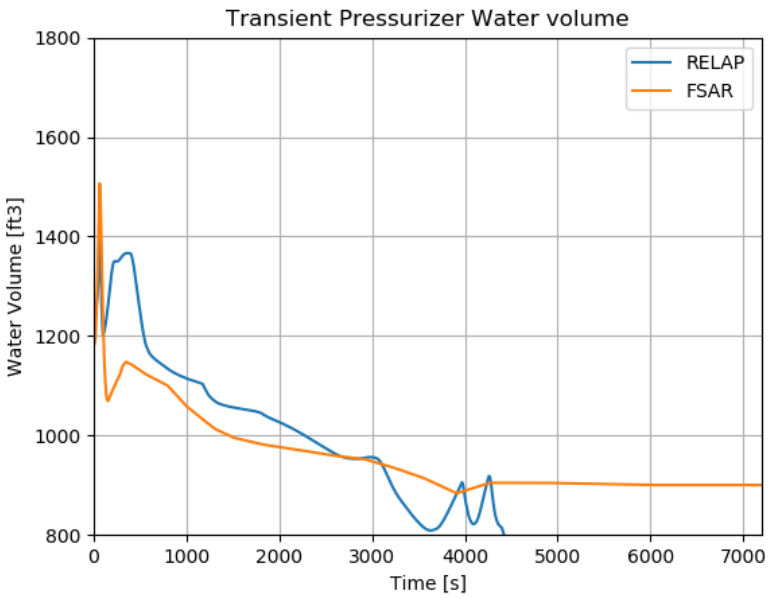

(B)

Figure 73 - Transient Pressurizer Water Volume for the LOOP Scenario (Base Case)

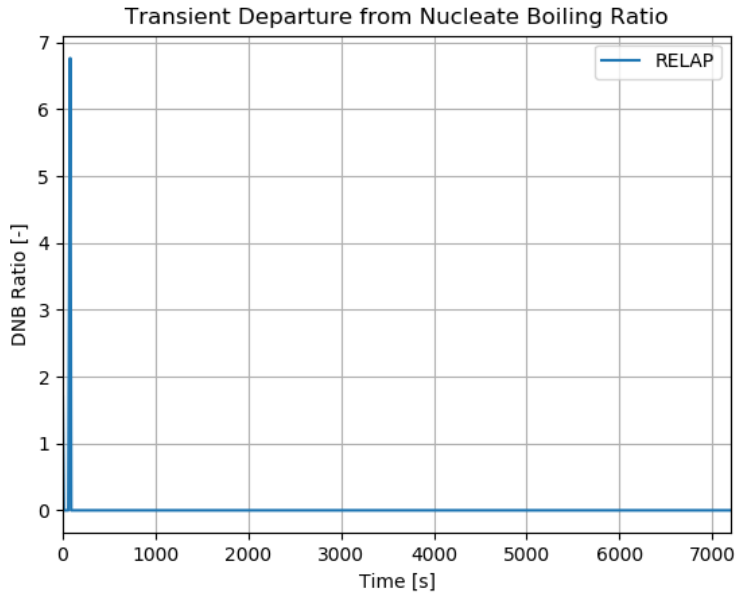

Figure 74 - Transient DNBR for the LOOP Scenario (Base Case)

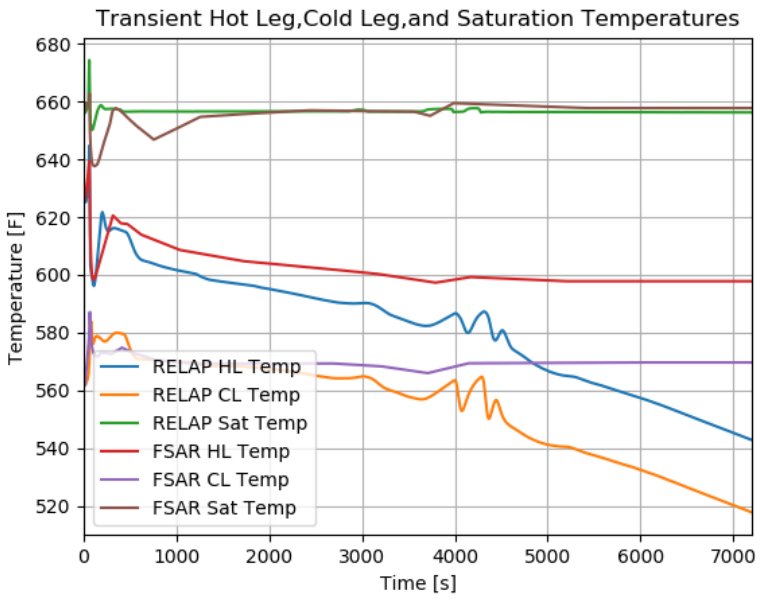

(B)

Figure 75 - Transient Hot Leg, Cold Leg, and Saturation Temperatures for the LOOP Scenario (Base Case)

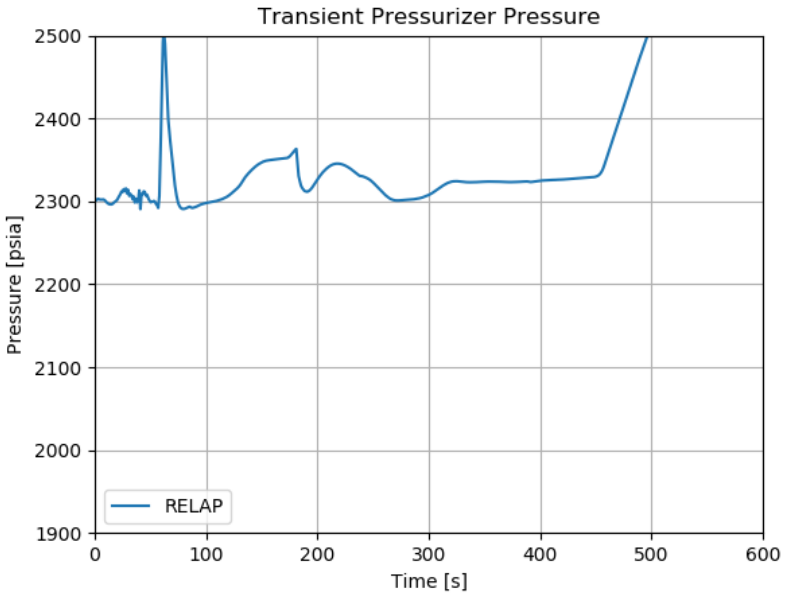

Figure 76 - Transient Pressurizer Pressure for the LOOP Scenario (Case with Charging Flows)

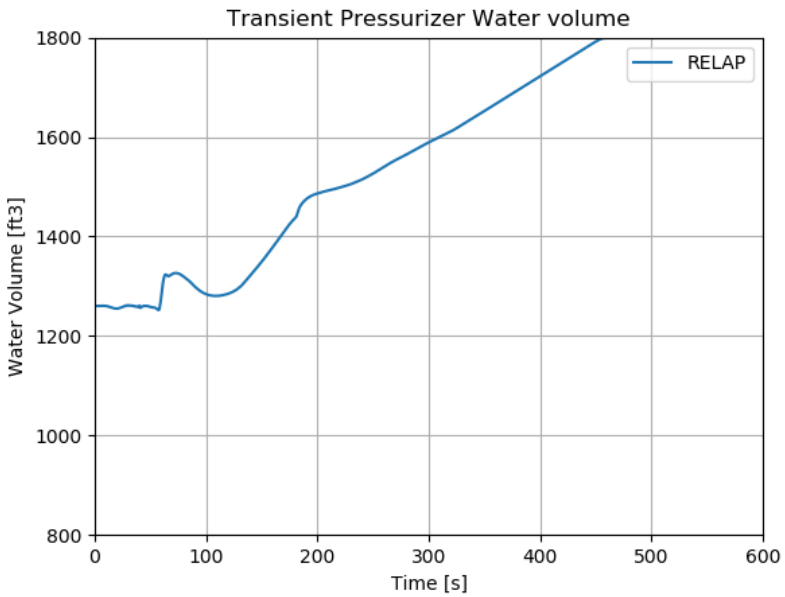

(B)

Figure 77 - Transient Pressurizer Water Volume for the LOOP Scenario (Case with Charging Flows)

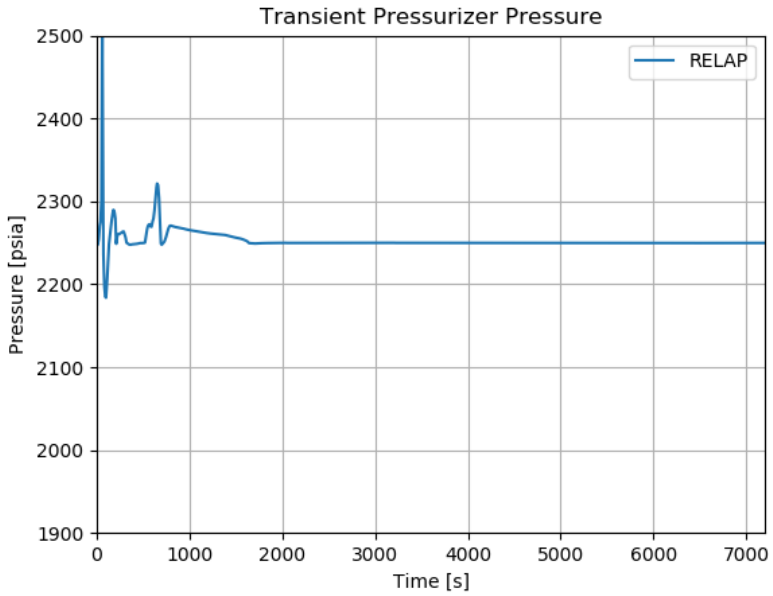

Figure 78 - Transient Pressurizer Pressure for the LOOP Scenario (Case with Altered AFW Flow for TMI Concerns)

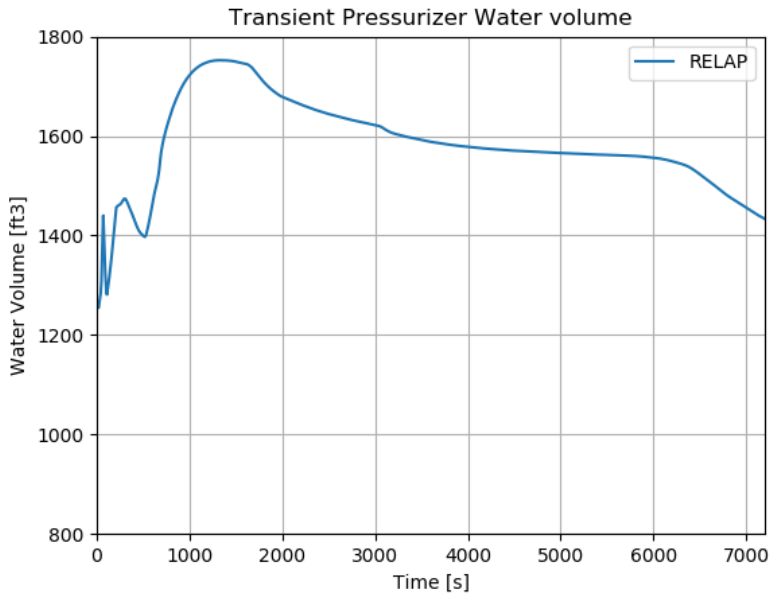

(B)

Figure 79 - Transient Pressurizer Water Volume for the LOOP Scenario (Case with Altered AFW Flow for TMI Concerns)

4.2.5 Chemical and Volume Control System Malfunction That Results in A Decrease in The Boron Concentration in The Reactor Coolant

Injecting primary grade water into the RCS via the reactor makeup portion of the chemical and volume control (CVCS) adds reactivity to the core. Boron dilution is a manual operation with strict administrative controls with procedures limiting the rate and duration of dilution. A boric acid blend system allows the operator to match the boron concentration of reactor coolant makeup water during normal charging to coolant in the RCS. Even under various postulated failure modes, the design of the CVCS limits the potential rate of dilution to a value which gives the operator sufficient time to correct the situation in a safe and orderly manner.

The opening of the primary water makeup control valve supplies water to the RCS which can dilute the reactor coolant. Inadvertent dilution can be readily terminated by closing one of the valves in the makeup pathway. To add makeup water to the RCS at pressure, at least one charging pump, in addition to the primary makeup water pumps, must be running. Normally, only one primary water supply pump is operating while the other is on standby.

The boric acid from the boric acid tank blends with primary grade water at the mixing tee, and the preset flowrates of boric acid and primary grade water on the control board determine the composition.

To cover all phases of the plant operation, the reference plant FSAR analysis considers boron dilution during refueling, cold shutdown, hot shutdown, hot standby, startup, and power operation. The analysis assumes conservative values for the critical parameters; i.e., high RCS critical boron concentrations, most negative boron worths, minimum shutdown margins, and small RCS volumes. These result in conservative calculations of the time available for the operator to determine the cause of the addition and take corrective action before shutdown margin is lost.

Although not explicitly stated, the analyses described for refueling, cold shutdown, hot shutdown, and hot standby appear to be done with some simplified calculation, and not a simulation.

It is unclear if simulations are even performed for the startup and full power operation analyses, but the following simulations are run:

- Dilution during startup or full power with manual control.
- Dilution during full power operation with automatic reactor control.

The assumptions for the automatic reactor control case are the same as the manual reactor control case, except that letdown flow is considered.

The objective of this analysis is to find the time when the RCS boron concentration drops to 300 ppm below the initial condition.

4.2.5.1 Results

The RELAP results are compared to each other in the paragraphs below, as there are no FSAR results given, other than the RCS dilution time. Note that the figures labeled with -A are for manual reactor control and the figures labeled with -B are for automatic reactor control.

The transient pressurizer pressure is shown in Figures 80-A and 80-B. From Figure 80-A, the RELAP run with manual reactor control has significant de-pressurization early in the transient. As the pressurizer begins to refill, though, the pressure starts to rise again. From Figure 80-B, the

RELAP run with automatic reactor control de-pressurizes consistently throughout the transient, due to the letdown flow.

The transient core power as a fraction of the nominal power is shown in Figures 81-A and 81-B. From Figures 81-A and 81-B, the RELAP runs have a similar core power transient which shows a standard reduction from operating power to just decay heat.

The transient maximum clad temperature is shown in Figures 82-A and 82-B. From Figures 82-A and 82-B, both runs have a consistent reduction in peak temperature.

The transient cladding oxidation at the peak power location of the hot rod is shown in Figures 83-A and 83-B. From Figures 83-A and 83-B, the RELAP runs both experience consistent and negligible oxidation.

The transient SG pressure is shown in Figures 84-A and 84-B. From Figures 84-A and 84-B, the RELAP runs both experience an initial large decrease in steam pressure, likely due to the reduction in heat from the core. However, at about 1200 seconds, the pressure starts rapidly increasing. This is presumably due to the continuous operation of the AFW.

The transient pressurizer water volume is shown in Figures 85-A and 85-B. From Figure 85-A, the RELAP run with manual reactor control has minimal water volume early in the transient, but eventually begins to refill. From Figure 85-B, the RELAP run with automatic reactor control never has a significant amount of water volume, due to the continuous letdown flow.

The transient core boron concentration and critical concentration is shown in Figures 86-A and 86-B. From Figure 86-A, the RELAP run with manual reactor control crosses the critical concentration line at about 2300 seconds. From Figure 86-B, the RELAP run with manual reactor control crosses the critical concentration line at about 2200 seconds.

The transient DNBR is shown in Figures 87-A and 87-B. From Figures 87-A and 87-B, both runs have a consistent DNBR of 0 throughout the transients, which is interpreted to mean a very high value.

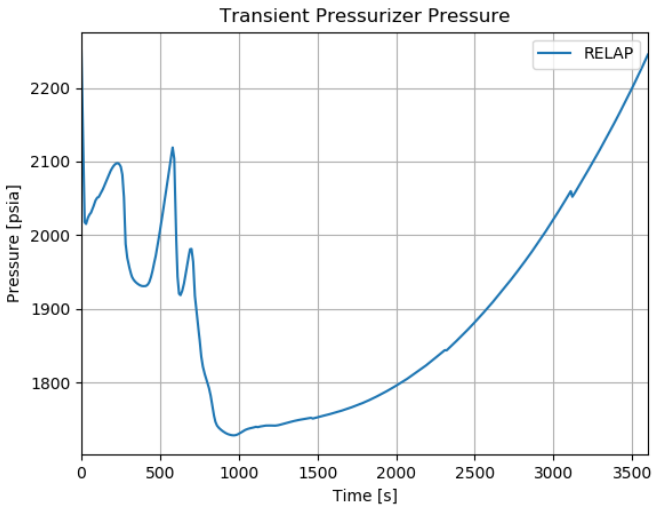

(A)

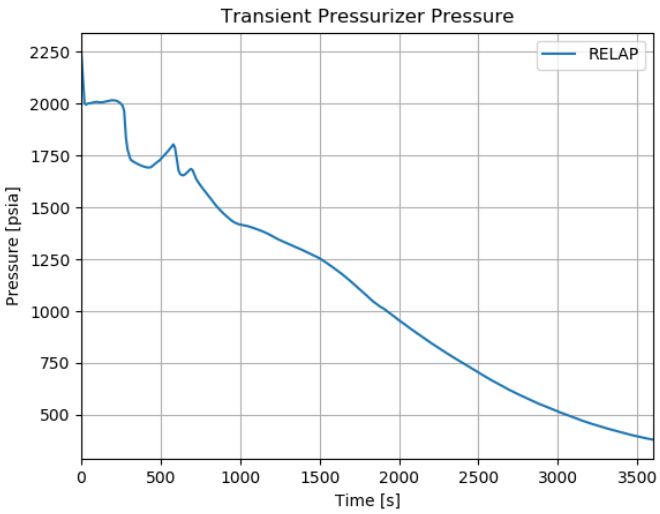

(B)

Figure 80 - Transient Pressurizer Pressure for the CVCS Malfunction Scenario (both Manual and Automatic Controls)

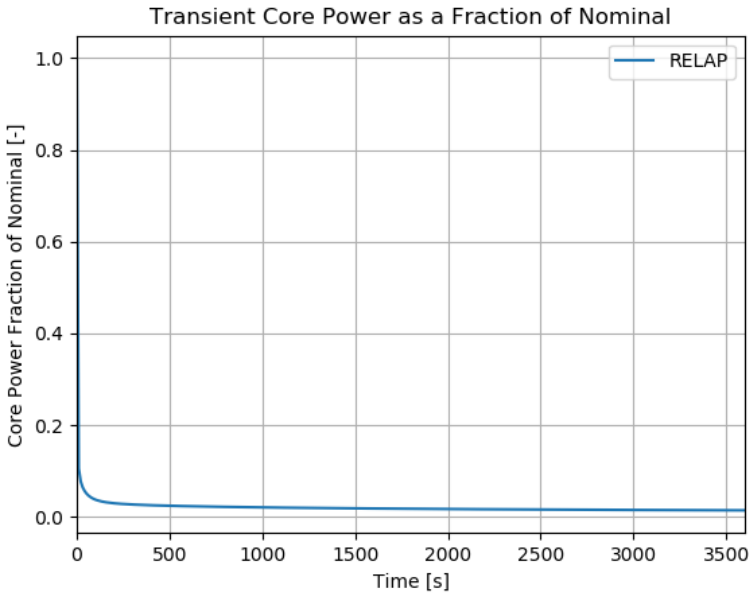

(A)

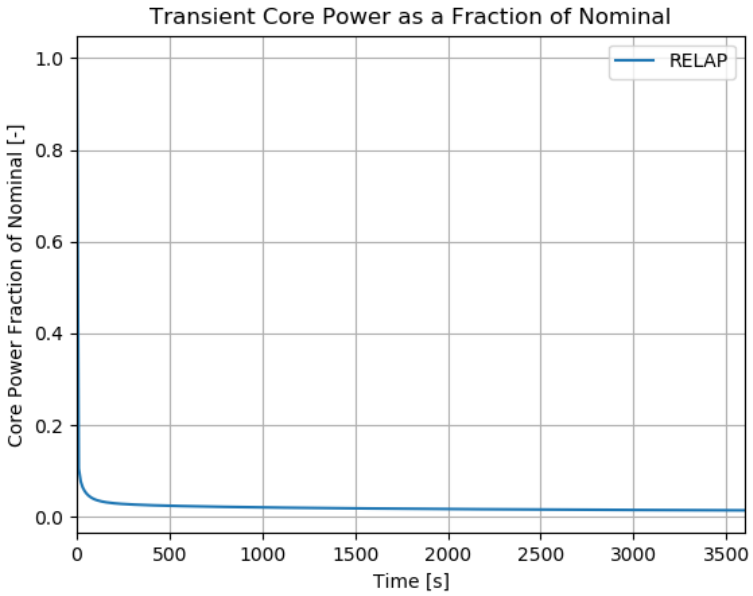

(B)

Figure 81 - Transient Core Power as a Fraction of the Nominal Power for the CVCS Malfunction Scenario (both Manual and Automatic Controls)

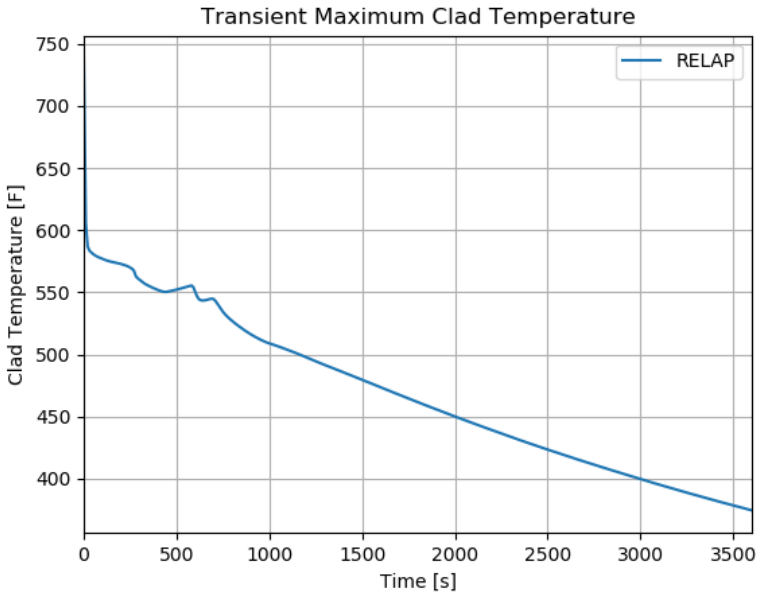

(A)

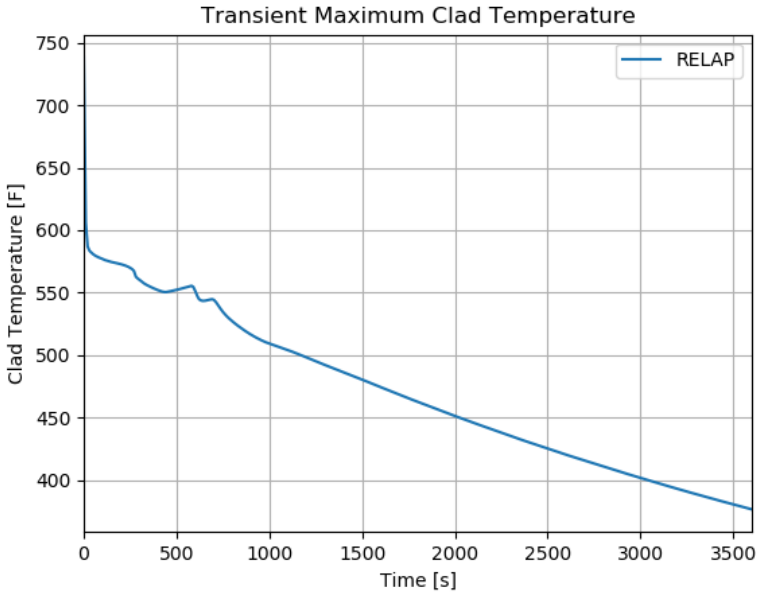

(B)

Figure 82 - Transient Maximum Clad Temperature for the CVCS Malfunction Scenario (both Manual and Automatic Controls)

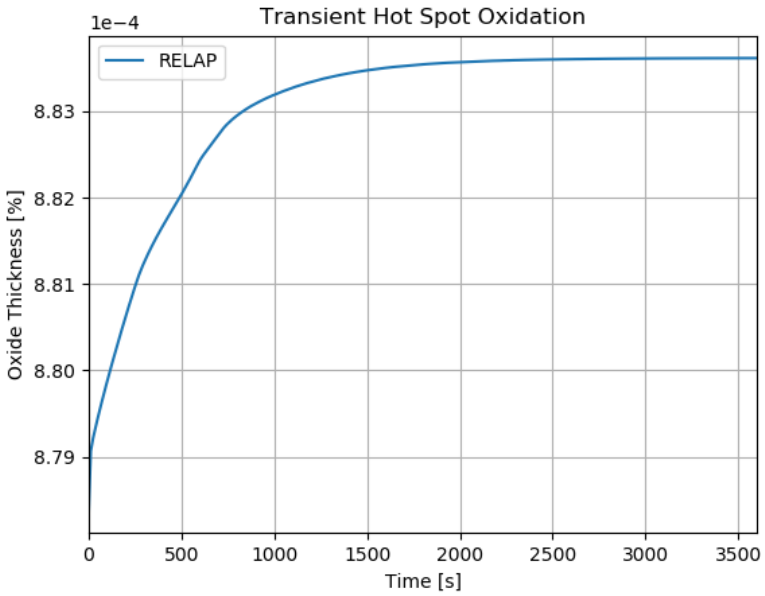

(A)

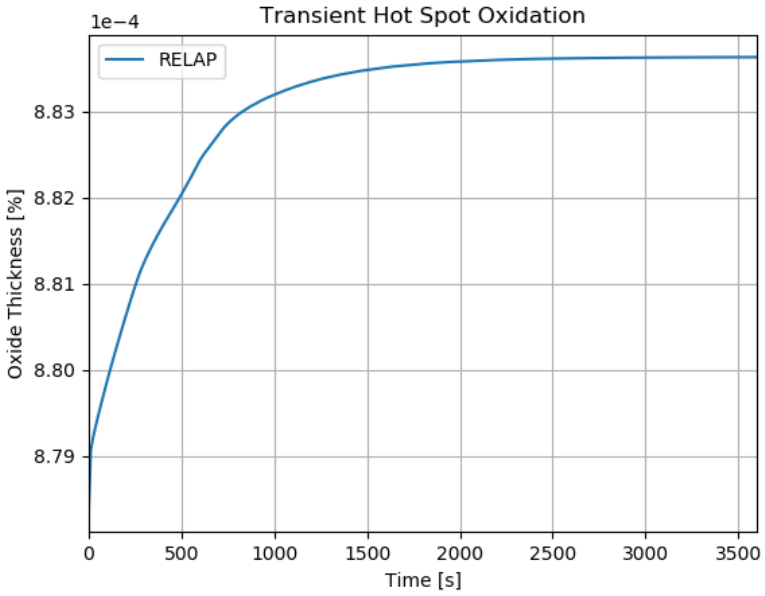

(B)

Figure 83 - Transient Cladding Oxidation at the Peak Power Location for the CVCS Malfunction Scenario (both Manual and Automatic Controls)

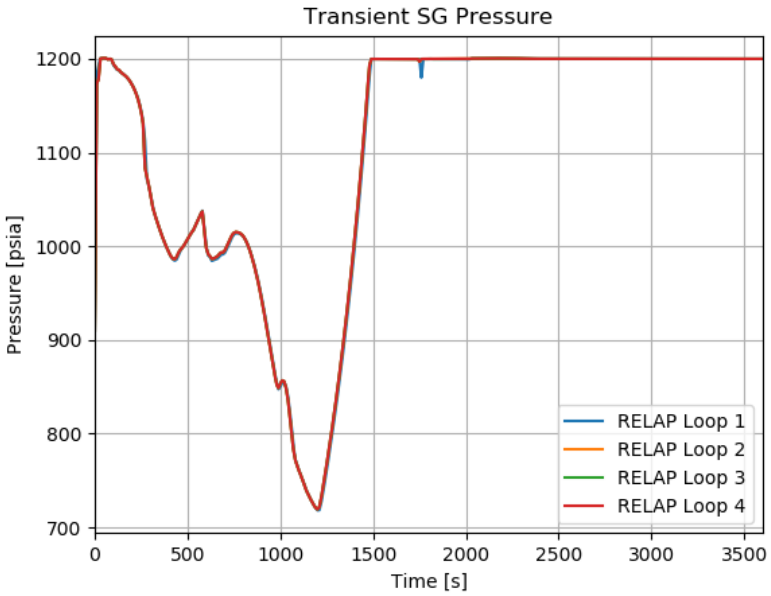

(A)

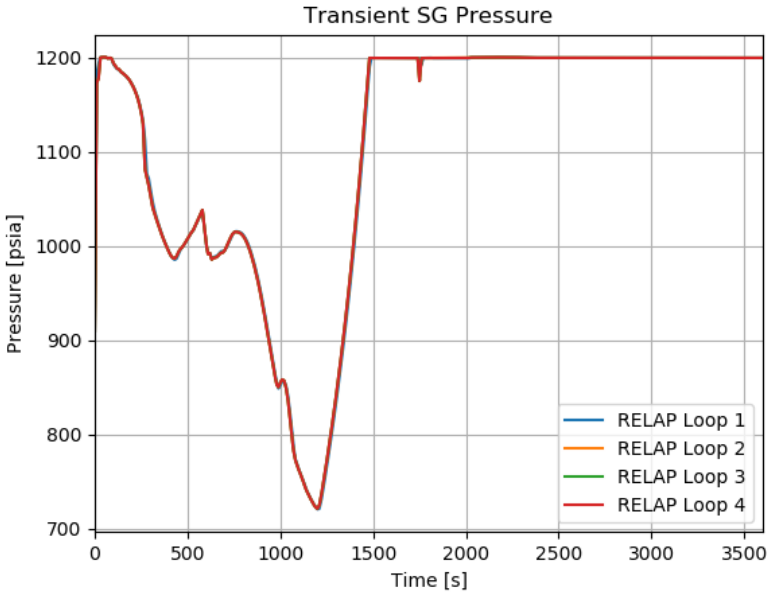

(B)

Figure 84 - Transient SG Pressure for the CVCS Malfunction Scenario (both Manual and Automatic Controls)

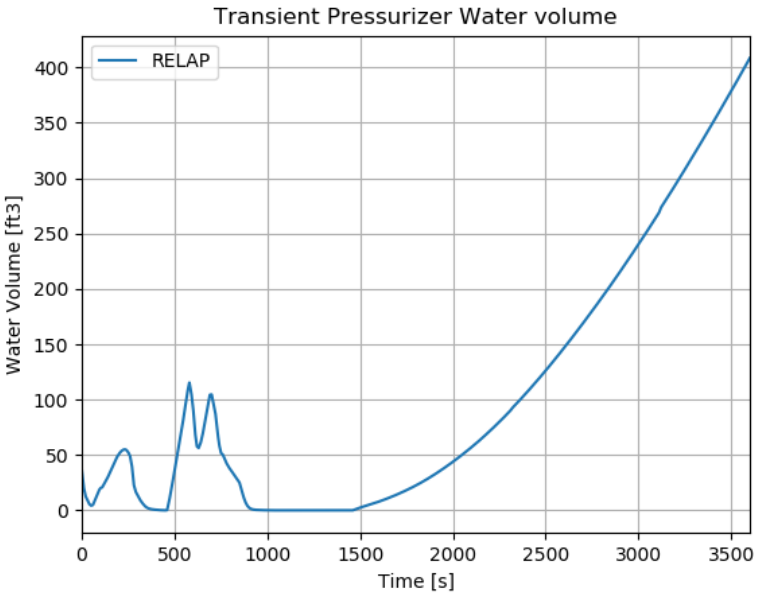

(A)

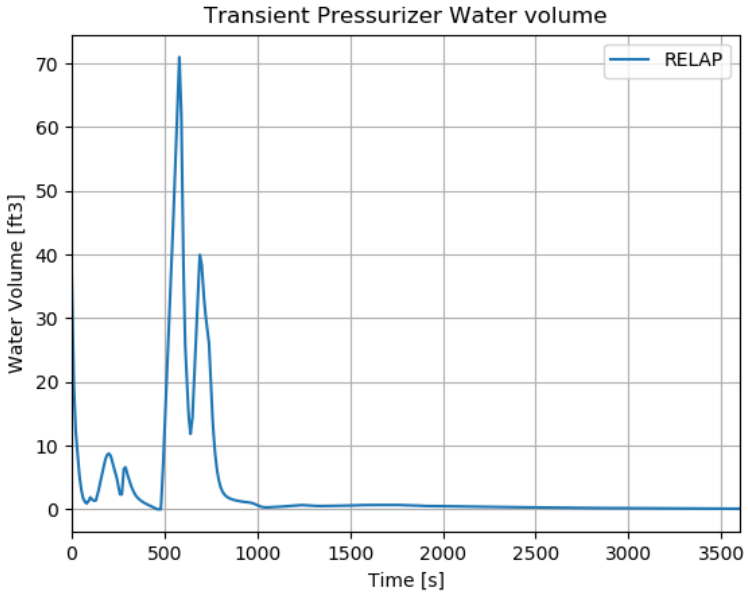

(B)

Figure 85 - Transient Pressurizer Water Volume for the CVCS Malfunction Scenario (both Manual and Automatic Controls)

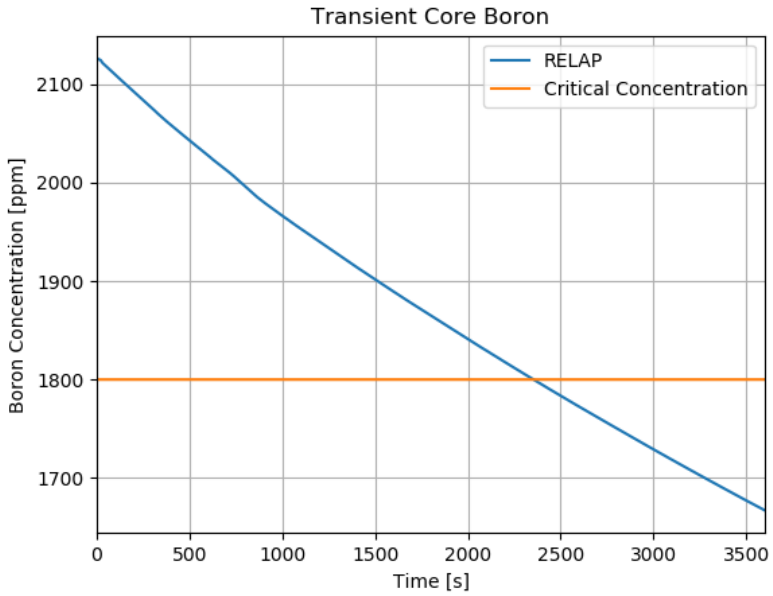

(A)

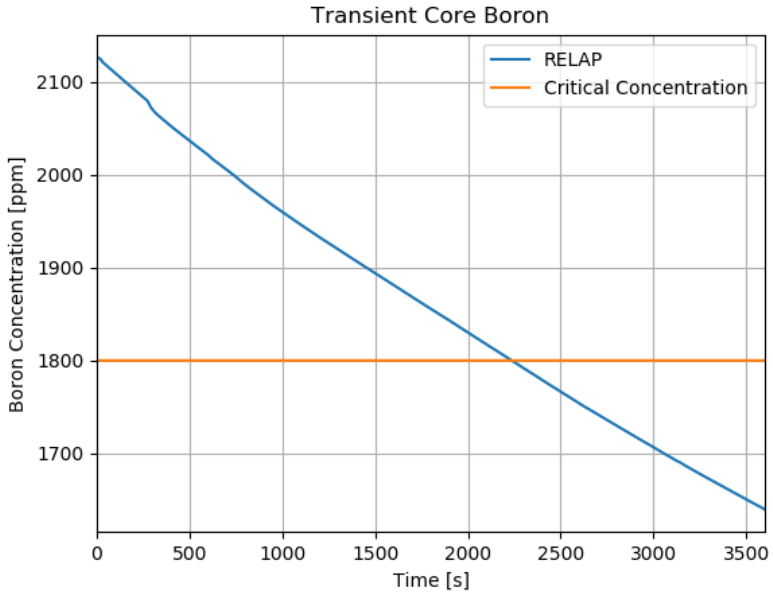

(B)

Figure 86 - Transient Core Boron Concentration for the CVCS Malfunction Scenario (both Manual and Automatic Controls)

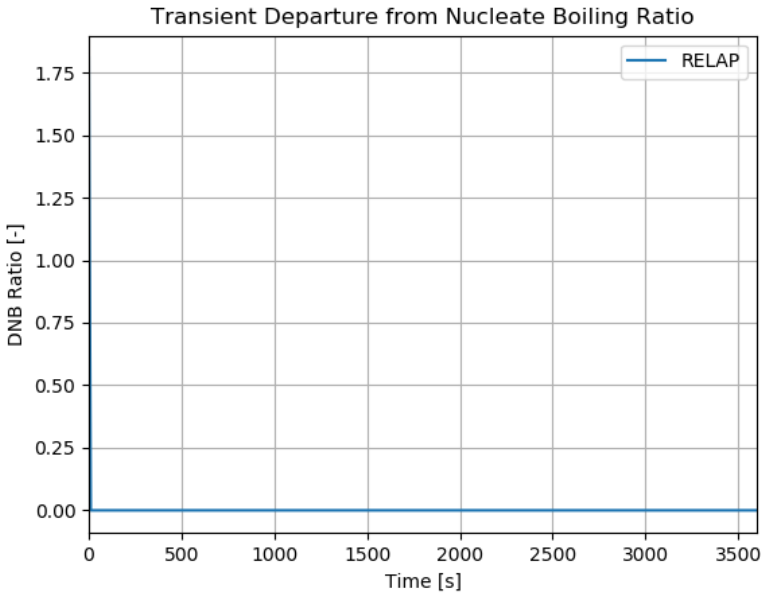

(A)

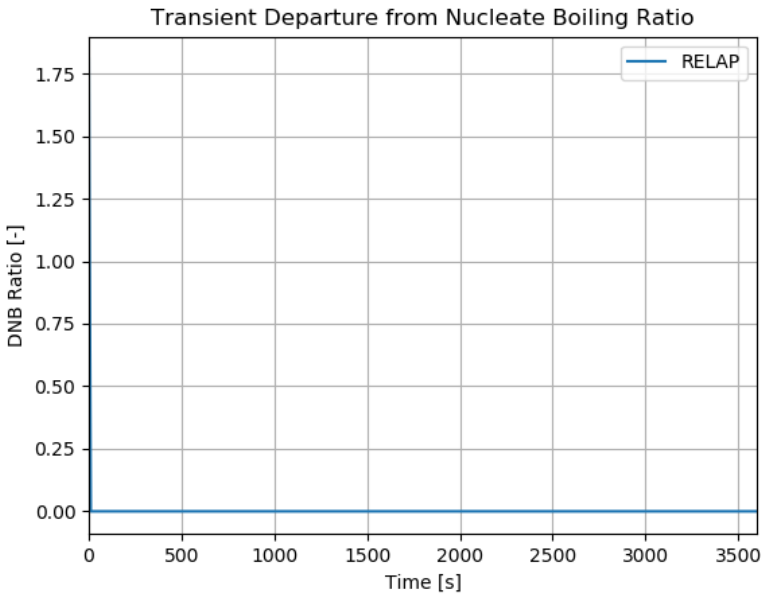

(B)

Figure 87 - Transient DNBR for the CVCS Malfunction Scenario (both Manual and Automatic Controls)

4.2.6 Loss-of-Coolant Accidents

A loss-of-coolant accident (LOCA) is the result of a pipe rupture of the reactor coolant system (RCS) pressure boundary. For the analyses described performed herein, a major pipe break (large break, LB) is defined as a rupture with a total cross-sectional area equal to or greater than 1.0 ft^2. This event is considered a limiting fault, an American Nuclear Society (ANS) Condition IV event,

in that it is not expected to occur during the lifetime of the plant but is postulated as a conservative design basis.

A minor pipe break (small break, SB), as considered in this subsection, is defined as a rupture of the reactor coolant pressure boundary with a total cross-sectional area less than 1.0 ft^2, in which the normally operating charging system flow is not sufficient to sustain pressurizer level and pressure. This is considered a Condition III event in that it is an infrequent fault that may occur during the life of the plant.

Both the limiting large break and small break cases are simulated.

4.2.6.1 Results

The RELAP results are compared to the LOCA runs from the FSAR in the paragraphs below.

Large Break

The transient pressurizer pressure is shown in Figure 88. The FSAR run depressurizes much more rapidly than the RELAP run. This is due to the change in the broken loop cold leg nozzle reverse loss coefficient. This is a known issue that should be corrected downstream.

The transient core power as a fraction of nominal is shown in Figure 89. The FSAR run shuts down much more rapidly. This is due to two factors. The first is that the 1971 decay heat model models a normal exponential decay that accounts for some residual fission, while RELAP explicitly calculates residual fissions. This is amplified by the fact that the RELAP run de-pressurizes much more slowly, and thus shuts down the residual fissions via voiding much more slowly. This is a known issue that should be corrected downstream when the de-pressurization is fixed, although some amount of slower decrease may persist due to the calculation of residual fissions.

The transient maximum clad temperature is shown in Figure 90. The FSAR run shows a very typical LB transient, with a period of distinct blowdown heatup followed by some cooling, then a rapid heatup during refill, and a more gradual heatup through reflood, until the heatup is terminated and slow cooling begins. The RELAP transient shows somewhat similar behavior, although generally much more exaggerated heatups and cooldowns.

The transient hot spot oxidation is shown in Figure 91. There is no FSAR plot for this. This plot shows that the RELAP run produces a result of ~0.23%, and most of this oxidation accumulates over the period of significant reflood heatup.

The transient liquid levels in the downcomer and core are shown in Figure 92. The core levels show a similar trend between RELAP and the FSAR, although the RELAP case has a consistently lower level. The downcomer level is initially somewhat similar, but the FSAR case retains significant inventory through the transient, while the RELAP case expels significant inventory.

The transient containment pressure is shown in Figure 93. This plot shows that the RELAP boundary condition was specified consistent with the FSAR analysis.

The transient core inlet and outlet mass flow rates are shown in Figure 94. The RELAP results show that the normal flow path is maintained, and no reverse flow is observed. This is due to the large reverse loss coefficient at the broken loop cold leg nozzle.

The transient heat transfer coefficient is shown in Figure 95. The RELAP results differ significantly from the FSAR results, but this is not investigated further, as the transient results will change significantly in downstream analyses.

The transient vapor temperature at the hot spot is shown in Figure 96. The RELAP results differ significantly from the FSAR results, but this is not investigated further, as the transient results will change significantly in downstream analyses.
The transient break mass flow rate is shown in Figure 97. The RELAP run has significantly lower break flow, consistent with the much slower de-pressurization. This is due to the large reverse loss coefficient at the broken loop cold leg nozzle.
The transient break energy release rate is shown in Figure 98. The RELAP run has a significantly lower energy release rate, consistent with the break flow.
The transient fluid quality at the PCT elevation is shown in Figure 99. The RELAP results differ significantly from the FSAR results, but this is not investigated further, as the transient results will change significantly in downstream analyses.
The transient mass flux at the PCT elevation is shown in Figure 100. The RELAP results differ significantly from the FSAR results, consistent with the difference in core mass flow.
The transient accumulator mass flow rate during blowdown is shown in Figure 101. This shows that the RELAP run does not even have accumulator injection in this time frame, consistent with the de-pressurization.
The transient combined SI mass flow rate is shown in Figure 102. This shows that the RELAP run has accumulator flow shortly after ~40 seconds. By this point, the FSAR accumulators are nearly empty, and the flow quickly falls to the purely SI level. Once the RELAP accumulators empty, the RELAP SI produces flow at a similar level to the FSAR run.

Small Break

The transient pressurizer pressure is shown in Figure 103. The FSAR and RELAP runs follow a somewhat similar depressurization path. The FSAR results lower much more quickly initially, but then plateau by about 200 seconds. This is likely due to the loop seal formation. The RELAP run shows slower depressurization, but it is not apparent that a loop seal forms at all.
The transient core power as a fraction of nominal is shown in Figure 104. There is no FSAR plot for this. This plot shows that the reactor is shut down almost immediately and follows a reasonable looking decay heat curve.
The transient clad temperature is shown in Figure 105. The RELAP run shows no heatup, while the FSAR run shows a significant heatup. This is due to the core not uncovering in the RELAP run. This is likely due to a number of issues with the RELAP model. The lack of loop seal formation likely contributes to this, as does the inconsistent break flow model. More investigation should be done downstream.
The transient oxidation at the hot spot is shown in Figure 106. There is no FSAR plot for this. This shows negligible oxidation accrual throughout the transient, consistent with a lack of heatup.
The transient core liquid level is shown in Figure 107. There is no FSAR plot for this, although this is a surrogate for the transient mixture level plot shown in the FSAR. The RELAP options for mixture level tracking did not appear to work correctly, and this should be investigated downstream. From the RELAP results presented, however, it is apparent that the mixture level would not have dropped below the top of the core, as there is only a very brief decrease from being liquid solid. As the mixture level includes a two-phase region, it is extremely

unlikely that the small drop in liquid level shown in this figure indicates a mixture level below the top of the core.
The transient core outlet steam mass flow rate is shown in Figure 108. The RELAP run shows no steam mass flow, other than the short period where the level dropped below the top of the core. This is because the core remains purely liquid otherwise, so there is no steam flow.
The transient heat transfer coefficient at the PCT elevation is shown in Figure 109. This shows a fairly consistent heat transfer level throughout the transient, notably missing the period of little to no heat transfer during core uncovery.
The transient vapor temperature at the PCT elevation is shown in Figure 110. This follows the same trend as the clad temperature.
The transient intact loops SI mass flow rate is shown in Figure 111. The RELAP flows are very similar to the FSAR flows, and the differences largely follow the pressure differences.

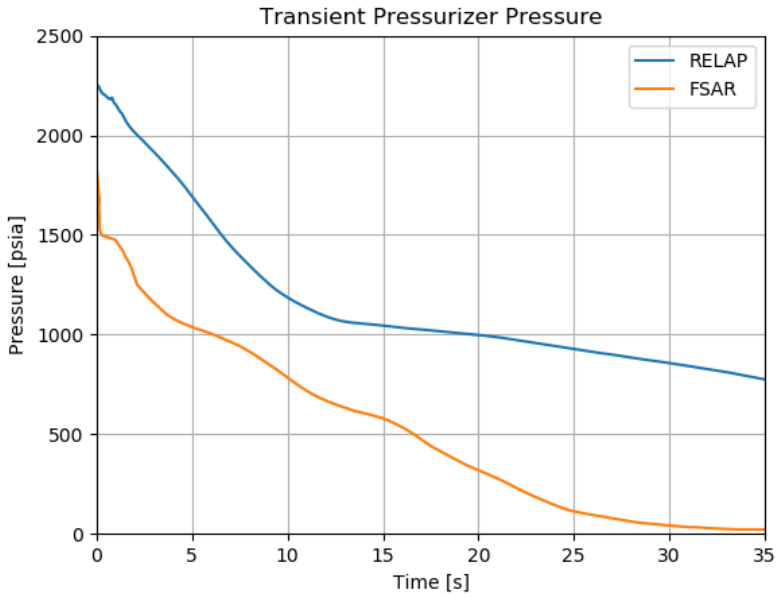

Figure 88 - Transient Pressurizer Pressure for the LOCA Scenario (LB)

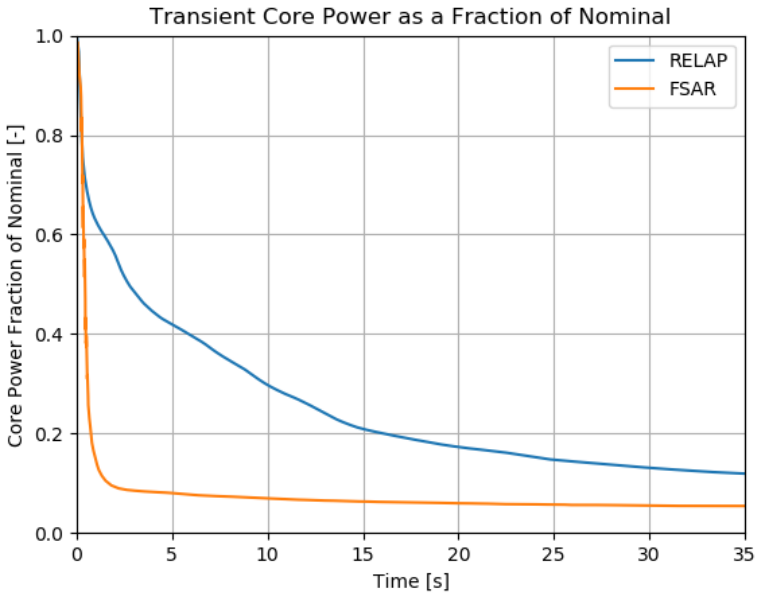

Figure 89 - Transient Core Power as a Fraction of Nominal for the LOCA Scenario (LB)

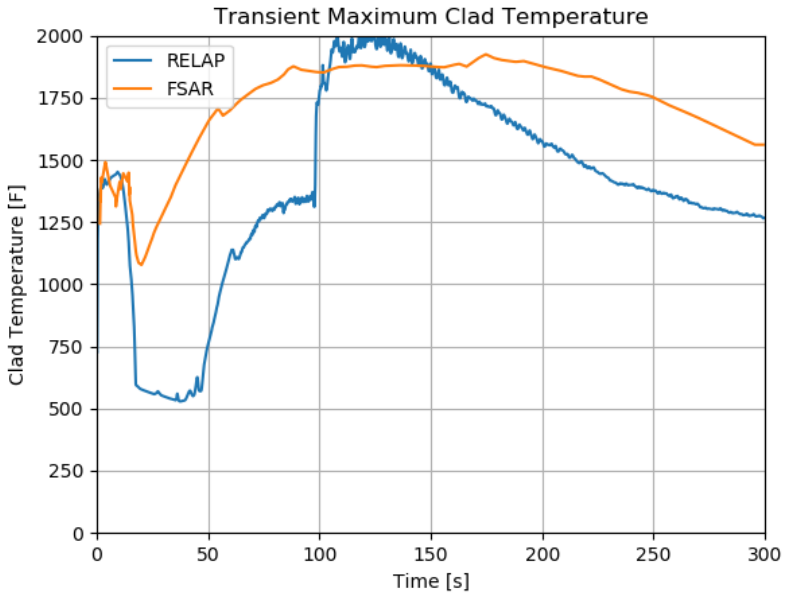

Figure 90 - Transient Maximum Clad Temperature for the LOCA Scenario (LB)

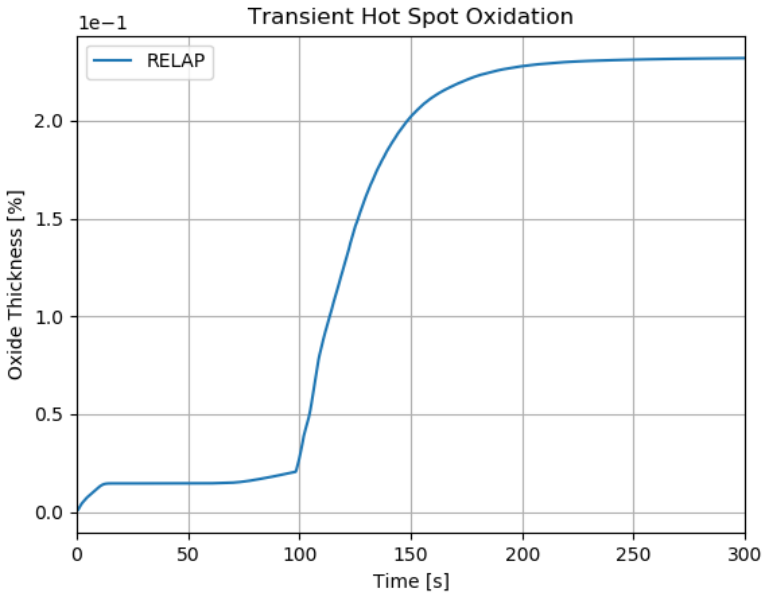

Figure 91 - Transient Hot Spot Oxidation for the LOCA Scenario (LB)

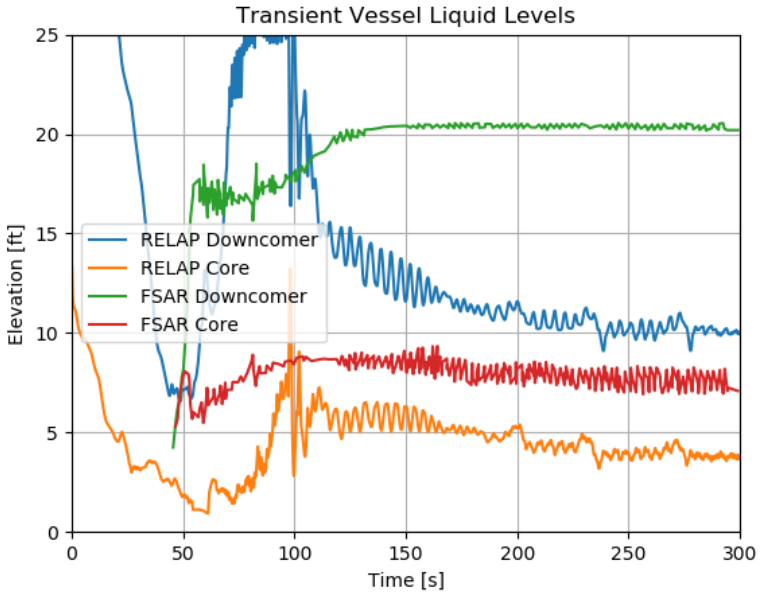

Figure 92 - Transient Vessel Liquid Levels for the LOCA Scenario (LB)

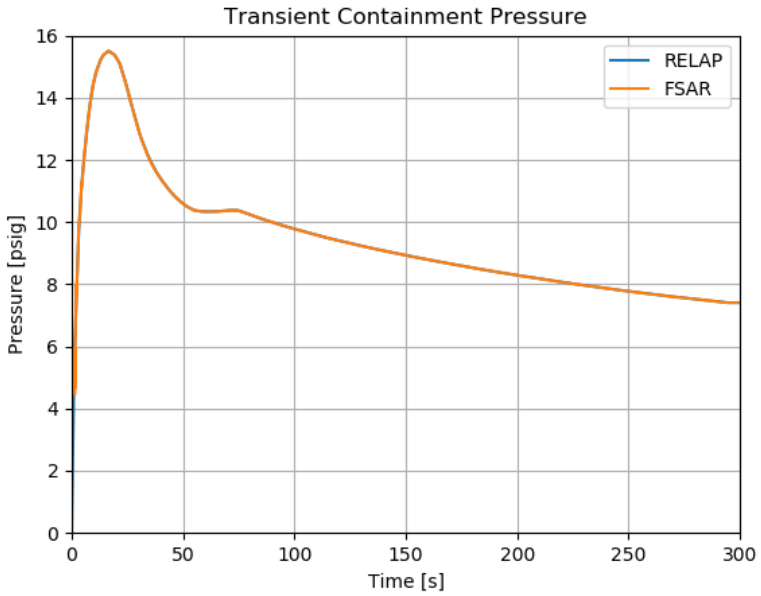

Figure 93 - Transient Containment Pressure for the LOCA Scenario (LB)

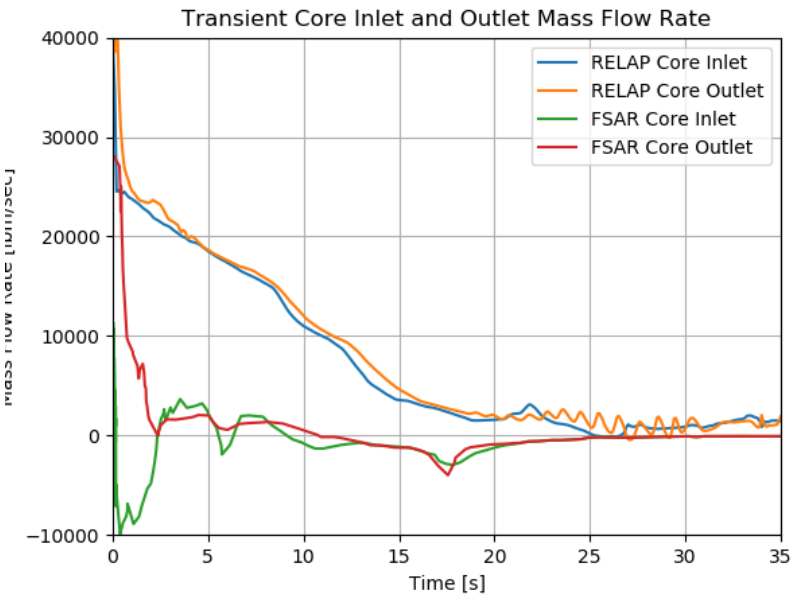

Figure 94 - Transient Core Inlet and Outlet Mass Flow Rate for the LOCA Scenario (LB)

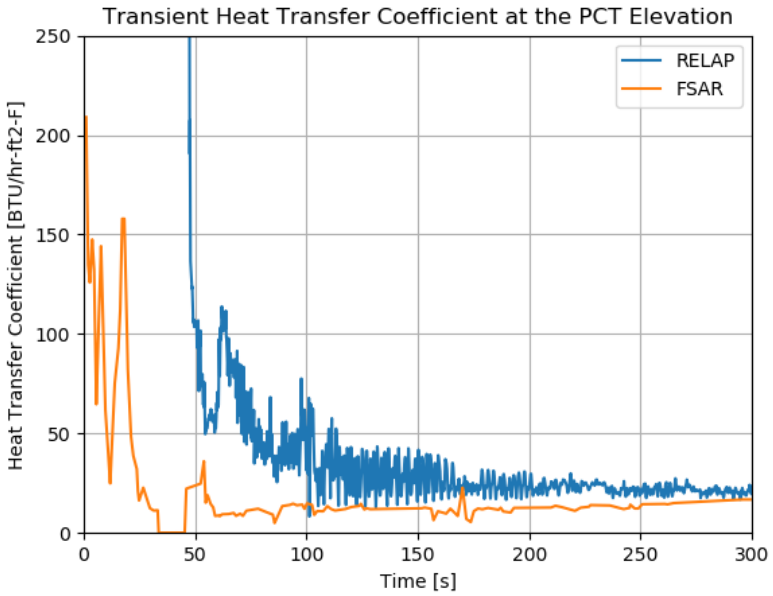

Figure 95 - Transient Heat Transfer Coefficient at the PCT Elevation for the LOCA Scenario (LB)

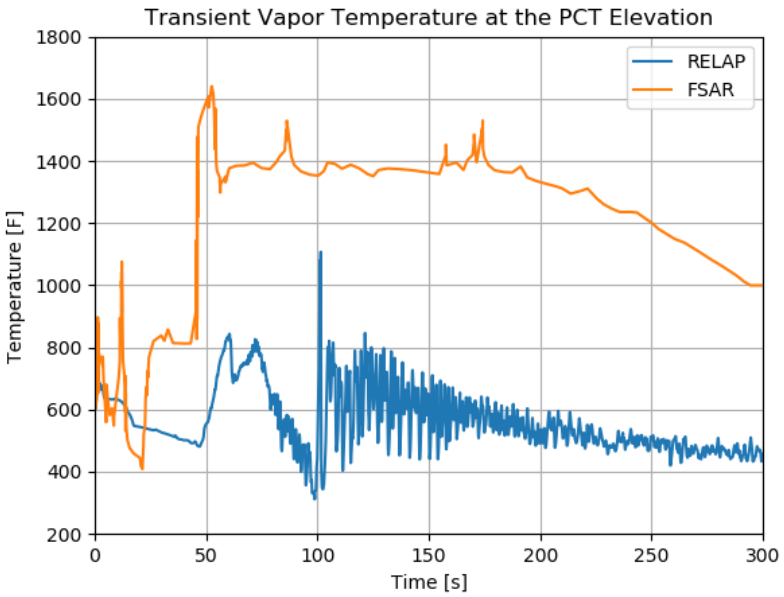

Figure 96 - Transient Vapor Temperature at the PCT Elevation for the LOCA Scenario (LB)

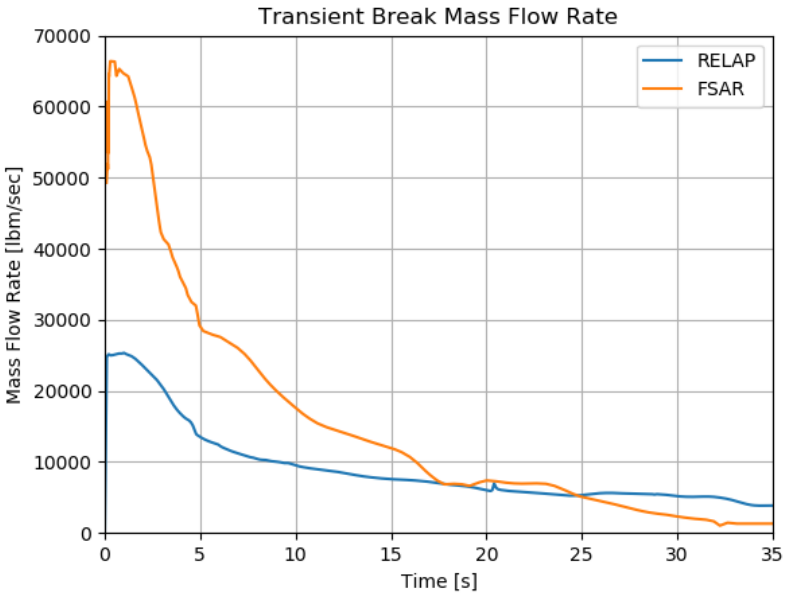

Figure 97 - Transient Break Mass Flow Rate for the LOCA Scenario (LB)

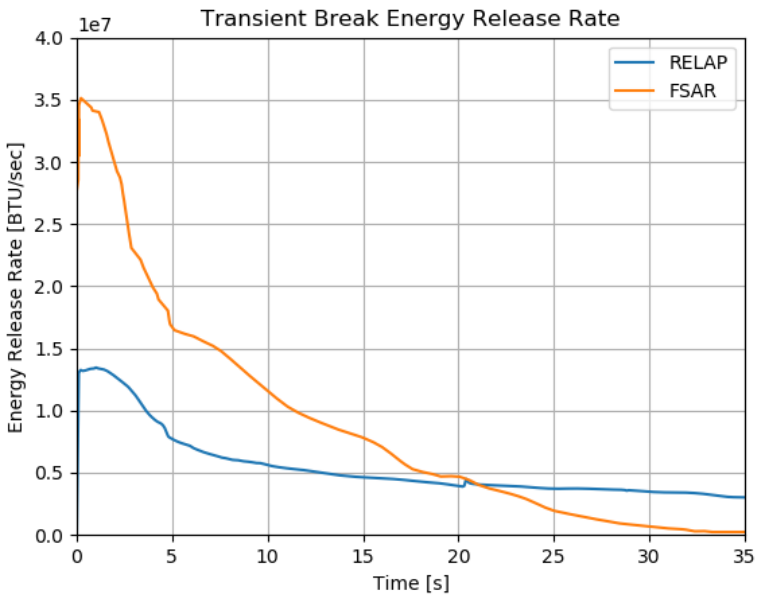

Figure 98 - Transient Break Energy Release Rate for the LOCA Scenario (LB)

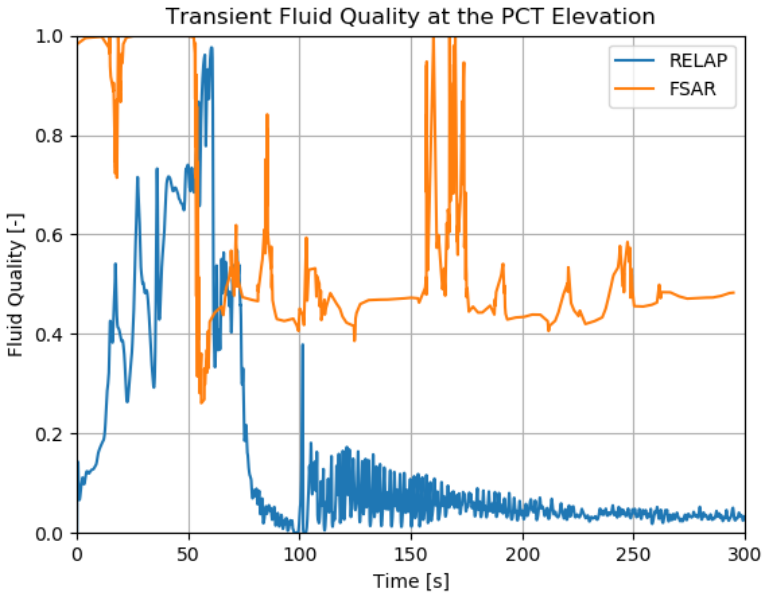

Figure 99 - Transient Fluid Quality at the PCT Elevation for the LOCA Scenario (LB)

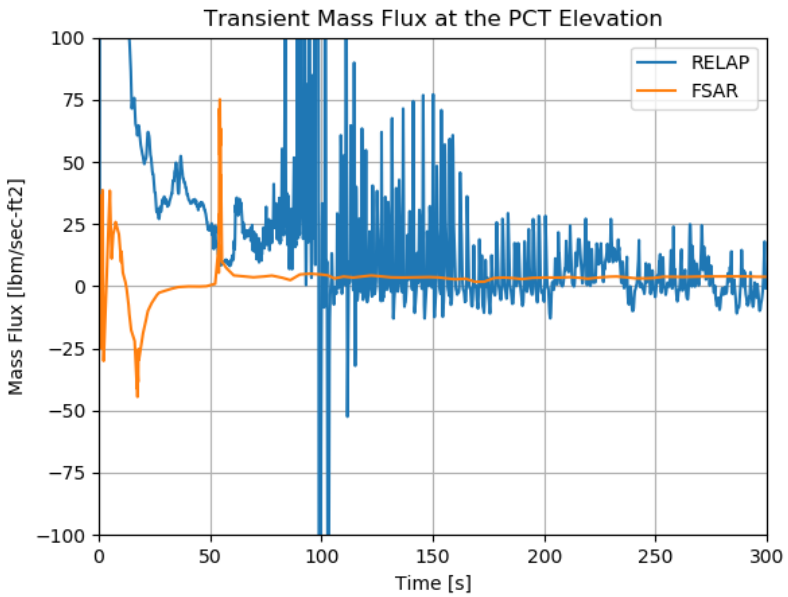

Figure 100 - Transient Mass Flux at the PCT Elevation for the LOCA Scenario (LB)

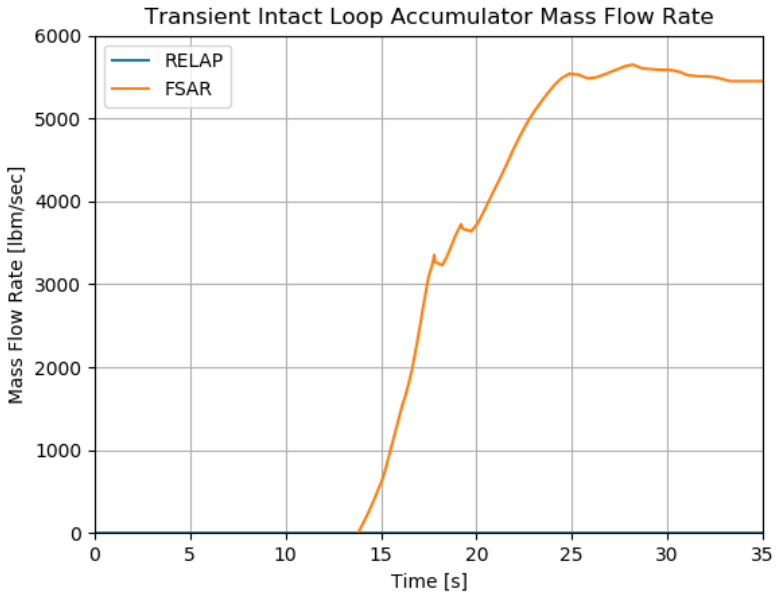

Figure 101 - Transient Intact Loop Accumulator Mass Flow Rate for the LOCA Scenario (LB)

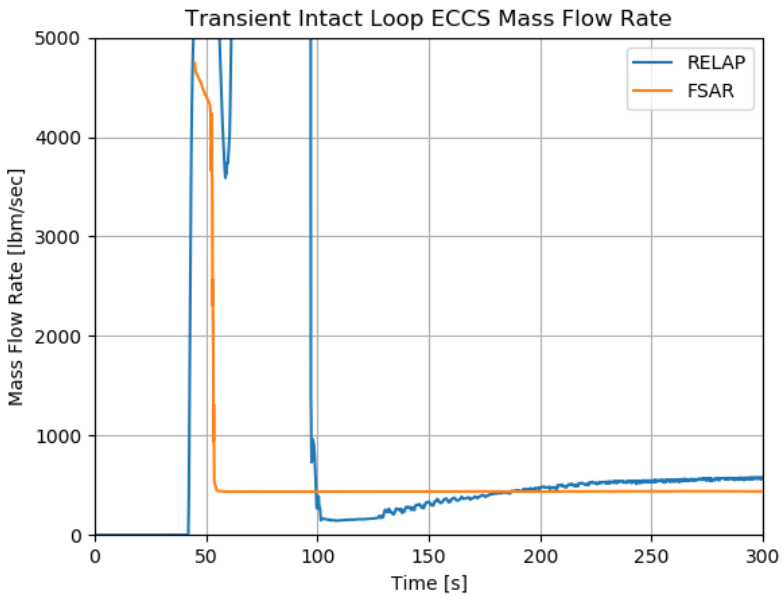

Figure 102 - Transient Intact Loop ECCS Mass Flow Rate for the LOCA Scenario (LB)

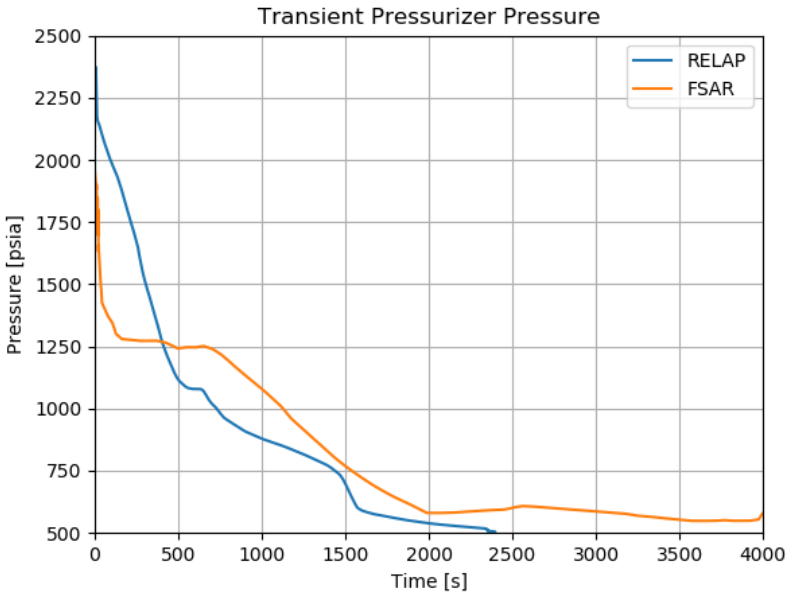

Figure 103 - Transient Pressurizer Pressure for the LOCA Scenario (SB)

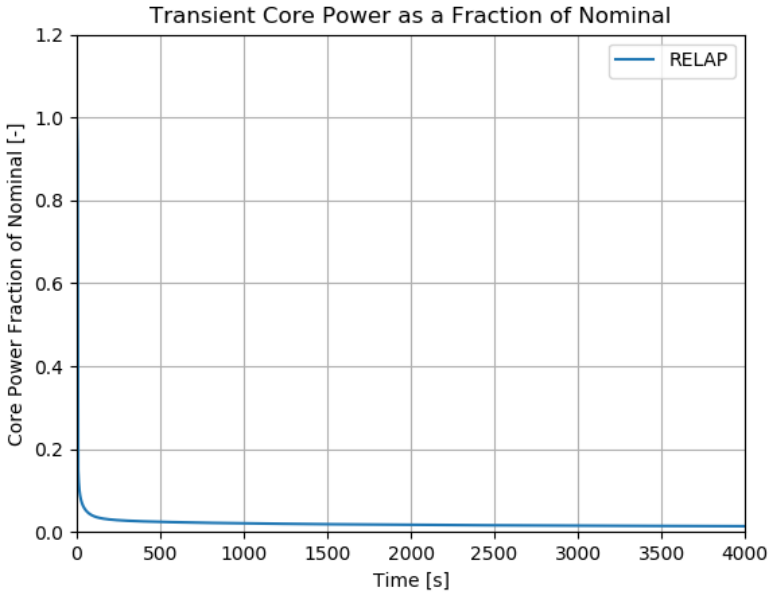

Figure 104 - Transient Core Power as a Fraction of Nominal for the LOCA Scenario (SB)

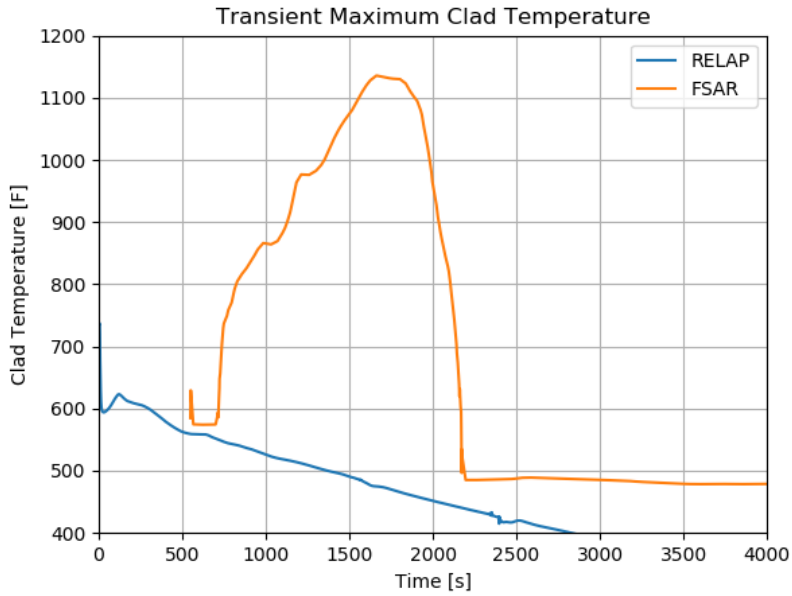

Figure 105 - Transient Maximum Clad Temperature for the LOCA Scenario (SB)

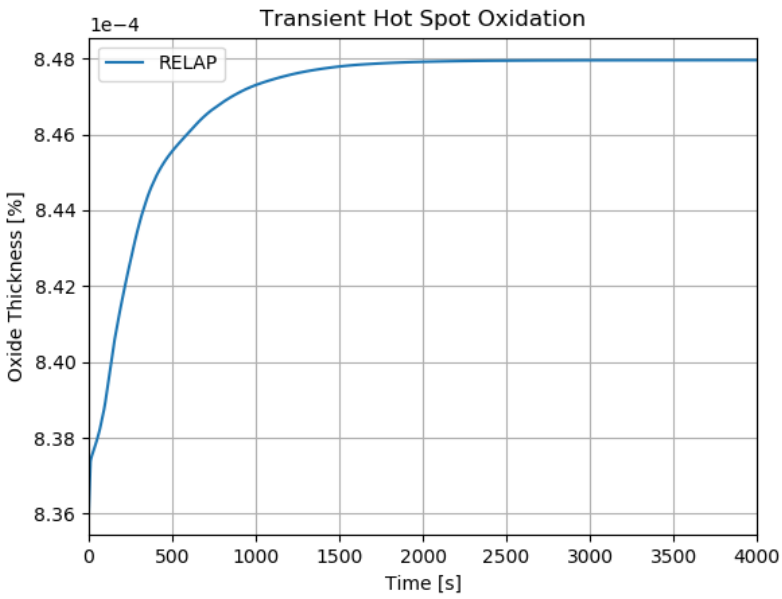

Figure 106 - Transient Hot Spot Oxidation for the LOCA Scenario (SB)

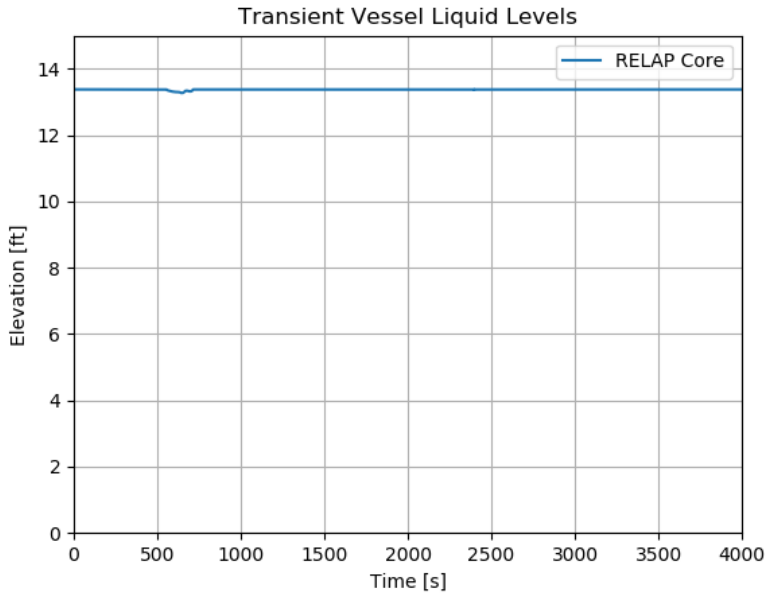

Figure 107 - Transient Vessel Liquid Levels for the LOCA Scenario (SB)

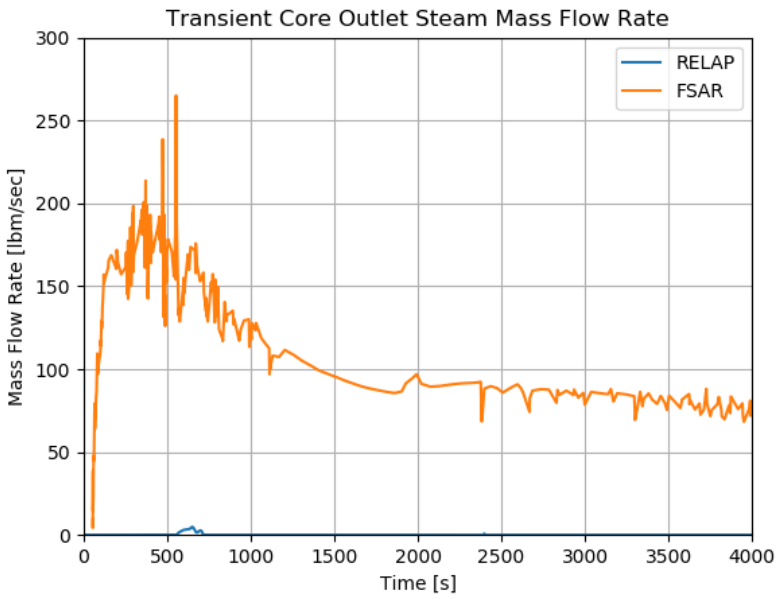

Figure 108 - Transient Core Outlet Steam Mass Flow Rate for the LOCA Scenario (SB)

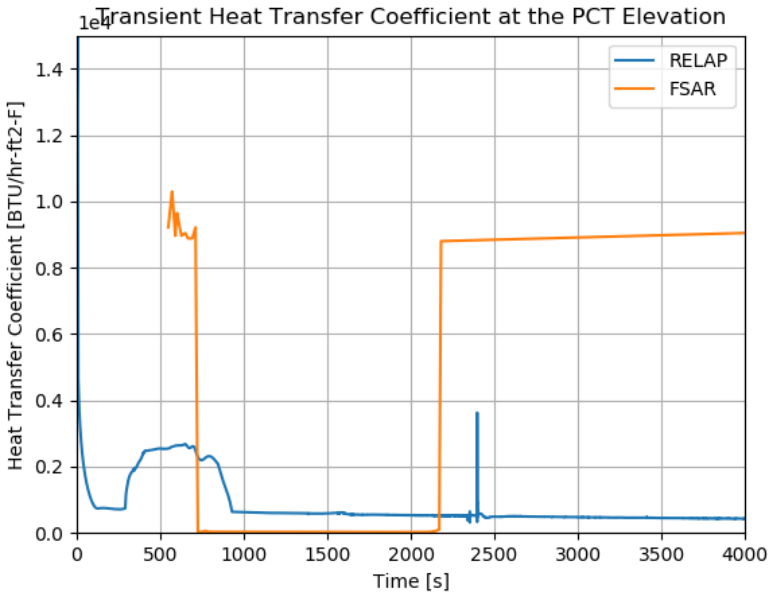

Figure 109 - Transient HTC at the PCT Elevation for the LOCA Scenario (SB)

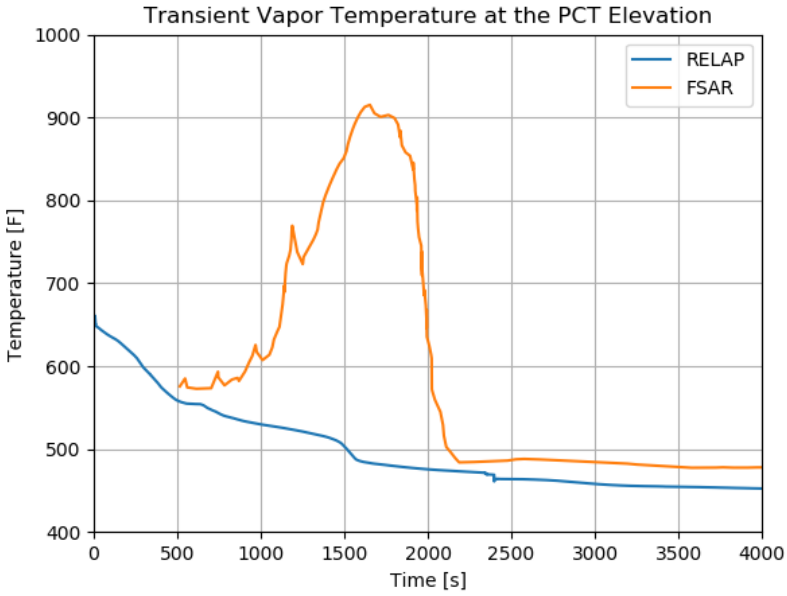

Figure 110 - Transient Vapor Temperature at the PCT Elevation for the LOCA Scenario (SB)

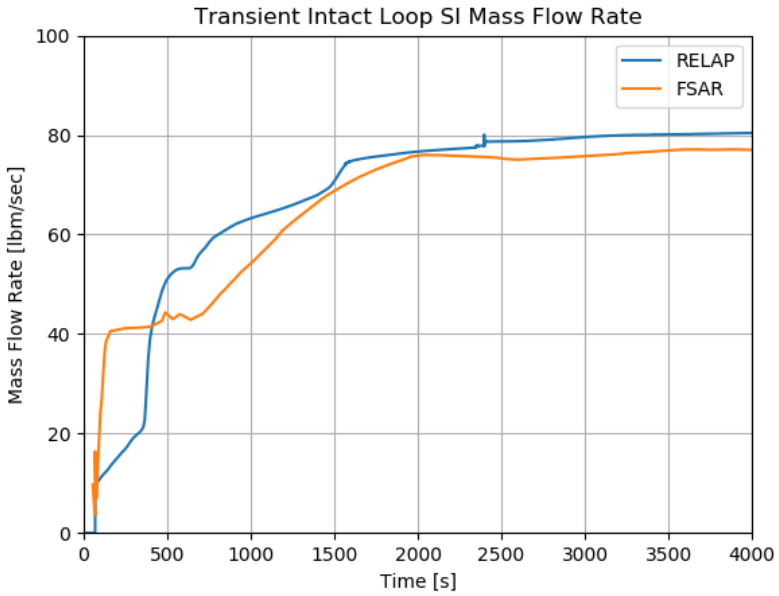

Figure 111 - Transient Intact Loop SI Mass Flow Rate for the LOCA Scenario (SB)

4.2.7 Inadvertent Operation of the Emergency Core Cooling System During Power Operation

Inadvertent operation of the ECCS at power could be caused by operator error, test sequence error, or a false electrical actuation signal. A spurious signal initiated after the logic circuitry in one protection system train for any of the following engineered safety feature (ESF) functions could cause this incident by actuating the ESF equipment associated with the affected train.

- High containment pressure.
- Low pressurizer pressure.
- Low steam line pressure.

Following the actuation signal, the suction of the coolant charging pumps diverts from the volume control tank to the refueling water storage tank. Simultaneously, the valves isolating the injection header from the charging pumps open and the normal charging line isolation valves close. The charging pumps force the borated water from the RWST through the pump discharge header, the injection line, and into the cold leg of each loop. The safety injection (SI) pumps also start automatically but provide no flow when the reactor coolant system (RCS) is at normal pressure. The passive accumulator tank safety injection and low head system are available. However, they do not provide flow when the reactor coolant system (RCS) is at normal pressure.

An SI signal normally results in a direct reactor trip and a turbine trip. However, any single fault that actuates the ECCS will not necessarily produce a reactor trip. If the reactor protection system does not produce an immediate trip as a result of the spurious SI signal, the reactor experiences a negative reactivity addition due to the injected boron, which causes a decrease in reactor power. The power mismatch causes a drop in TAVG and consequent coolant shrinkage. The pressurizer pressure and water level decrease. Load decreases due to the effect of reduced steam pressure on load after the turbine throttle valve is fully open.

If automatic rod control is used, these effects will lessen until the rods have moved out of the core. The transient is eventually terminated by the reactor protection system low pressurizer pressure trip or by manual trip.

The limiting cases presented in the FSAR section are re-created. This includes:

- A case for analysis of DNBR.
- A case for analysis of pressurizer filling using low TAVG.
- A case for analysis of pressurizer filling using high TAVG.

4.2.7.1 Results

The RELAP results are compared to the runs from the FSAR in the paragraphs below.

DNBR Case Results

The transient pressurizer pressure is shown in Figure 112. The FSAR run depressurizes slightly more than the RELAP run, but the behavior is similar. After the initial repressurization, the RELAP run goes through two cycles of the pressurizer safety valve while the FSAR run does not. This is likely due to the unknown exact nature of the pressurizer pressure control modeling.

The transient core power as a fraction of nominal is shown in Figure 113. The power is very similar, with the RELAP run staying slightly higher for slightly longer.

The transient maximum clad temperature is shown in Figure 114. There is no FSAR plot for this. The cladding temperature immediately drops significantly, and then more or less flattens out after reactor trip.

The transient hot spot oxidation is shown in Figure 115. There is no FSAR plot for this. There is no appreciable oxidation accrual during the transient.

The transient average core moderator temperature is shown in Figure 116. The FSAR run decreases slightly more than the RELAP run and takes longer to increase, but the behavior is generally similar.

The transient pressurizer water volume is shown in Figure 117. The transients are very similar until about 250 seconds, at which point the FSAR increases significantly above the RELAP run.

The transient steam flow as a fraction of nominal is shown in Figure 118. The transients are very similar, with the main difference being due to the timing of reactor trip.

The transient DNBR is shown in Figure 119. The behavior is similar for about 50 seconds, at which time the RELAP run drops to 0. In RELAP, this indicates that the heat structure is in a HT mode which does not even calculate CHF (i.e., single phase liquid). As such, this is consistent with the very high DNBR observed in the FSAR run.

Pressurizer Filling High TAVG Case Results

The transient pressurizer pressure is shown in Figure 120. After the initial decrease, the RELAP run re-pressurizes much faster and quickly goes through 2 cycles of the pressurizer safety valve. The FSAR run pressure flattens out for several hundred seconds before going through its pressurizer safety valve cycles.

The transient core power as a fraction of nominal is shown in Figure 121. The power is nearly identical between RELAP and the FSAR.

The transient maximum clad temperature is shown in Figure 122. There is no FSAR plot for this. The cladding temperature immediately drops significantly, and then more or less flattens out after reactor trip.

The transient hot spot oxidation is shown in Figure 123. There is no FSAR plot for this. There is no appreciable oxidation accrual during the transient.

The transient average core moderator temperature is shown in Figure 124. The RELAP run decreases slightly more than the FSAR run and flattens out at a lower temperature.

The transient pressurizer water volume is shown in Figure 125. A fairly significant difference develops in the first 20-30 seconds, and this difference more or less persists throughout the transient. The slope of increase is very similar through the transient.

The transient steam flow as a fraction of nominal is shown in Figure 126. The transients are the same, with the steam being turned off immediately due to immediate reactor trip.

The transient DNBR is shown in Figure 127. There is no FSAR plot for this. The RELAP run immediately goes to 0. In RELAP, this indicates that the heat structure is in a HT mode which does not even calculate CHF (i.e., single phase liquid).

Pressurizer Filling Low TAVG Case Results

The transient pressurizer pressure is shown in Figure 128. After the initial decrease, the RELAP run repressurizes much faster and quickly goes through a cycle of the pressurizer safety valve. The FSAR run pressure flattens out for several hundred seconds before going through its pressurizer safety valve cycles.

The transient core power as a fraction of nominal is shown in Figure 129. The power is nearly identical between RELAP and the FSAR.

The transient maximum clad temperature is shown in Figure 130. There is no FSAR plot for this. The cladding temperature immediately drops significantly, and then more or less flattens out after reactor trip.

The transient hot spot oxidation is shown in Figure 131. There is no FSAR plot for this. There is no appreciable oxidation accrual during the transient.

The transient average core moderator temperature is shown in Figure 132. The RELAP run initially decreases significantly less than the FSAR run and then also increases significantly less, resulting in it flattening out at a slightly lower temperature.

The transient pressurizer water volume is shown in Figure 133. A fairly significant difference develops in the first 20 seconds which sees the RELAP run with significantly more volume, but the FSAR run then increases much faster. This results in the FSAR run hitting maximum volume earlier.

The transient steam flow as a fraction of nominal is shown in Figure 133. The transients are the same, with the steam being turned off immediately due to immediate reactor trip.

The transient DNBR is shown in Figure 134. There is no FSAR plot for this. The RELAP run immediately goes to 0. In RELAP, this indicates that the heat structure is in a HT mode which does not even calculate CHF (i.e., single phase liquid). As such, this is consistent with the very high DNBR observed in the FSAR run.

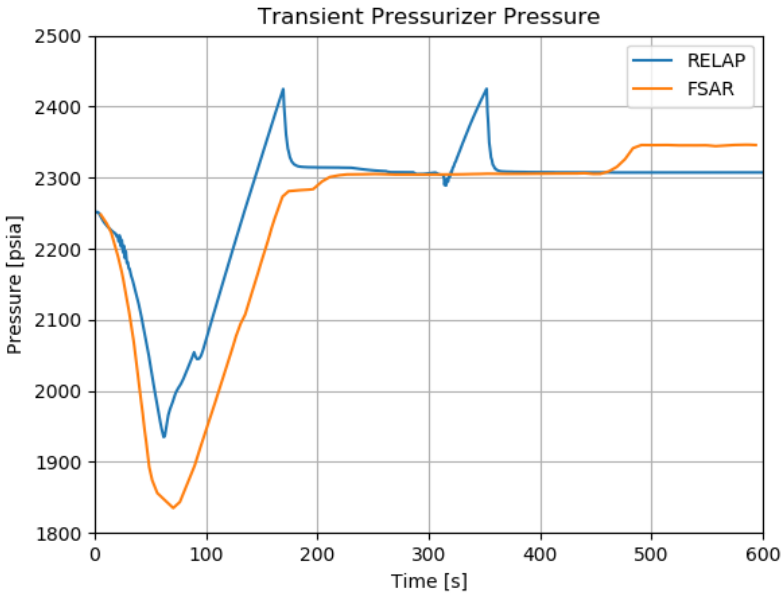

Figure 112 - Transient Pressurizer Pressure for the Inadvertent Operation of the ECCS Scenario (DNBR Case)

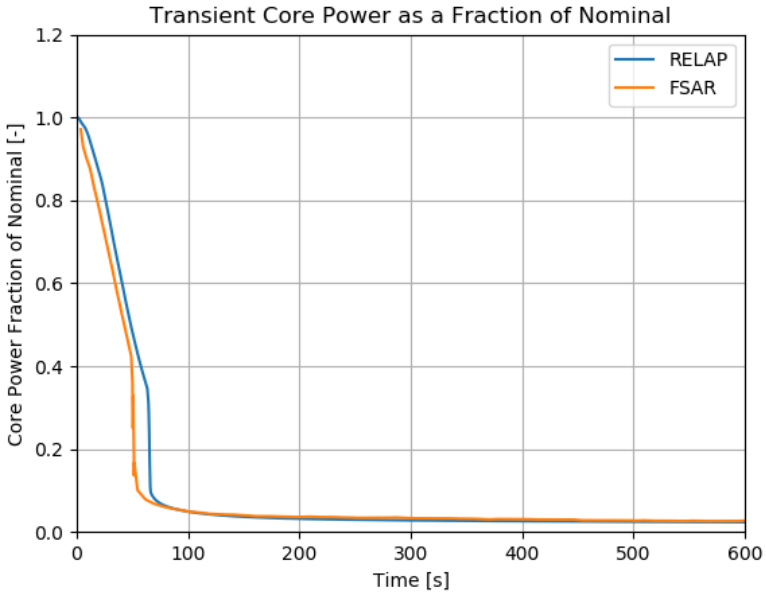

Figure 113 - Transient Core Power as a Fraction of Nominal for the Inadvertent Operation of the ECCS Scenario (DNBR Case)

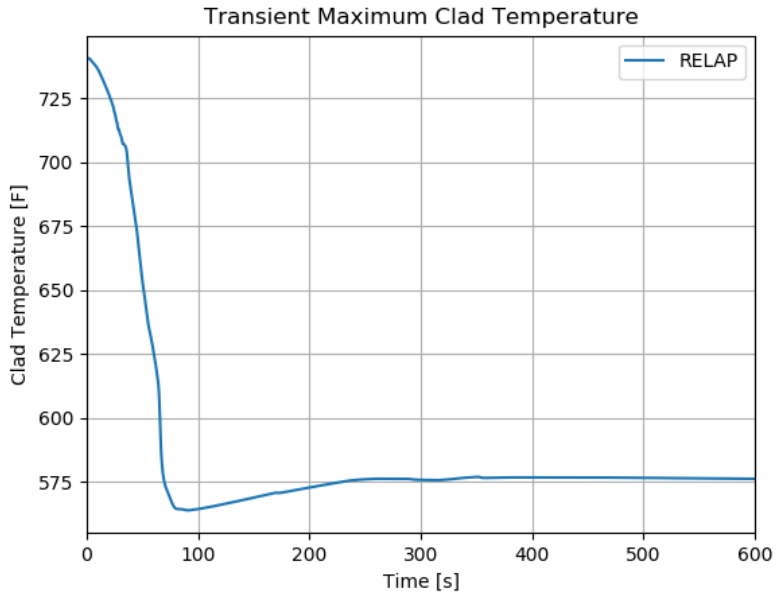

Figure 114 - Transient Maximum Cladding Temperature for the Inadvertent Operation of the ECCS Scenario (DNBR Case)

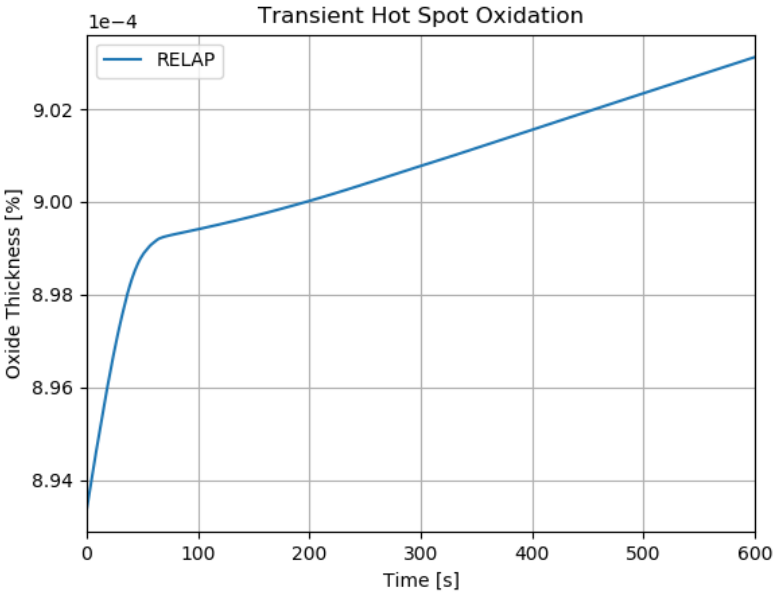

Figure 115 - Transient Hot Spot Oxidation for the Inadvertent Operation of the ECCS Scenario (DNBR Case)

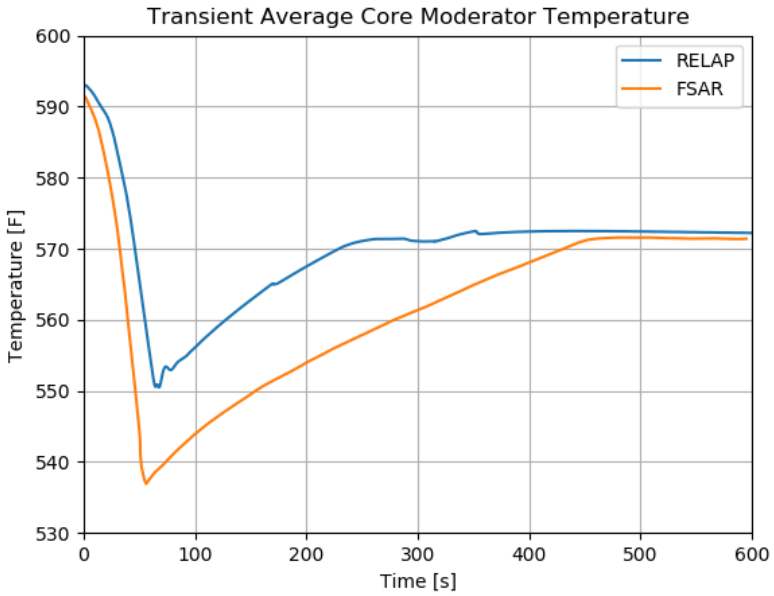

Figure 116 - Transient Average Core Moderator Temperature for the Inadvertent Operation of the ECCS Scenario (DNBR Case)

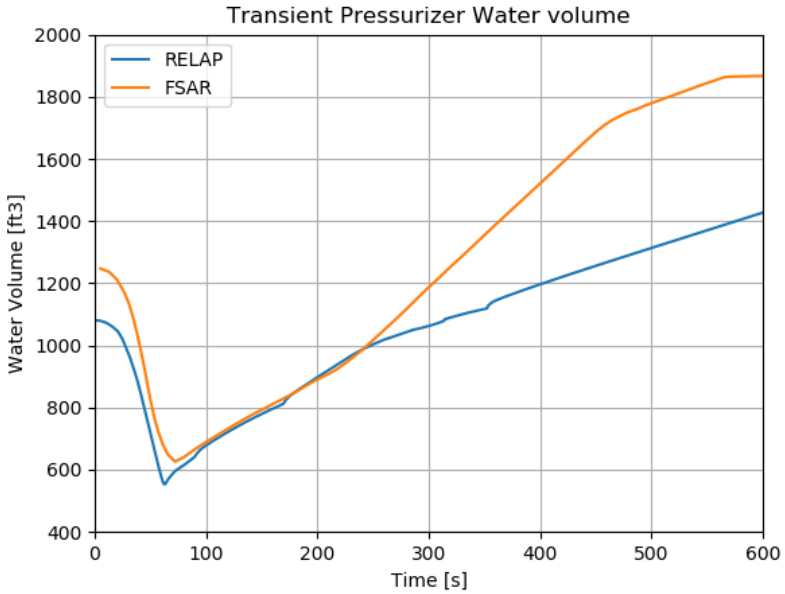

Figure 117 - Transient Pressurizer Water Volume for the Inadvertent Operation of the ECCS Scenario (DNBR Case)

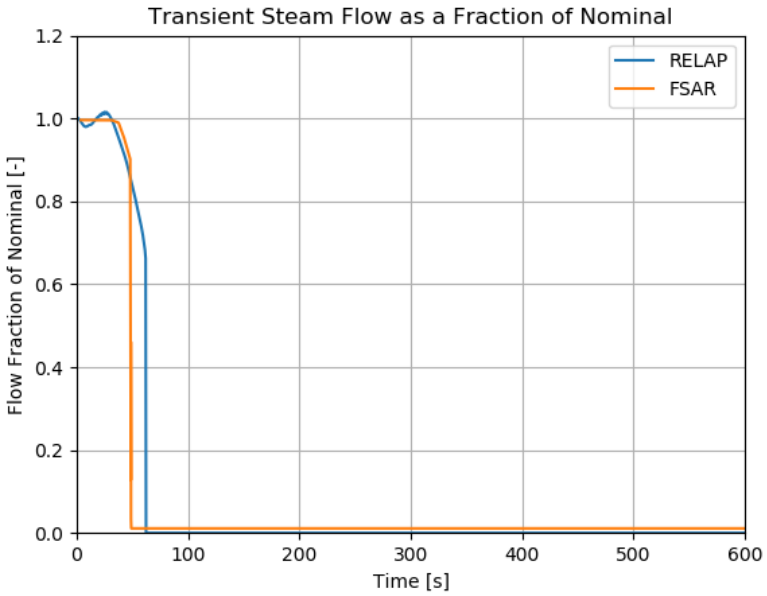

Figure 118 - Transient Steam Flow as a Fraction of Nominal for the Inadvertent Operation of the ECCS Scenario (DNBR Case)

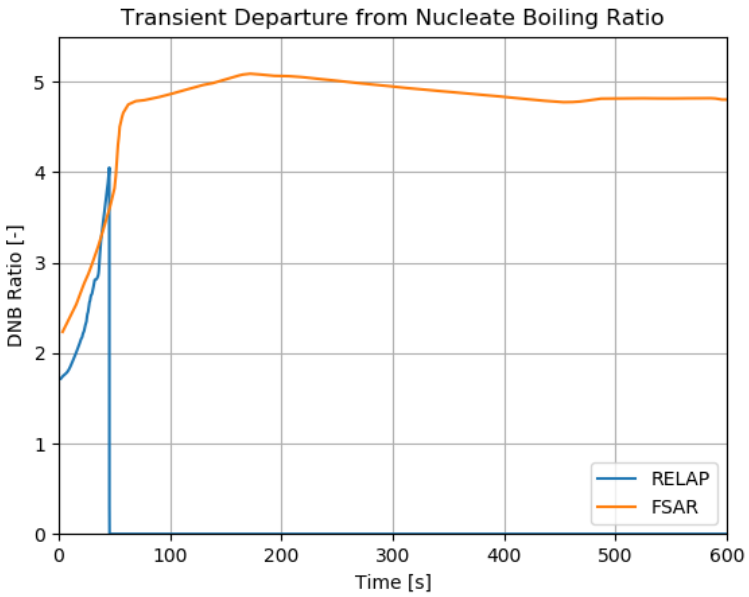

Figure 119 - Transient DNBR for the Inadvertent Operation of the ECCS Scenario (DNBR Case)

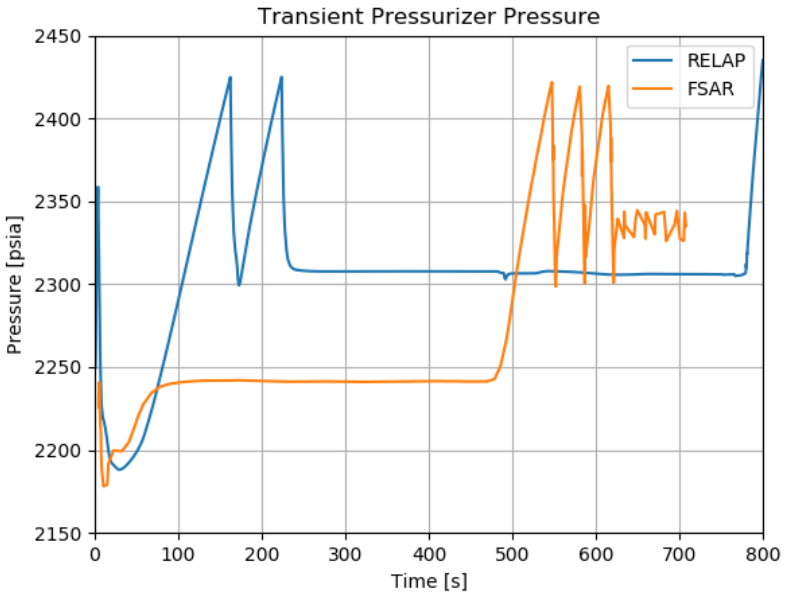

Figure 11.5-2-A: Transient Pressurizer Pressure for the Inadvertent Operation of the ECCS Scenario (Pressurizer Filling High TAVG Case)

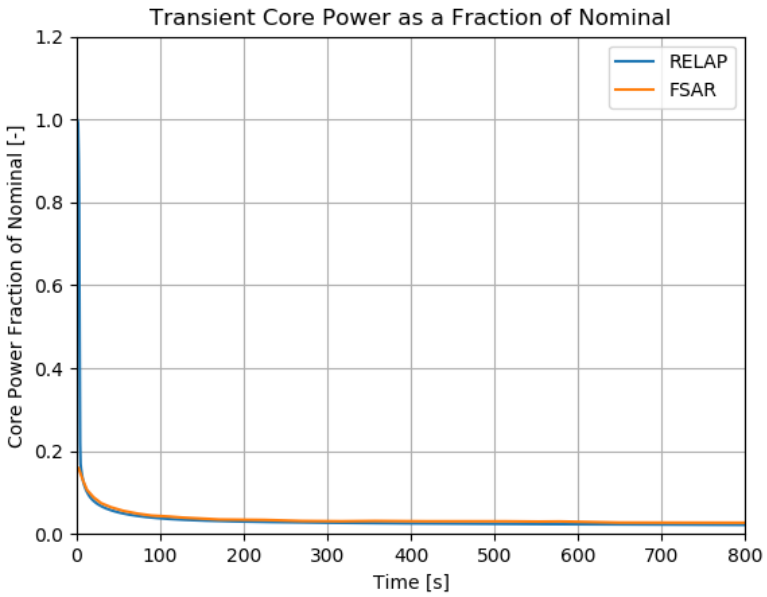

Figure 120 - Transient Core Power as a Fraction of Nominal for the Inadvertent Operation of the ECCS Scenario (Pressurizer Filling High TAVG Case)

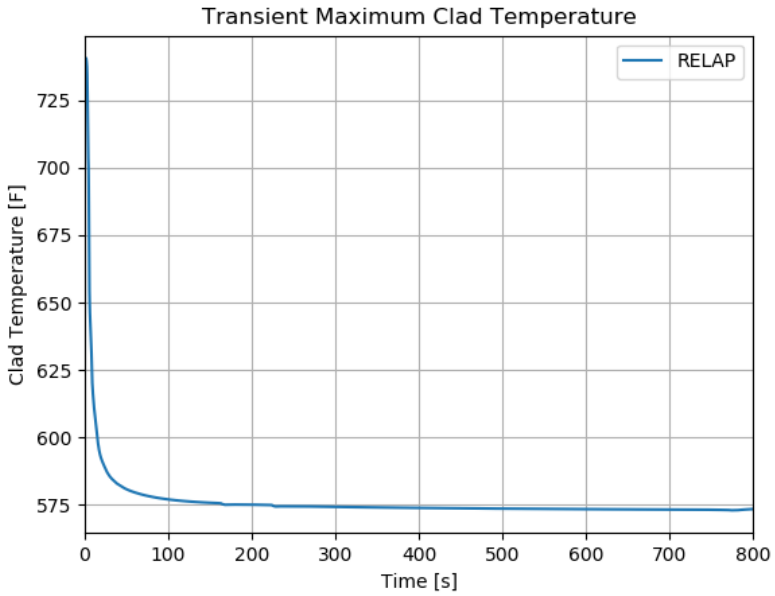

Figure 121 - Transient Maximum Cladding Temperature for the Inadvertent Operation of the ECCS Scenario (Pressurizer Filling High TAVG Case)

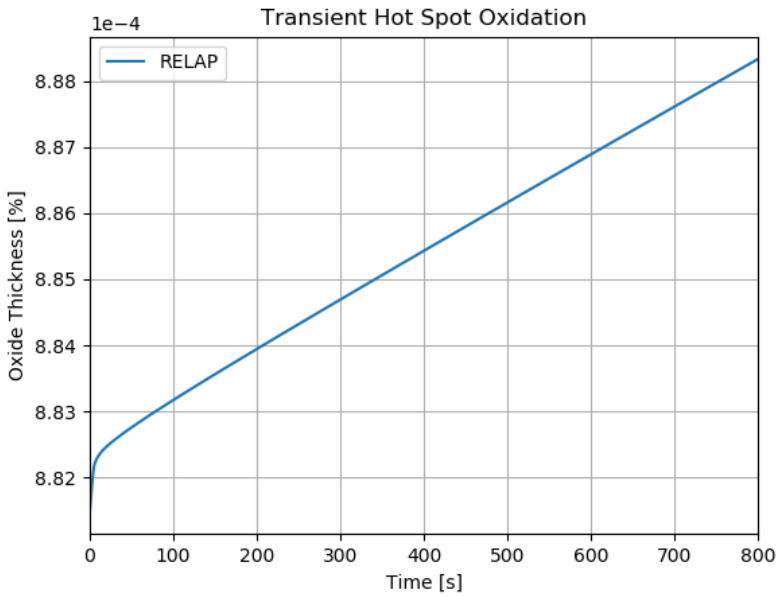

Figure 122 - Transient Hot Spot Oxidation for the Inadvertent Operation of the ECCS Scenario (Pressurizer Filling High TAVG Case)

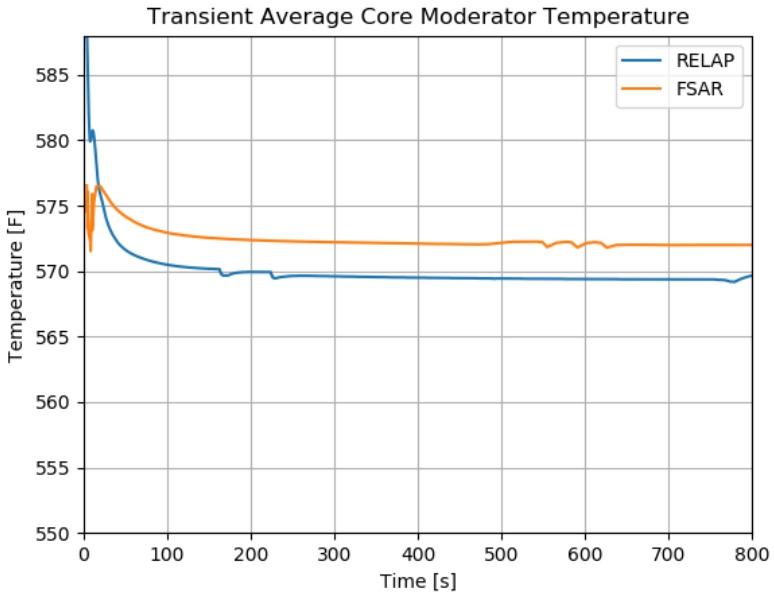

Figure 123 - Transient Average Core Moderator Temperature for the Inadvertent Operation of the ECCS Scenario (Pressurizer Filling High TAVG Case)

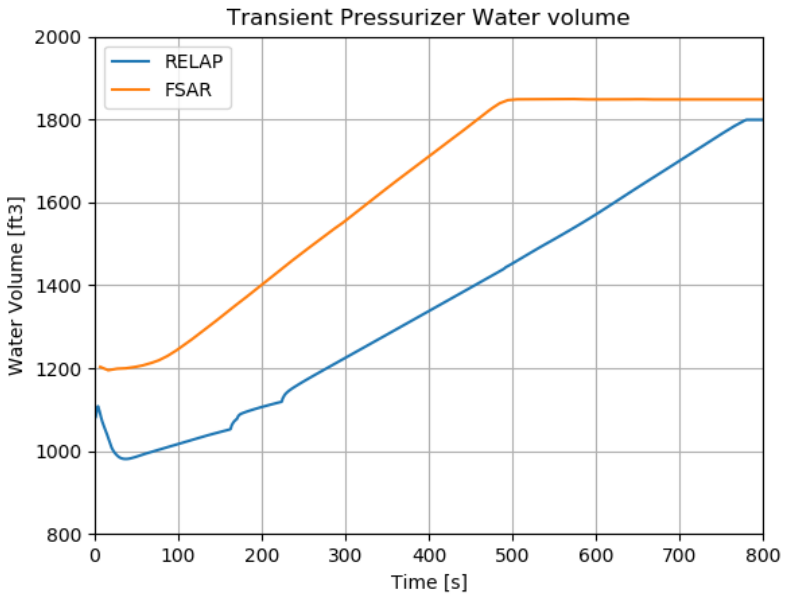

Figure 124 - Transient Pressurizer Water Volume for the Inadvertent Operation of the ECCS Scenario (Pressurizer Filling High TAVG Case)

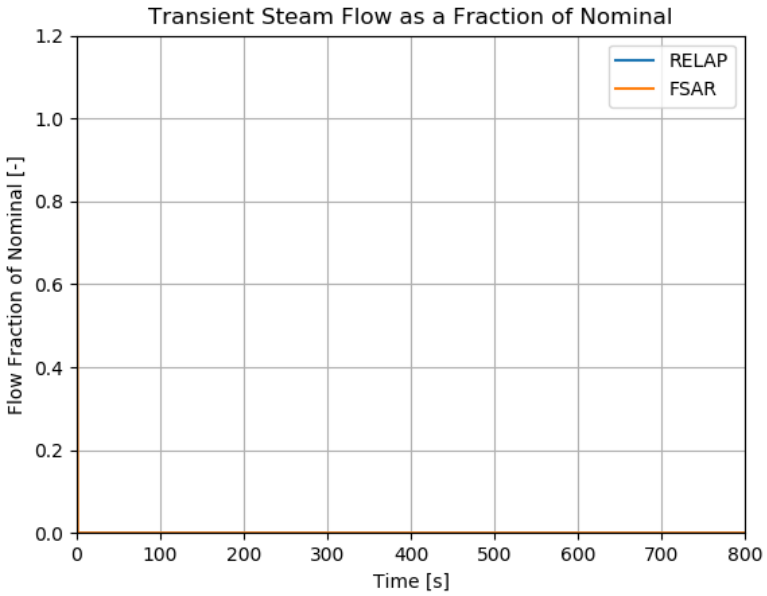

Figure 125 - Transient Steam Flow as a Fraction of Nominal for the Inadvertent Operation of the ECCS Scenario (Pressurizer Filling High TAVG Case)

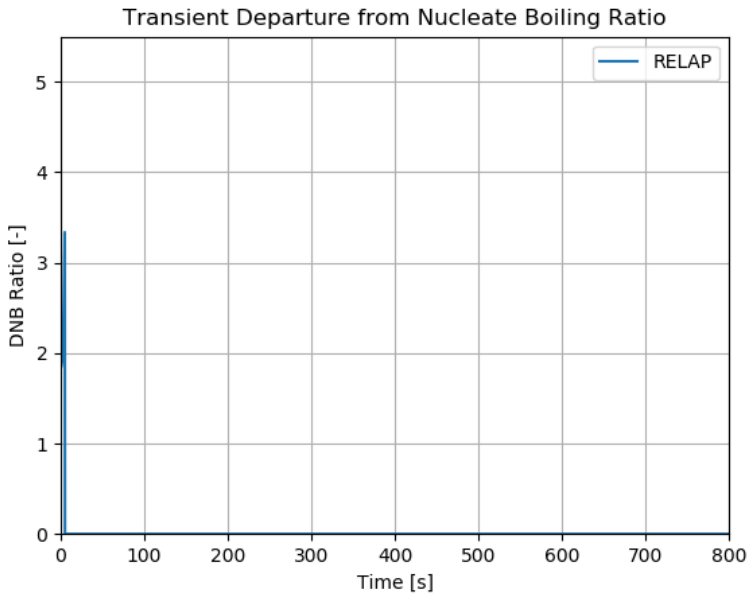

Figure 126 - Transient DNBR for the Inadvertent Operation of the ECCS Scenario (Pressurizer Filling High TAVG Case)

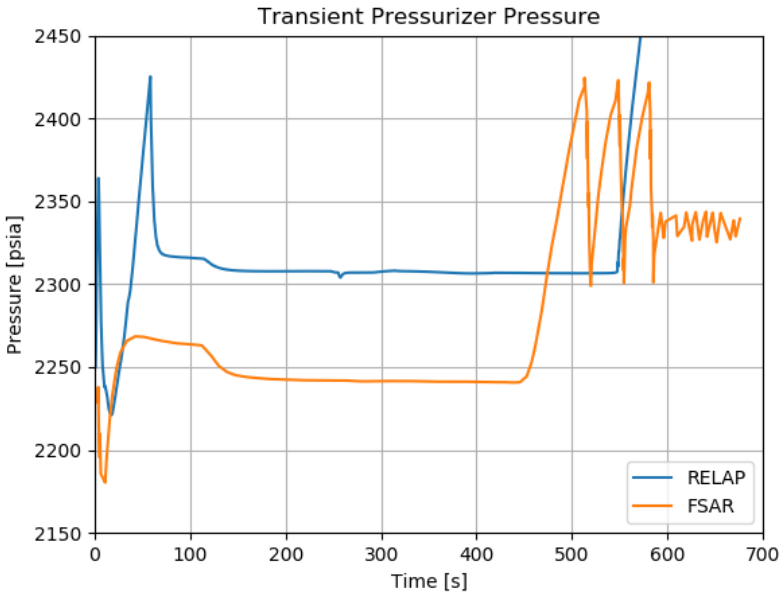

Figure 127 - Transient Pressurizer Pressure for the Inadvertent Operation of the ECCS Scenario (Pressurizer Filling Low TAVG Case)

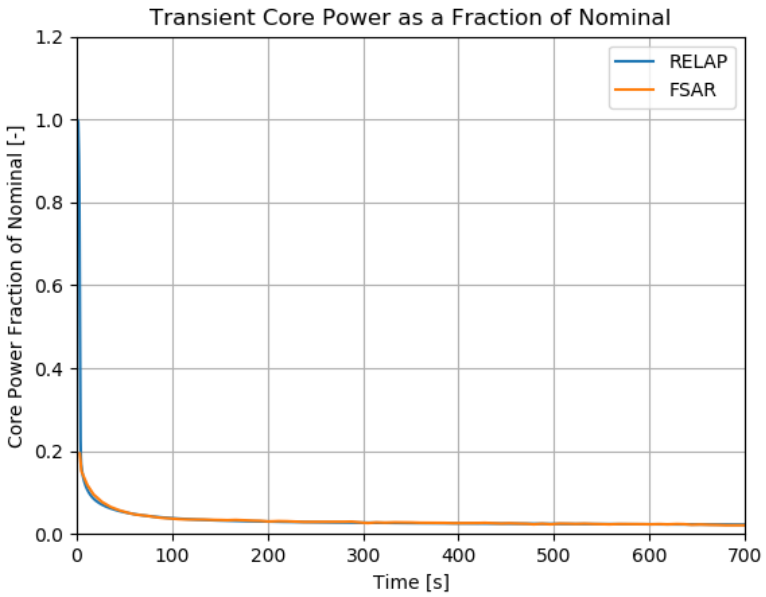

Figure 128 - Transient Core Power as a Fraction of Nominal for the Inadvertent Operation of the ECCS Scenario (Pressurizer Filling Low TAVG Case)

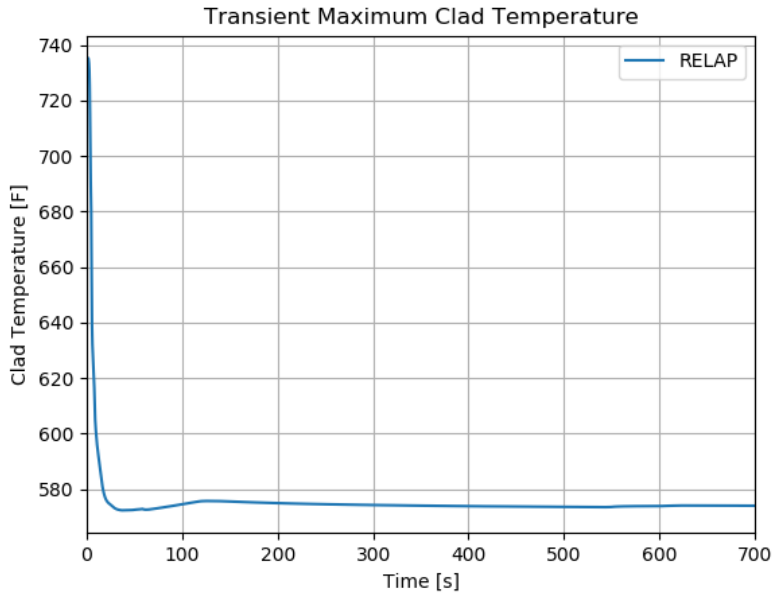

Figure 129 - Transient Maximum Cladding Temperature for the Inadvertent Operation of the ECCS Scenario (Pressurizer Filling Low TAVG Case)

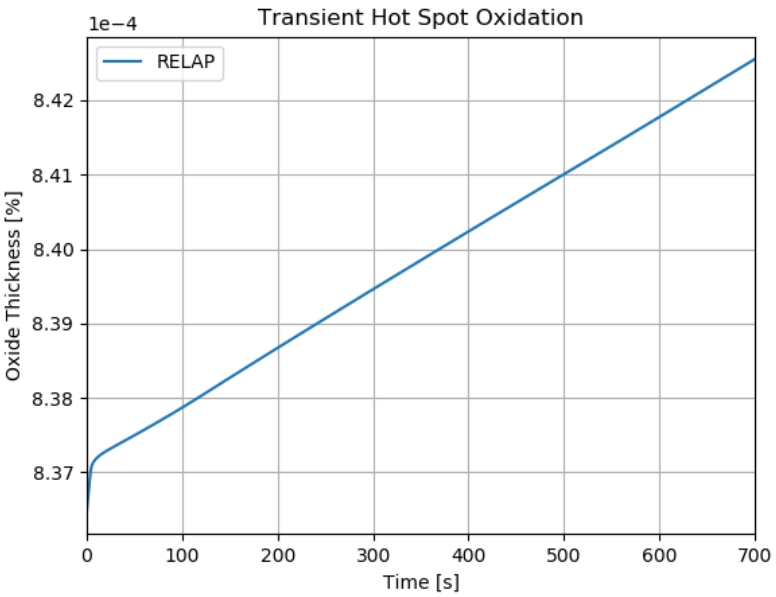

Figure 130 - Transient Hot Spot Oxidation for the Inadvertent Operation of the ECCS Scenario (Pressurizer Filling Low TAVG Case)

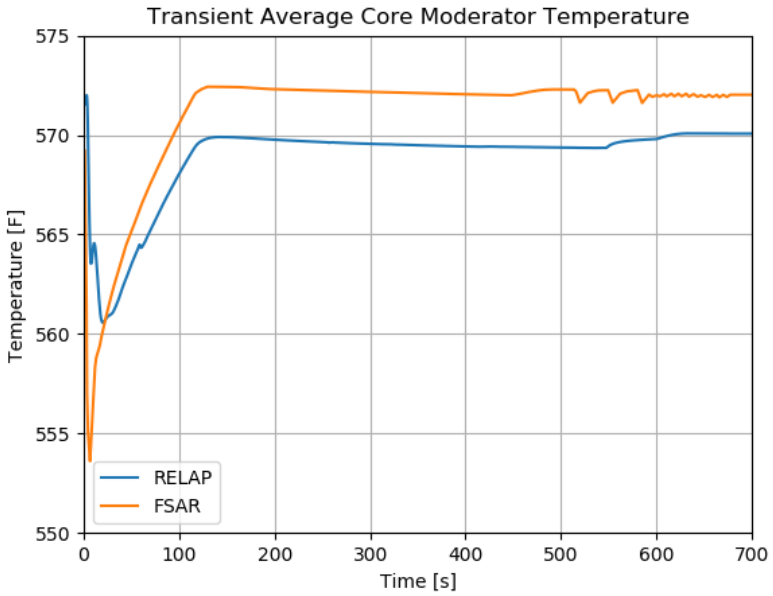

Figure 131 - Transient Average Core Moderator Temperature for the Inadvertent Operation of the ECCS Scenario (Pressurizer Filling Low TAVG Case)

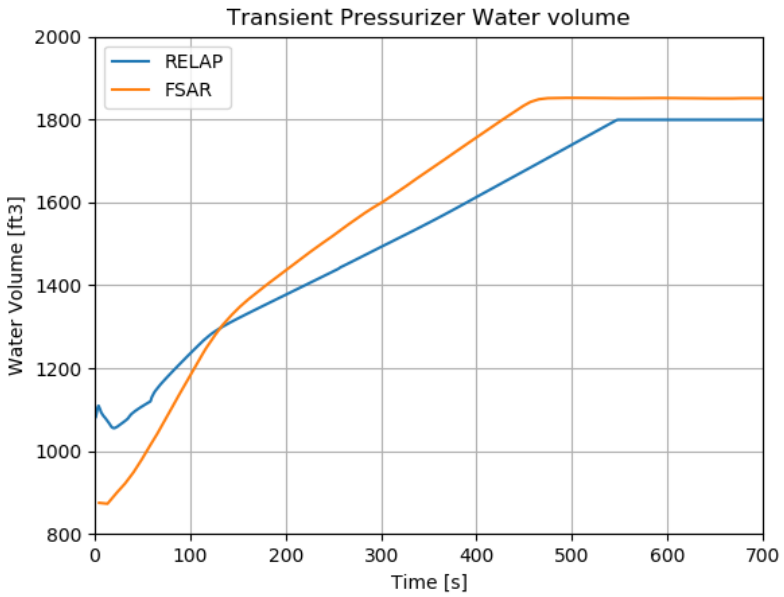

Figure 132 - Transient Pressurizer Water Volume for the Inadvertent Operation of the ECCS Scenario (Pressurizer Filling Low TAVG Case)

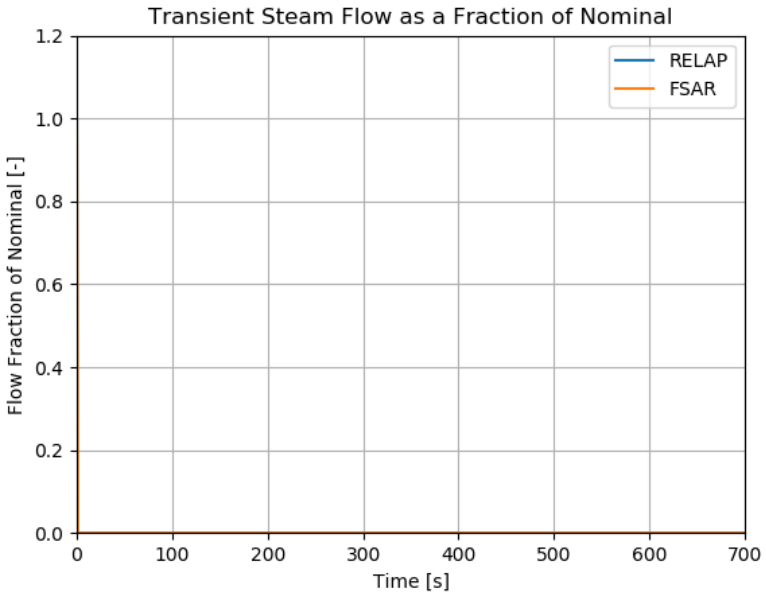

Figure 133 - Transient Steam Flow as a Fraction of Nominal for the Inadvertent Operation of the ECCS Scenario (Pressurizer Filling Low TAVG Case)

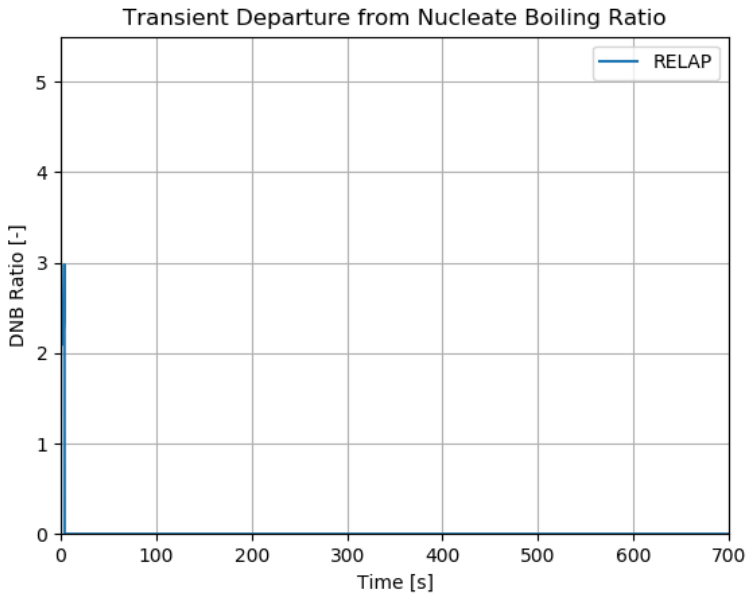

Figure 134 - Transient DNBR for the Inadvertent Operation of the ECCS Scenario (Pressurizer Filling Low TAVG Case)

4.2.8 Feedwater System Malfunctions that Result in an Increase in Feedwater Flow

Feedwater System Malfunctions that Result in an Increase in Feedwater Flow are classified as American Nuclear Society Condition II events, fault of moderate frequency.

Addition of excessive feedwater will cause an increase in core power by decreasing reactor coolant temperature. The thermal capacity of the secondary side of the plant and the RCS attenuates such transients. The steam generator high-high water level signal terminates the excessive feedwater flow. It also initiates a turbine trip that results in a reactor trip and trips the SG feedwater pumps. Should the turbine trip not initiate a reactor trip, the subsequent reduction in steam generator water level will initiate a reactor trip on steam generator low-low level.

The full opening of a feedwater regulating valve due to a feedwater control system malfunction or an operator error may cause excessive feedwater flow. At power conditions, this excess flow causes a greater load demand on the RCS due to increased subcooling in the steam generator. With the plant at no-load conditions, the addition of cold feedwater may cause a decrease in RCS temperature and thus a reactivity insertion due to the effects of the negative moderator temperature coefficient of reactivity.

The steam generator high-high water level ESF signal does the following:

- Closes the feedwater valves.
- Closes the feedwater pump discharge valves.
- Trips the turbine.
- Trips the main feedwater pumps.
- Prevents continuous addition of excessive feedwater.

The turbine trip signal initiates a reactor trip.

4.2.8.1 Results

The RELAP results are compared to the run from the FSAR in the paragraphs below.

The transient pressurizer pressure is shown in Figure 135. The RELAP run pressurizes earlier than the FSAR run due to earlier reactor trip, and the pressurizer is higher, but much shorter in duration.

The transient hot rod heat flux as a fraction of nominal is shown in Figure 136. The RELAP run has a much smaller heat flux increase and the reactor trips earlier.

The transient core power as a fraction of nominal is shown in Figure 137. The RELAP run has a much smaller power increase and the reactor trips earlier.

The transient maximum cladding temperature is shown in Figure 138. There is no FSAR plot for this. The RELAP run continues at the SS temperature until the reactor trip.

The transient hot spot oxidation is shown in Figure 139. There is no FSAR plot for this. There is no significant oxidation accrual during this transient.

The transient average core moderator temperature is shown in Figure 140. The RELAP run encounters a much smaller increase in temperature, and decreases earlier, due to the earlier reactor trip.

The transient DNBR is shown in Figure 141. The DNBR is similar prior to reactor trip, and in both cases, it increases after trip. The RELAP run immediately goes to 0 after trip. In RELAP, this indicates that the heat structure is in a HT mode which does not even calculate CHF (i.e., single phase liquid). As such, this is consistent with the very high DNBR observed in the FSAR run.

The transient reactor vessel change in temperature is shown in Figure 142. The transients are very similar, except that the RELAP run decreases much earlier due to the earlier reactor trip.

The transient fuel centerline temperature is shown in Figure 143. There is no FSAR plot for this. The fuel centerline temperature continues at approximately the SS temperature until reactor trip, when it drops very quickly.

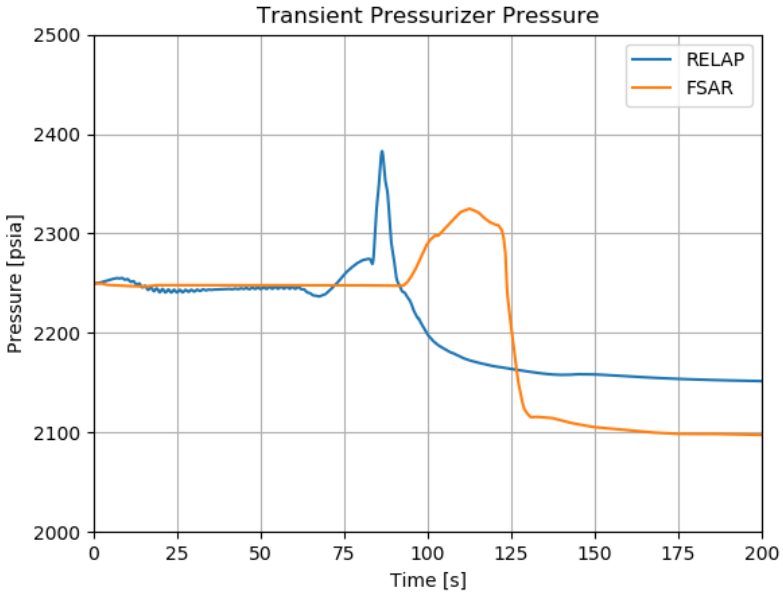

Figure 135 - Transient Pressurizer Pressure for the Feedwater Malfunction Scenario

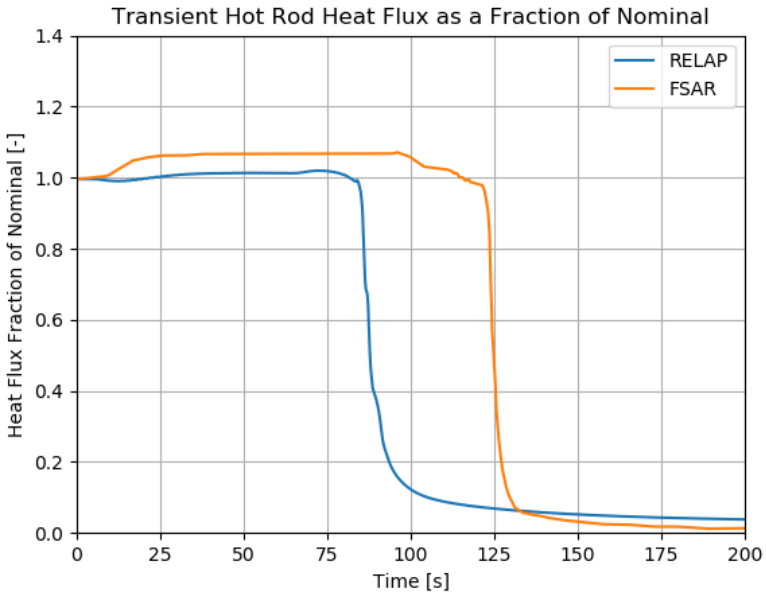

Figure 136 - Transient Hot Rod Heat Flux as a Fraction of Nominal for the Feedwater Malfunction Scenario

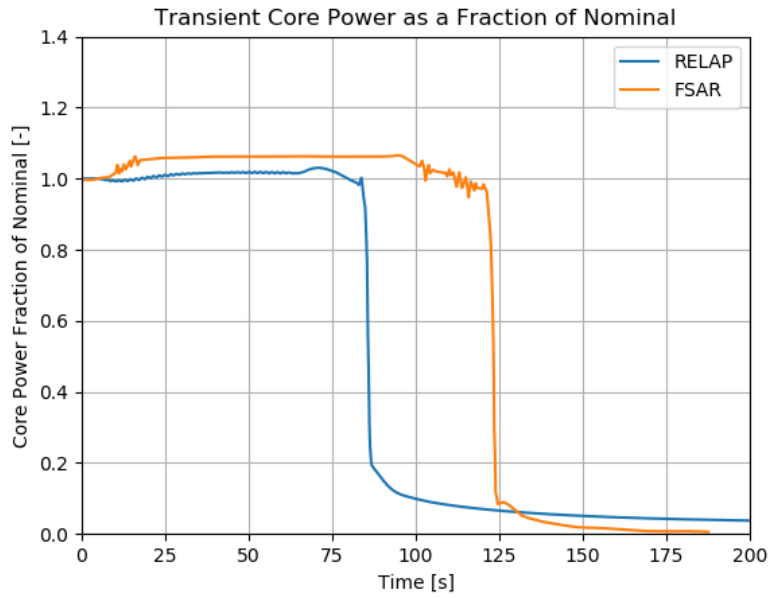

Figure 137 - Transient Core Power as a Fraction of Nominal for the Feedwater Malfunction Scenario

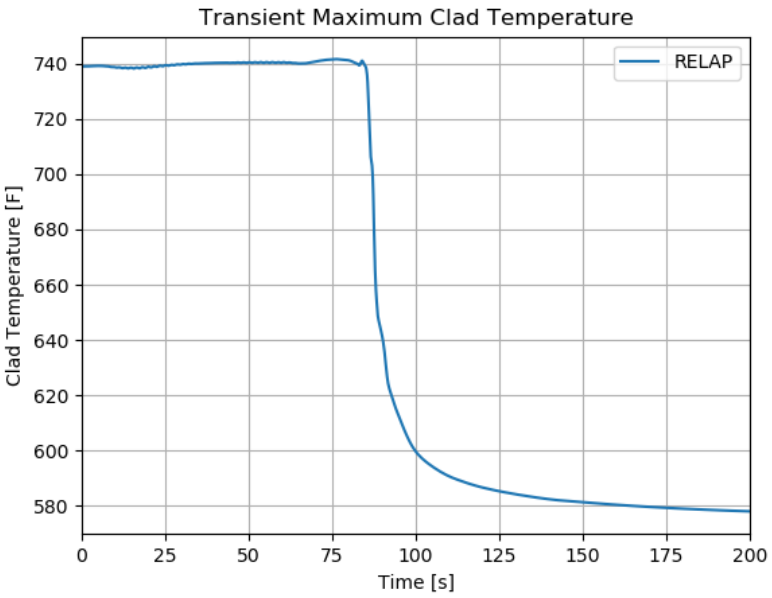

Figure 138 - Transient Maximum Clad Temperature for the Feedwater Malfunction Scenario

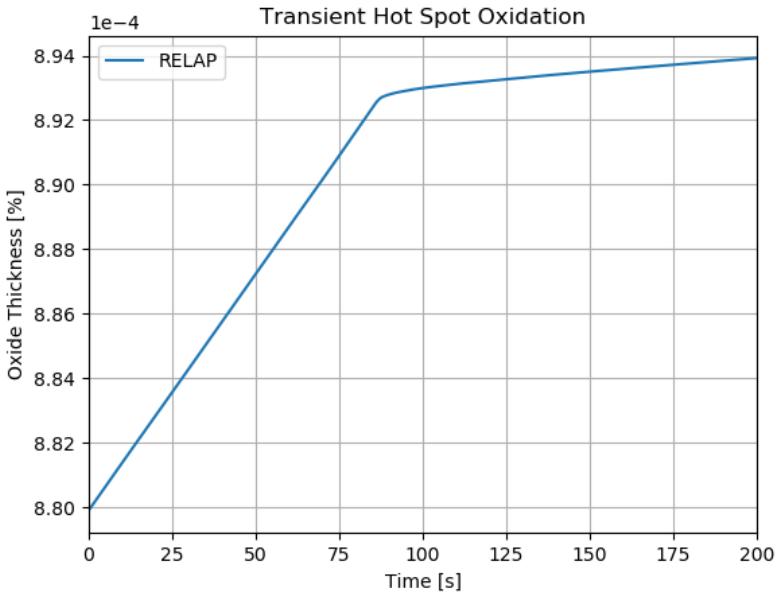

Figure 139 - Transient Hot Spot Oxidation for the Feedwater Malfunction Scenario

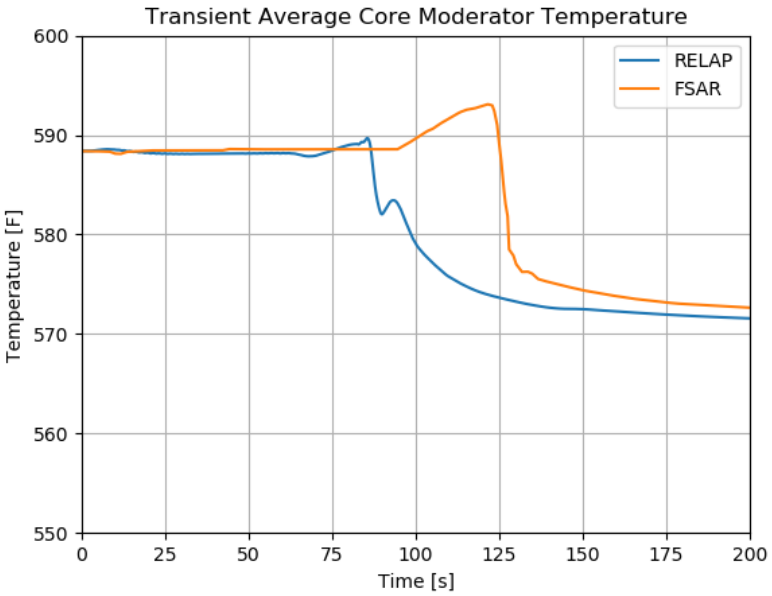

Figure 140 - Transient Average Core Moderator Temperature for the Feedwater Malfunction Scenario

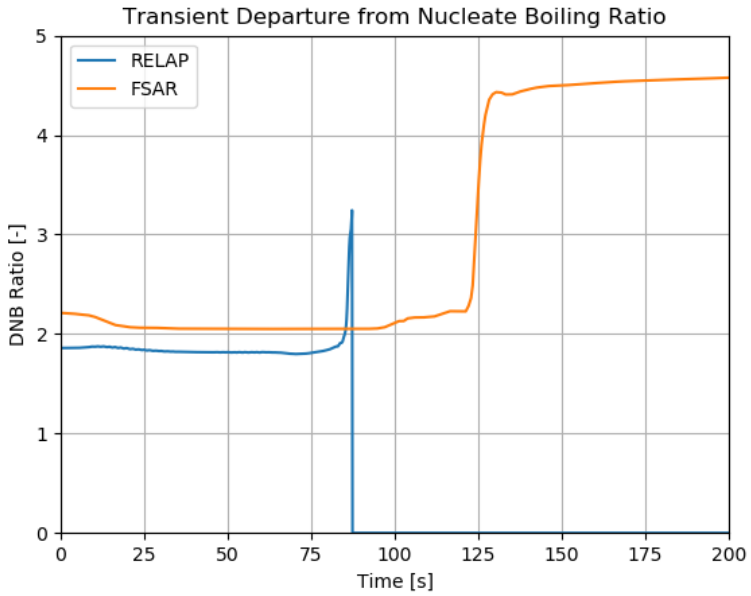

Figure 141 - Transient DNBR for the Feedwater Malfunction Scenario

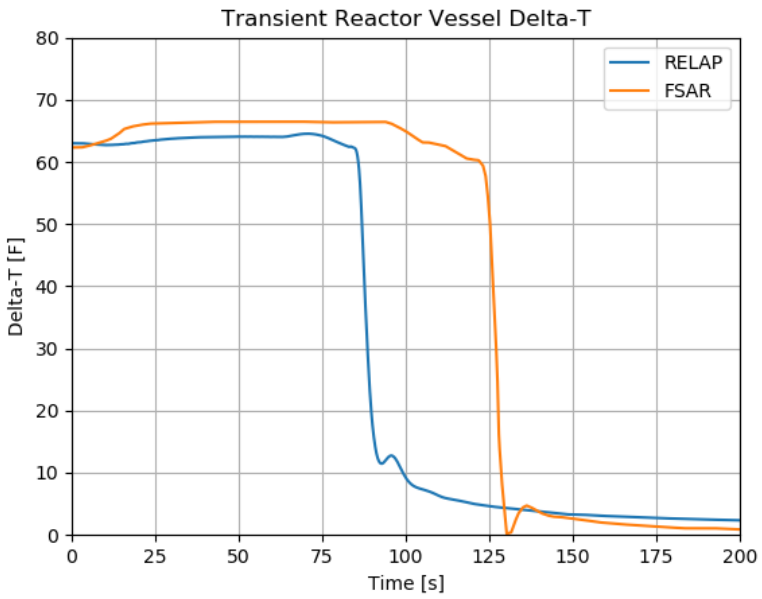

Figure 142 - Transient Reactor Vessel Change in Temperature for the Feedwater Malfunction Scenario

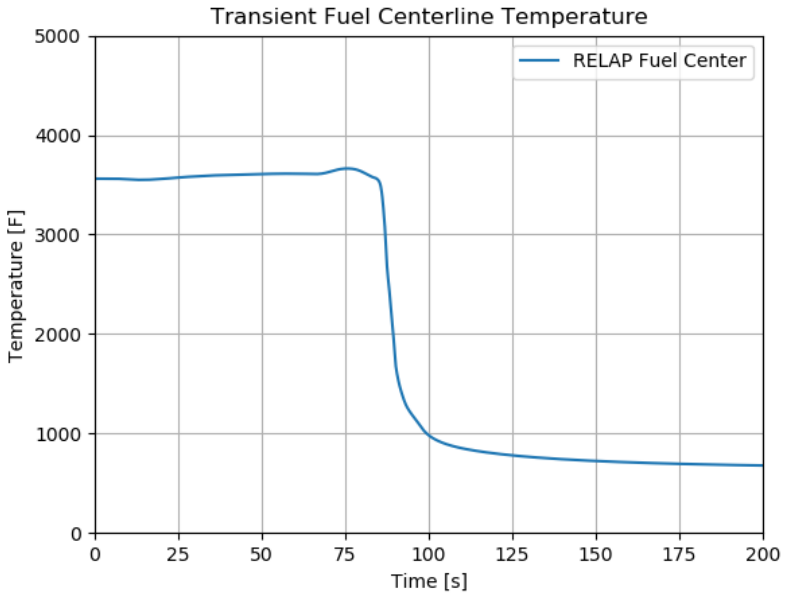

Figure 143 - Transient Fuel Centerline Temperature for the Feedwater Malfunction Scenario

4.2.9 Steam Generator Tube Failure

This event is also called a steam generator tube rupture (SGTR). The accident examined is the complete severance of a single steam generator tube. This event is considered an ANS Condition IV event, a limiting fault.

The accident is assumed to take place at full power with the reactor coolant contaminated with fission products corresponding to continuous operation with a number of defective fuel rods.

The accident leads increased contamination of the secondary system due to leakage of radioactive coolant from the reactor coolant system (RCS). In the event of a coincident loss of offsite power or failure of the condenser steam dump system, discharge of activity to the atmosphere takes place via the steam generator power-operated relief valves (and safety valves if their setpoint is reached).

The operator is assumed to determine that a steam generator tube rupture has occurred, to identify and isolate the faulted steam generator, and to complete the required recovery actions to stabilize the plant and terminate the primary to secondary break flow. These actions are performed on a restricted time scale in order to minimize contamination of the secondary system and ensure termination of radioactive release to the atmosphere.

If normal operation of the various plant control system is assumed, the following sequence of events is initiated by a tube rupture:

A. Pressurizer low-pressure and low-level alarms are actuated and charging pump flow increases in an attempt to maintain pressurizer level. On the secondary side, steam flow/feedwater flow mismatch occurs, since feedwater flow to the affected steam generator is reduced as a result of primary coolant break flow to that unit.
B. The main steamline radiation monitors, the condenser air ejector radiation monitor, and/or the steam generator blowdown liquid monitor will alarm, indicating a sharp

increase in radioactivity in the secondary system. The high radiation level alarm from the steam generator blowdown process monitor automatically isolates the system and terminates discharge. The high radiation level alarm from the air ejector monitor automatically diverts the air ejector and steam seal exhauster blower discharges through a filtration unit.

C. The decrease in RCS pressure due to continued loss of reactor coolant inventory leads to a reactor trip signal on low pressurizer pressure or OTΔT. Resultant plant cooldown following reactor trip leads to a rapid decrease in RCS pressure and pressurizer level, and a safety injection signal initiated by low pressurizer pressure follows soon after reactor trip. The safety injection signal automatically terminates normal feedwater supply and initiates auxiliary feedwater addition.
D. The reactor trip automatically trips the turbine, and if offsite power is available, the steam dump valves open, permitting steam dump to the condenser. In the event of a coincident loss of offsite power, the steam dump valves automatically close to protect the condenser. The steam generator pressure rapidly increases, resulting in steam discharge to the atmosphere through the steam generator power-operated relief valves (and safety valves if their setpoint is reached).
E. Following reactor trip and safety injection actuation, the continued action of the auxiliary feedwater supply and borated safety injection flow (supplied from the refueling water storage tank) provides a heat sink which absorbs some of the decay heat. This reduces the amount of steam bypass to the condenser, or in the case of loss of offsite power, steam relief to the atmosphere.

Safety injection flow results in increasing RCS pressure and pressurizer water level, and the RCS pressure trends toward the equilibrium value where the safety injection flow rate equals the break flow rate.

4.2.9.1 Results

The RELAP results are compared to the run from the FSAR in the paragraphs below.

The transient pressurizer pressure is shown in Figure 144. The RELAP run follows the FSAR run pretty well. Between about 1000 and 4000 seconds, the RELAP run is consistently lower than the FSAR run but follows similar behavior. After the large depressurization at ~3800 seconds, the RELAP run continues to repressurize, while the FSAR run goes back down. This is likely because the RELAP run never hits a point where the secondary side and primary side pressures are equal, so the SI keeps going in the RELAP run.

The transient core power as a fraction of nominal is shown in Figure 145. There is no FSAR plot for this. The RELAP run has a small power increase, and then reactor trip and a reasonable decay heat curve.

The transient maximum cladding temperature is shown in Figure 146. There is no FSAR plot for this. The RELAP run has a short, but large temperature excursion during the initial power excursion.

The transient hot spot oxidation is shown in Figure 147. There is no FSAR plot for this. A non-negligible amount of oxidation is accrued during the clad temperature spike, but no appreciable oxidation is accrued after that.

The transient DNBR is shown in Figure 148. There is no FSAR plot for this. The DNBR nearly always at 0 for this transient. During the power/clad temperature spike, there appears to be some movement, but its hard to see what. It is safe to say that during the clad temperature spike, it

undergoes CHF, and based on the low clad temperature for the rest of the transient, it is likely in single phase liquid.

The transient pressurizer level is shown in Figure 149. The RELAP run follows the FSAR run pretty well. Between about 1000 and 3500 seconds, the RELAP run is consistently lower than the FSAR run but follows similar behavior. After the large depressurization at ~3800 seconds, the RELAP run continues to increase the level, while the FSAR run goes back down. This is likely because the RELAP run never hits a point where the secondary side and primary side pressures are equal, so the SI keeps going in the RELAP run.

The transient secondary side pressures are shown in Figure 150. For the intact SGs, the RELAP run follows the FSAR run very well. For the ruptured SG, the patterns followed are similar, but the RELAP run has significantly lower pressure. This explains why the RELAP run never actually hits the requirement that the RCS pressure get below the secondary side pressure.

The transient intact loop primary temperatures are shown in Figure 151. The temperatures in the RELAP run drop significantly more than those in the FSAR run, but otherwise follows the FSAR run behavior pretty well.

The transient broken loop primary temperatures are shown in Figure 152. The temperatures in the RELAP run drop significantly more than those in the FSAR run, but otherwise follows the FSAR run behavior pretty well.

The transient differential pressure between the RCS and the ruptured SG is shown in Figure 153. The RELAP run follows the FSAR run well, until the end of the transient, when the continued SI operation causes the RELAP run to be significantly higher.

The transient mass flow between the RCS and the ruptured SG is shown in Figure 154. The RELAP run follows the FSAR run well, until the end of the transient, when the continued SI operation causes the RELAP run to be significantly higher.

The transient ruptured SG water volume is shown in Figure 155. The general behavior is consistent between the RELAP run and the FSAR run, but the RELAP run has generally more exaggerated reactions.

The transient ruptured SG water volume is shown in Figure 156. The general behavior is consistent between the RELAP run and the FSAR run, but the RELAP run has generally more exaggerated reactions.

The transient mass flow to the atmosphere from the ruptured SG is shown in Figure 157.The general behavior is consistent between the RELAP run and the FSAR run.

The transient mass flow to the atmosphere from the intact SGs is shown in Figure 158. The general behavior is consistent between the RELAP run and the FSAR run.

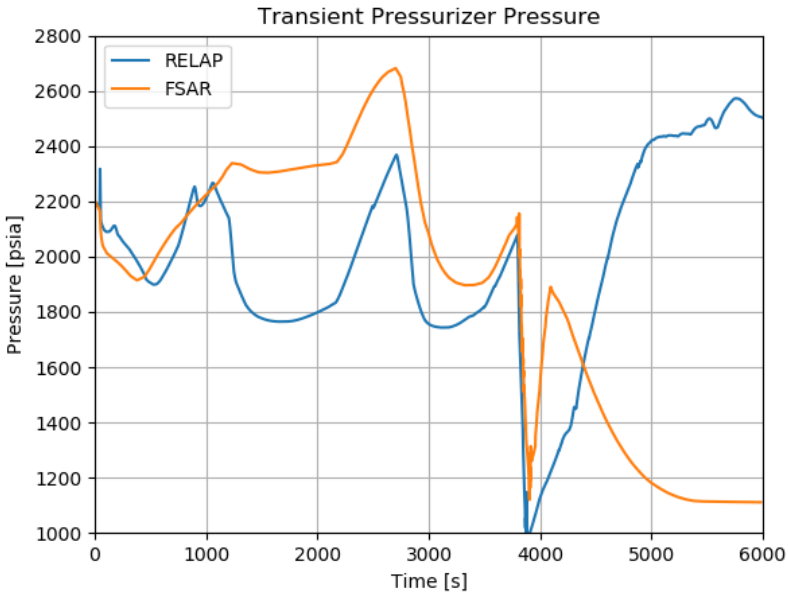

Figure 144 - Transient Pressurizer Pressure for the SGTR Scenario

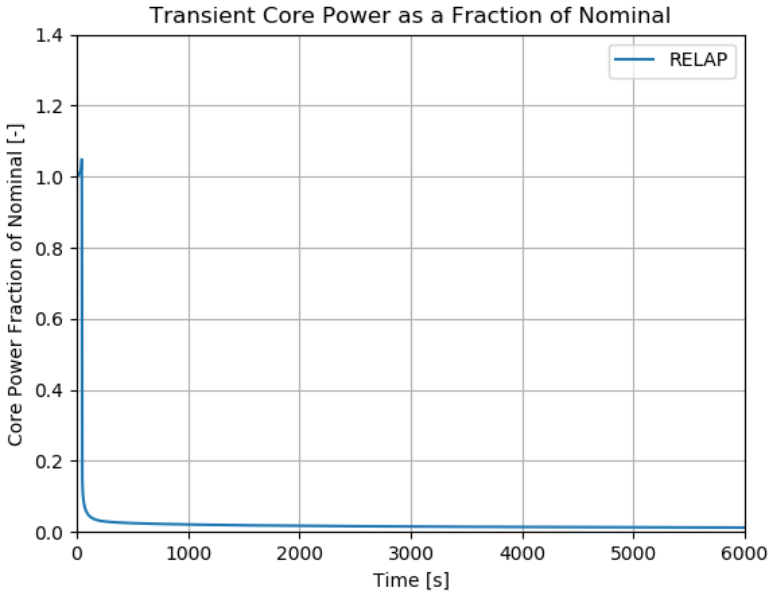

Figure 145 - Transient Core Power as a Fraction of Nominal for the SGTR Scenario

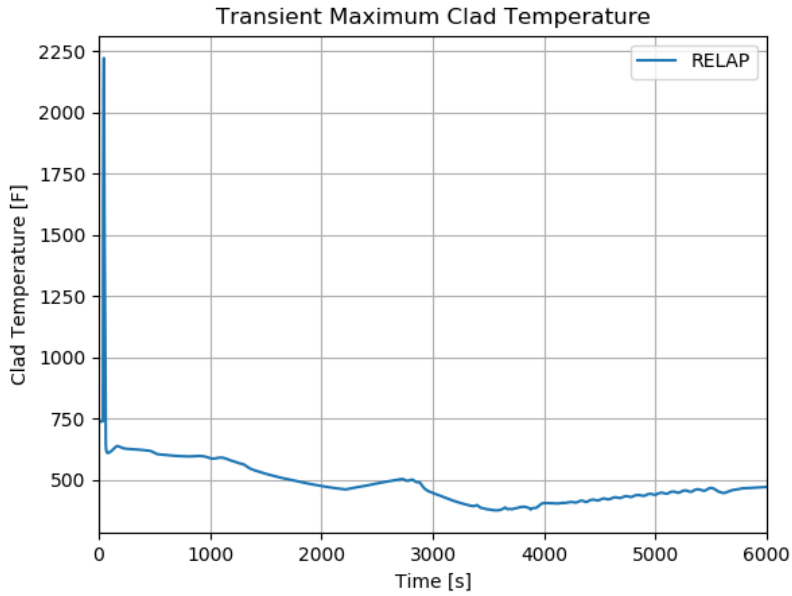

Figure 146 - Transient Maximum Clad Temperature for the SGTR Scenario

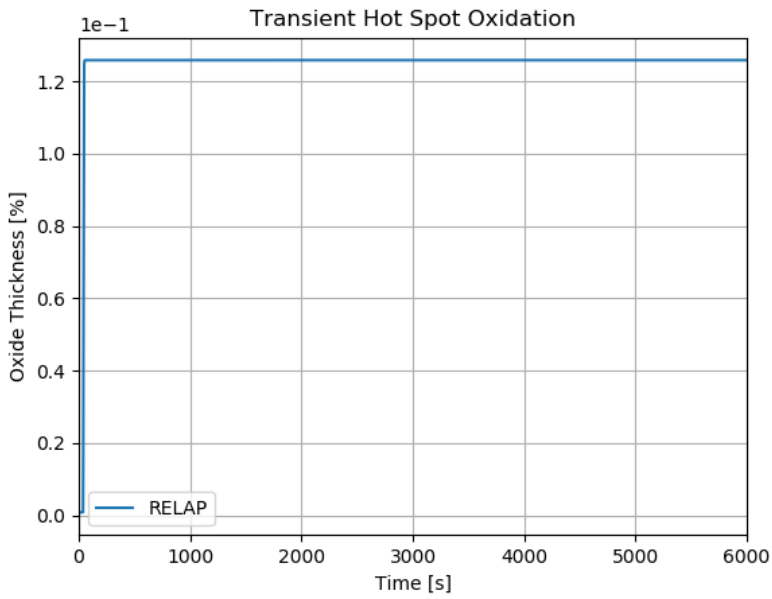

Figure 147 - Transient Hot Spot Oxidation for the SGTR Scenario

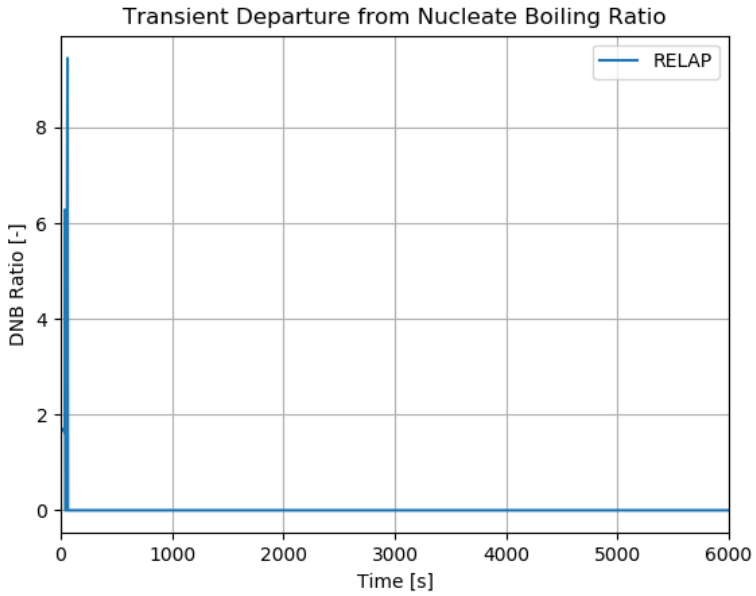

Figure 148 - Transient DNBR for the SGTR Scenario

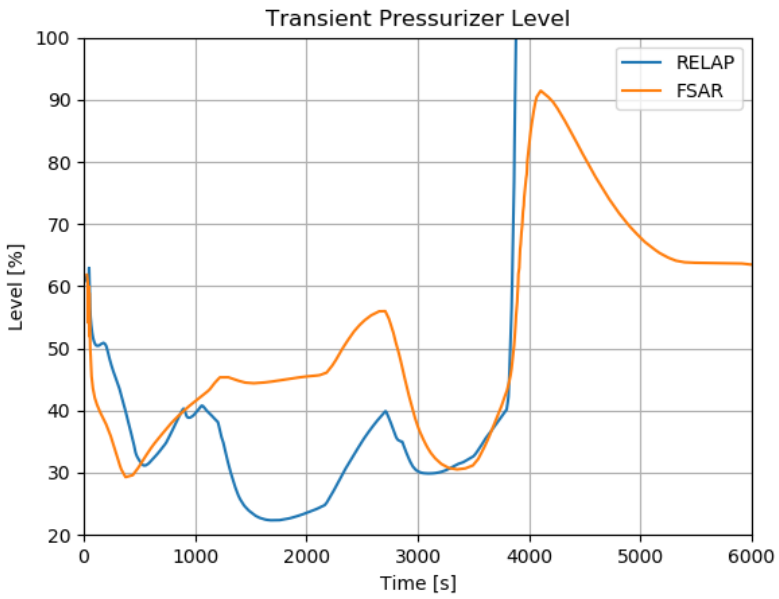

Figure 149 - Transient Pressurizer Level for the SGTR Scenario

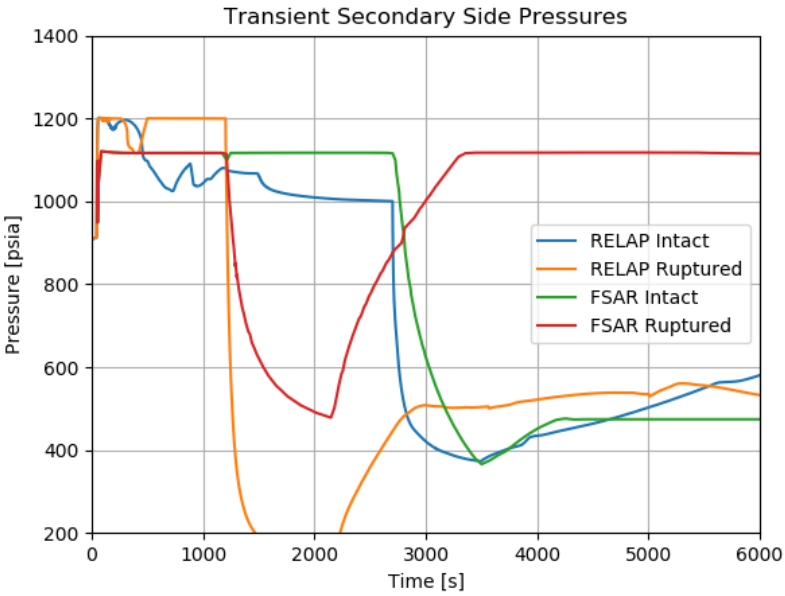

Figure 150 - Transient Secondary Side Pressures for the SGTR Scenario

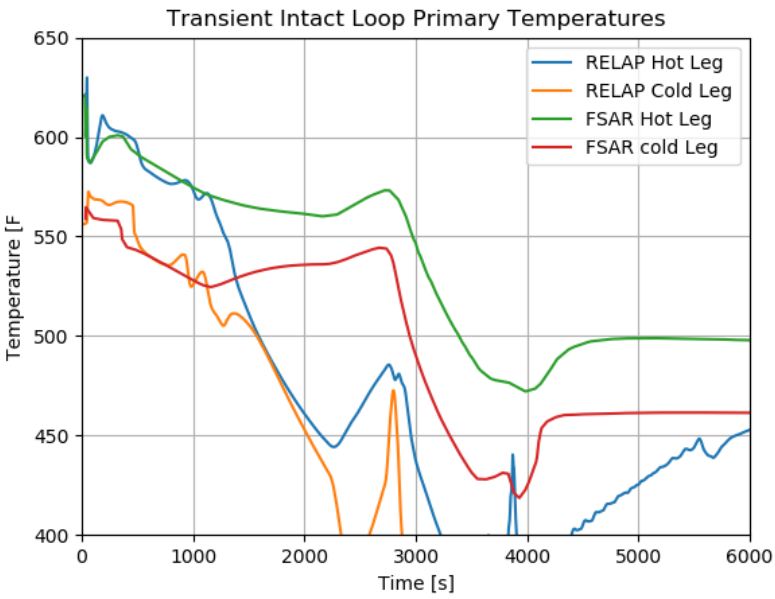

Figure 151 - Transient Intact Loop Primary Temperatures for the SGTR Scenario

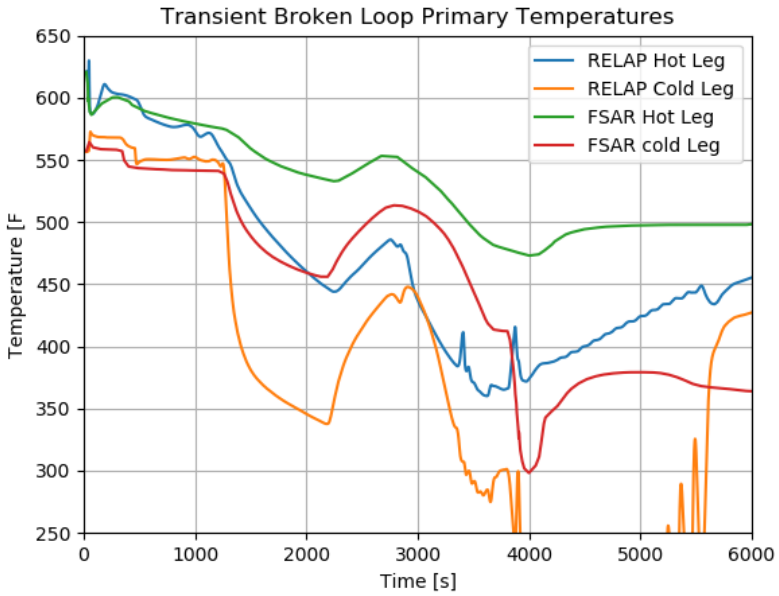

Figure 152 - Transient Broken Loop Primary Temperatures for the SGTR Scenario

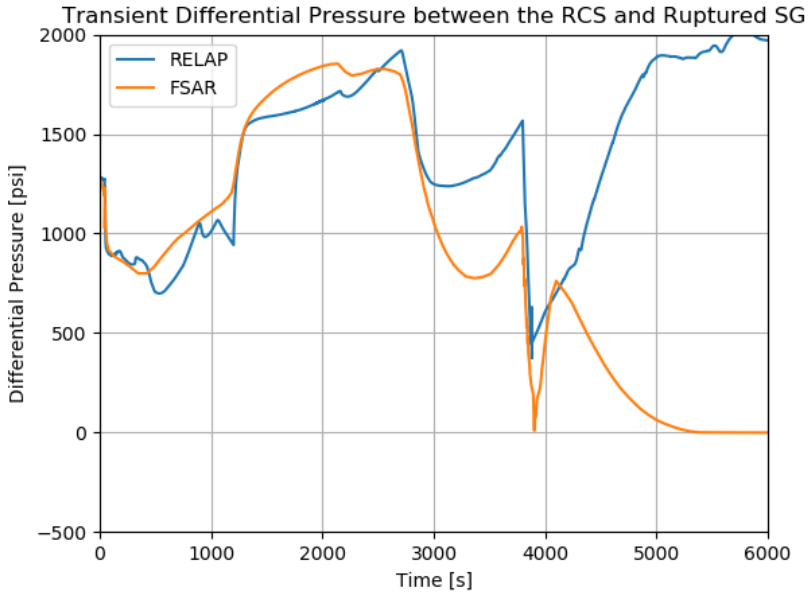

Figure 153 - Transient Differential Pressure between the RCS and Ruptured SG for the SGTR Scenario

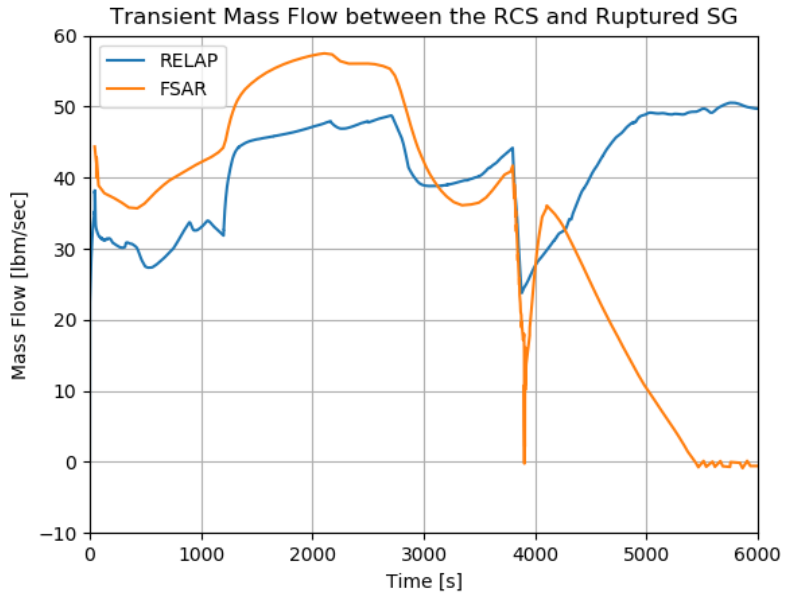

Figure 154 - Transient Mass Flow between the RCS and Ruptured SG for the SGTR Scenario

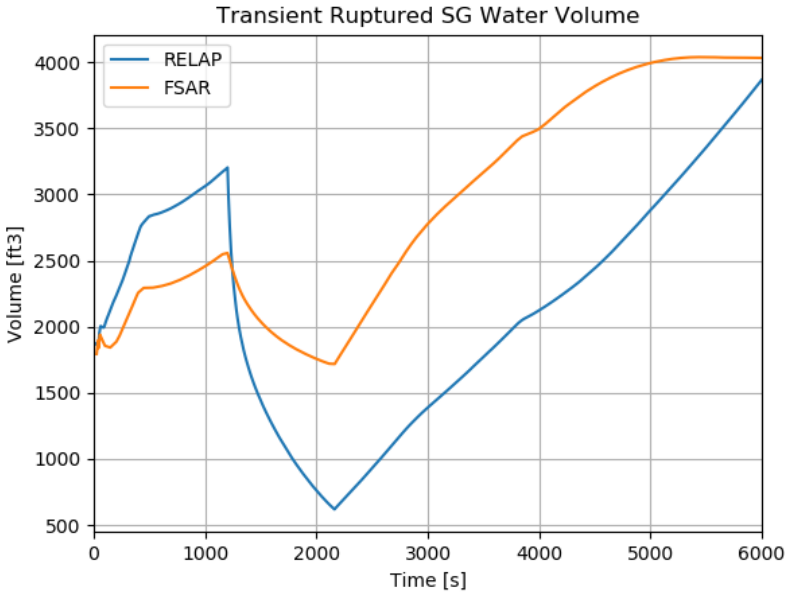

Figure 155 - Transient Ruptured SG Water Volume for the SGTR Scenario

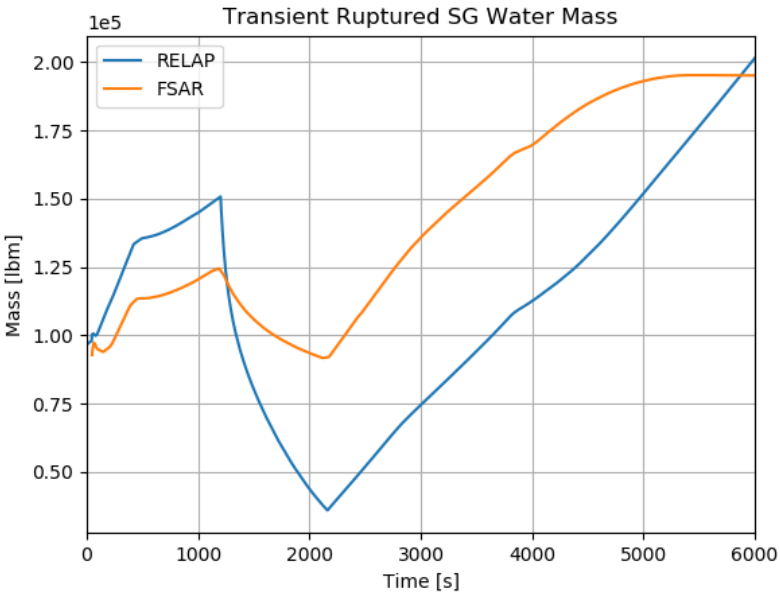

Figure 156 - Transient Ruptured SG Water Mass for the SGTR Scenario

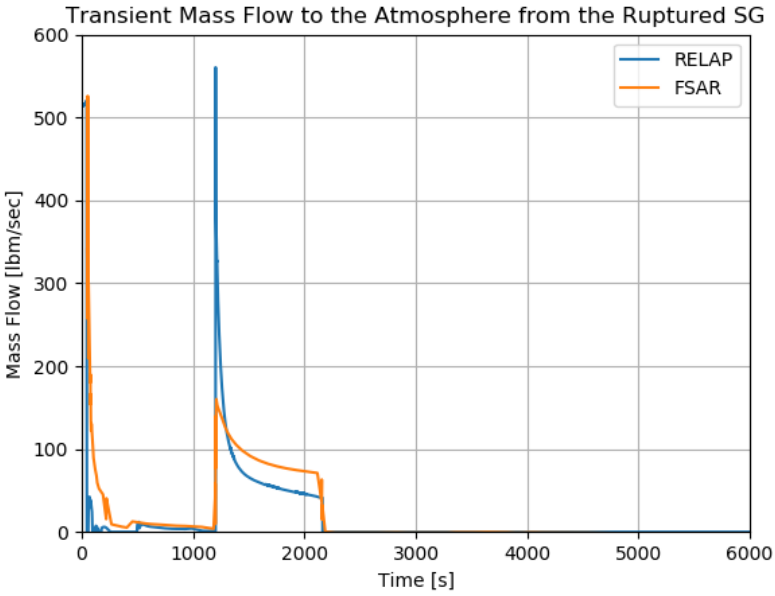

Figure 157 - Transient Mass Flow to the Atmosphere from the Ruptured SG for the SGTR Scenario

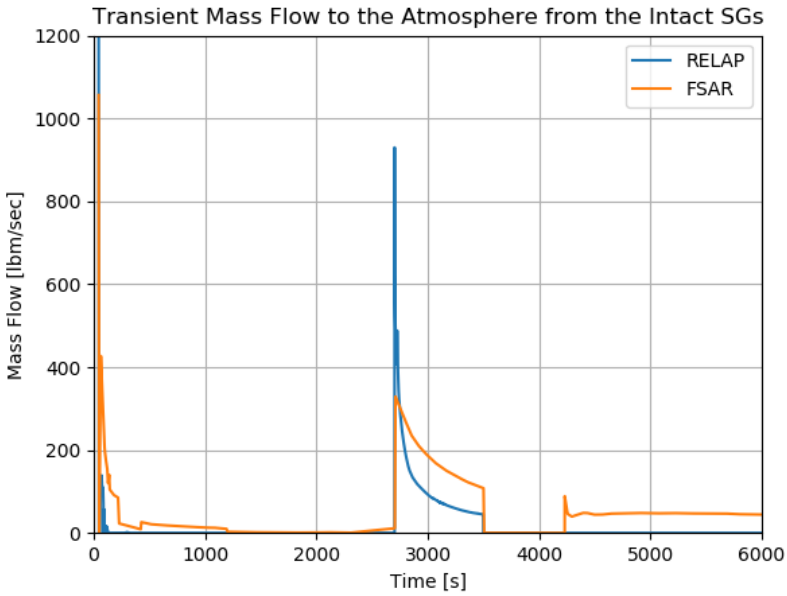

Figure 158 - Transient Mass Flow to the Atmosphere from the Intact SGs for the SGTR Scenario

4.2.10 Spectrum of Rod Cluster Control Assembly Ejection Accidents

This event is also called a rod ejection accident (REA). This event is classified as an American Nuclear Society (ANS) Condition IV incident.

This accident is defined as the mechanical failure of a control rod mechanism pressure housing, resulting in the ejection of a rod cluster control assembly (RCCA) and drive shaft. The consequence of this mechanical failure is a rapid positive reactivity insertion together with an adverse core power distribution, possibly leading to localized fuel rod damage.

There are two limiting runs which are simulated: beginning of life (BOL) hot full power (HFP) and end of life (EOL) hot zero power (HZP).

4.2.10.1 Results

The RELAP results are compared to the runs from the FSAR in the paragraphs below.

BOL HFP

The transient pressurizer pressure is shown in Figure 159. There is no FSAR plot for this. The RELAP run experiences a significant pressurization as the core power increases. This pressurization triggers all pressurizer de-pressurization devices.

The transient core power as a fraction of nominal is shown in Figure 160. The RELAP run has a very large power increase, over 2 times the nominal power. This is significantly more than the FSAR curve.

The transient maximum cladding temperature is shown in Figure 161. There is no FSAR plot for this. The RELAP run has a large temperature excursion during the initial power excursion, and gradually cools after the power reduces.

The transient hot spot oxidation is shown in Figure 162. There is no FSAR plot for this. A significant amount of oxidation is accrued during the power excursion, but the duration is short enough that it ends up being a small amount.

The transient DNBR is shown in Figure 163. There is no FSAR plot for this. The DNBR appears to drop to 0 around the time of the clad temperature excursion. This drop to 0 is interpreted to be due to CHF.

The transient fuel center, fuel average, and clad outer temperatures are shown in Figure 164.

The RELAP fuel center temperature is less than the FSAR value, while the RELAP fuel average temperature is higher than the FSAR value. This may indicate a higher thermal conductivity for the RELAP pellet material. In either case, the RELAP prediction is fairly close to the FSAR. The clad outer temperature is very close throughout the transient, though a bit lower.

EOL HZP

The transient pressurizer pressure is shown in Figure 165. There is no FSAR plot for this. The RELAP run experiences a significant pressurization as the core power increases. This pressurization triggers all pressurizer de-pressurization devices.

The transient core power as a fraction of nominal is shown in Figure 166. The RELAP run has a very large power increase, almost 10 times the nominal power. This is significantly less than the FSAR curve and is later. In addition, the excursion more gradually goes back down.

The transient maximum cladding temperature is shown in Figure 167. There is no FSAR plot for this. The RELAP run has a small temperature excursion during the initial power excursion and cools after the power reduces.

The transient hot spot oxidation is shown in Figure 168. There is no FSAR plot for this. A negligible amount of oxidation is accrued during the power excursion.

The transient DNBR is shown in Figure 169. There is no FSAR plot for this. The DNBR appears to be 0 early on and then 0 again after the clad temperature excursion. This drop to 0 is interpreted to be due to being in single phase liquid.

The transient fuel center, fuel average, and clad outer temperatures are shown in Figure 170. All three temperature curves are far lower for RELAP than for the FSAR analysis.

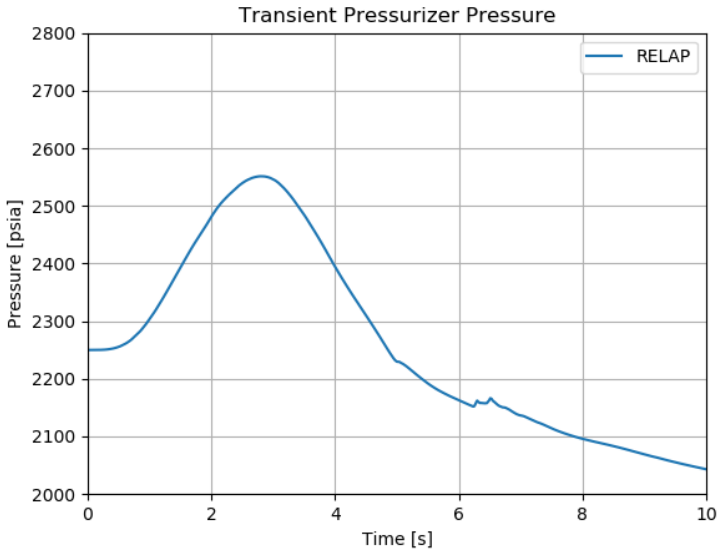

Figure 159 - Transient Pressurizer Pressure for the REA Scenario (BOL HFP)

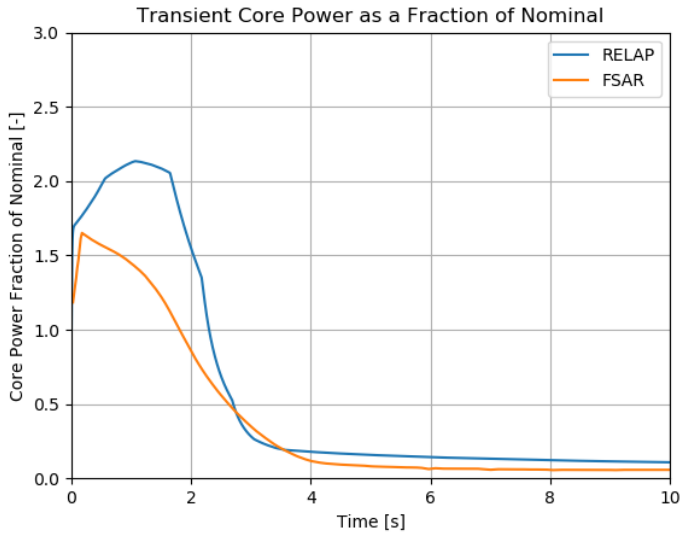

Figure 160 - Transient Core Power as a Fraction of Nominal for the REA Scenario (BOL HFP)

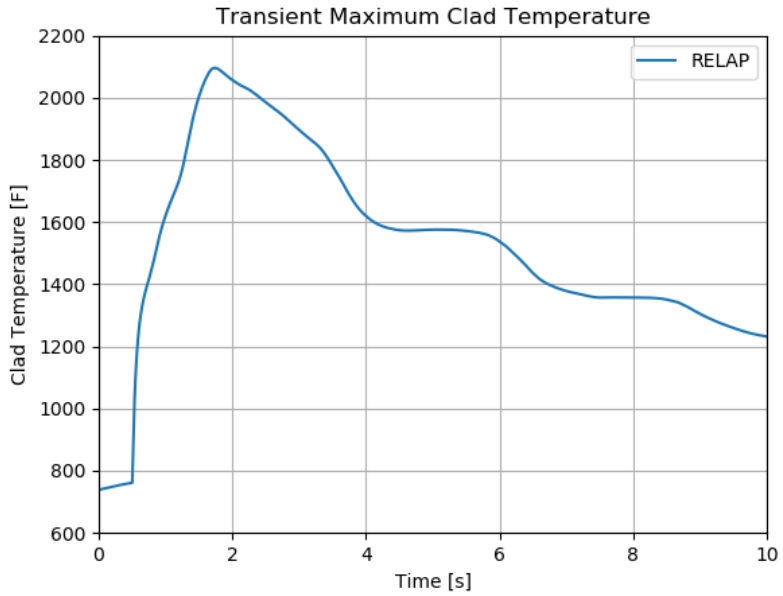

Figure 161 - Transient Maximum Clad Temperature for the REA Scenario (BOL HFP)

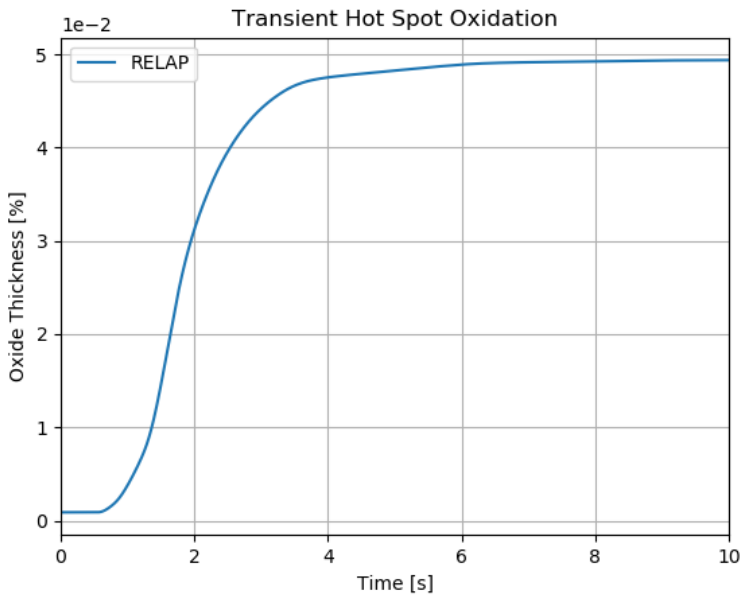

Figure 162 - Transient Hot Spot Oxidation for the REA Scenario (BOL HFP)

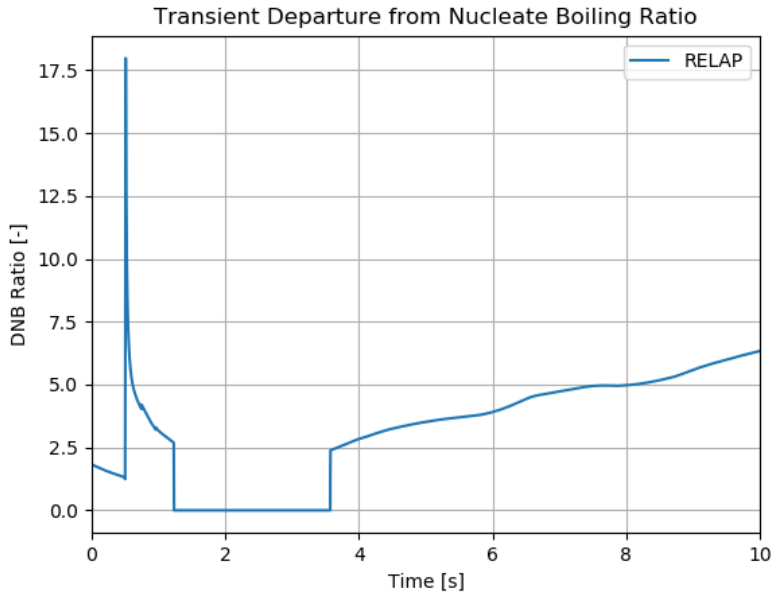

Figure 163 - Transient DNBR for the REA Scenario (BOL HFP)

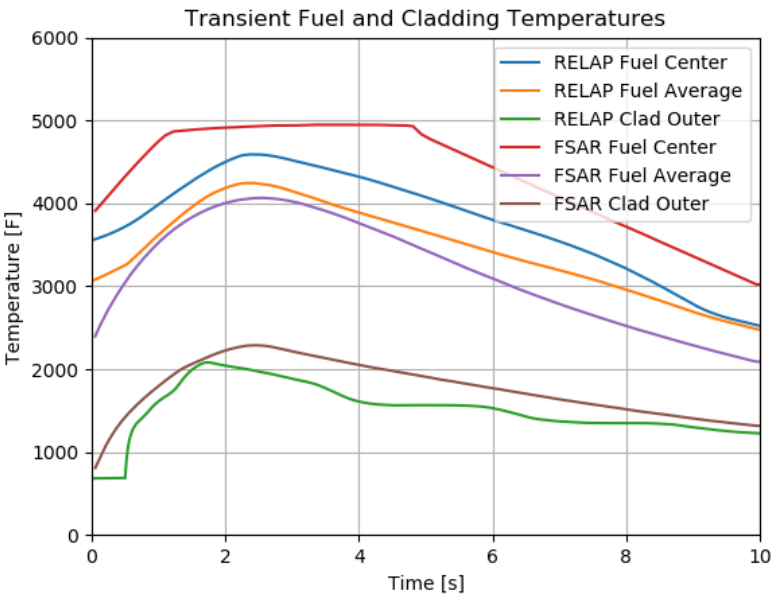

Figure 164 - Transient Fuel and Cladding Temperatures for the REA Scenario (BOL HFP)

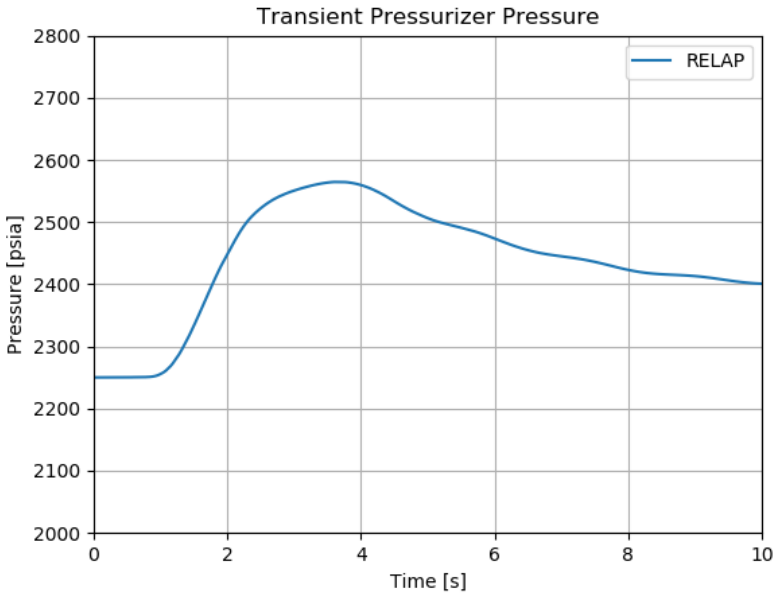

Figure 165 - Transient Pressurizer Pressure for the REA Scenario (EOL HZP)

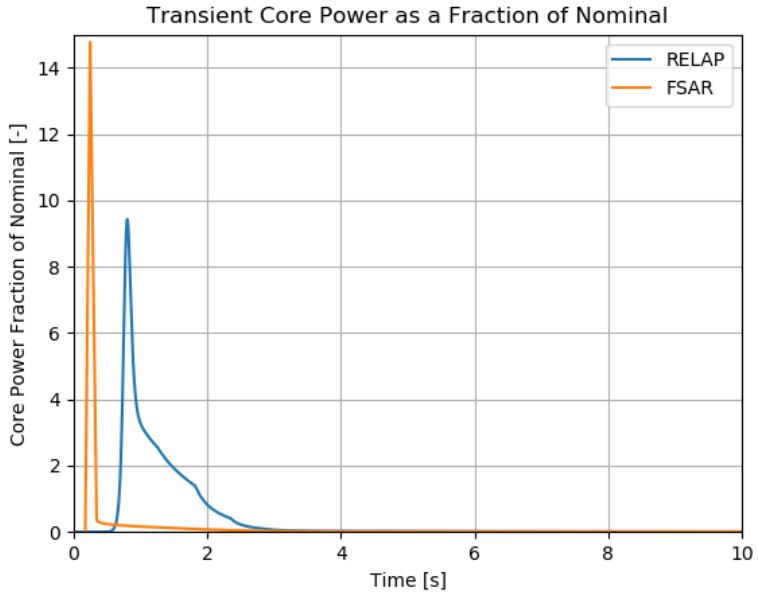

Figure 166 - Transient Core Power as a Fraction of Nominal for the REA Scenario (EOL HZP)

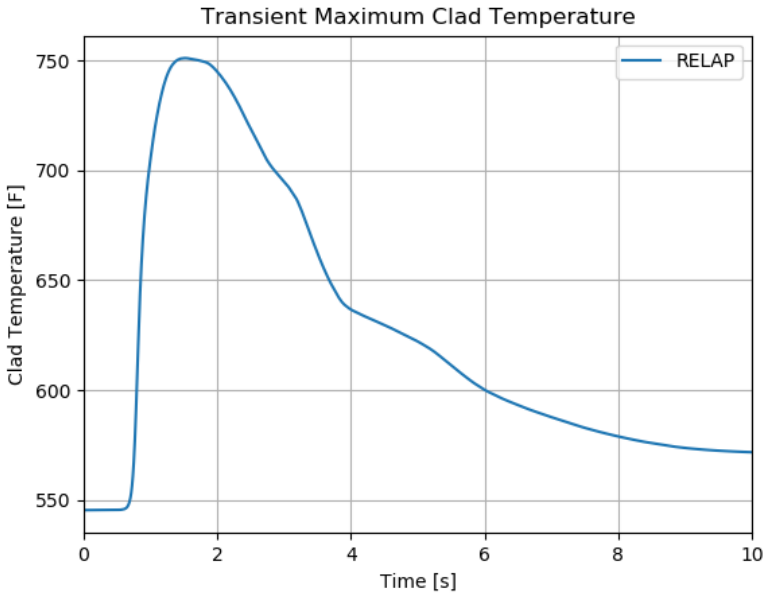

Figure 167 - Transient Maximum Clad Temperature for the REA Scenario (EOL HZP)

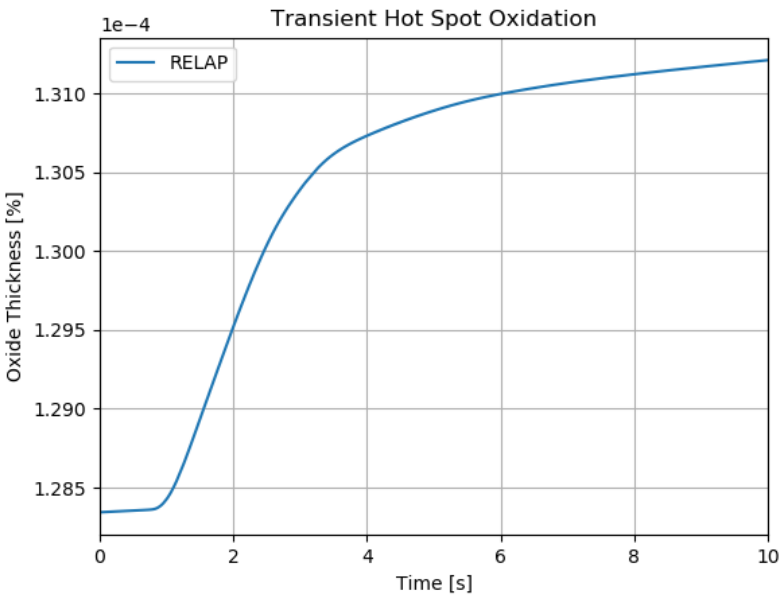

Figure 168 - Transient Hot Spot Oxidation for the REA Scenario (EOL HZP)

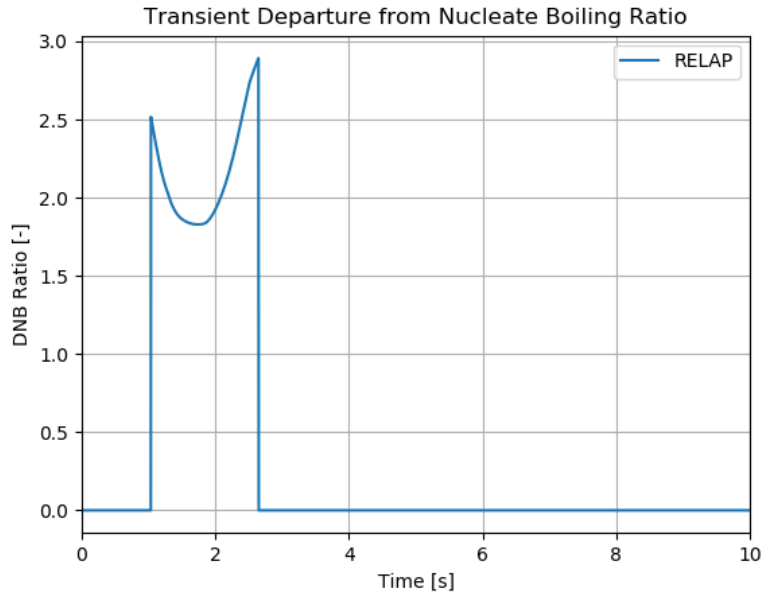

Figure 169 - Transient DNBR for the REA Scenario (EOL HZP)

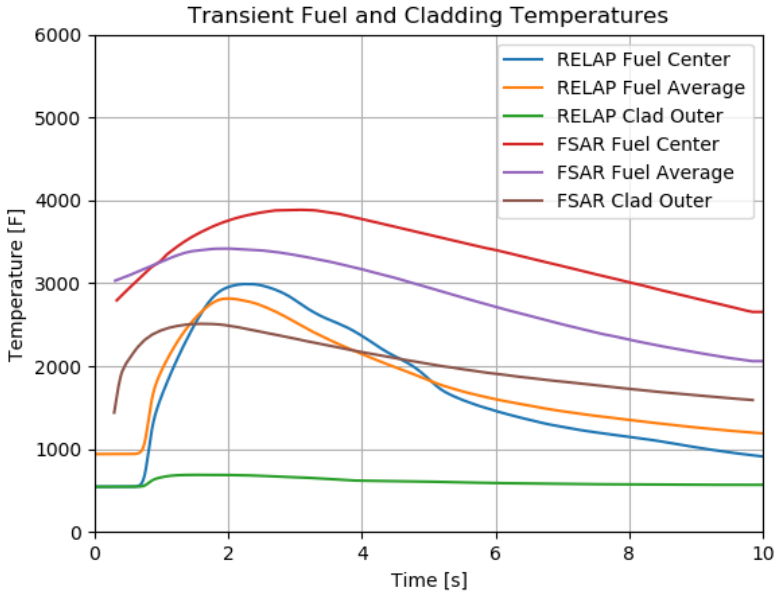

Figure 170 - Transient Fuel and Cladding Temperatures for the REA Scenario (EOL HZP)

4.3 DBA Simulation summary

The required transients have been simulated and the results have been discussed herein. In general, the RELAP simulations are good or acceptable approximations of the FSAR analyses.

The exercise to model, simulate and execute the 10 identified limiting cases is crucial for the deployment of the next phases in the project. In section 6, several updates of the models are proposed for the addressing the discrepancies of the model and the FSAR.

5. OPTIMIZATION ALGORITHMS

As reported in the introduction of this document, the final goal of this project is to provide a methodology for the optimization and automation of the fuel reload design and, consequentially, the thermal limits, considering the limiting events discussed herein.

Even if FY20 was focused on the identification and deployment of DBA cases described in the previous section, the "Plant Reload Licensing Process Optimization" project, in collaboration with the RISA "Risk Informed Asset Management" project (for the Genetic algorithms), has begun the development of optimization methods to efficiently fulfill the scope of the project.

Considering the nature of the optimization problem that is (and will be) the main focus in the next two phases, heuristic approaches looked the most suitable methods to be explored.

In FY20, two classes of heuristic approaches have been developed:

Simulating Annealing Optimization Methods [9]

Genetic Algorithms [10]

Both classes of algorithms have been developed within the RAVEN framework [6]. For the deployment of such methodologies, a modular approach has been followed, aiming to incorporate several flavors of algorithms in the same RAVEN optimization container. In the following sections, a brief introduction to the algorithms is reported.

5.1 Simulating Annealing

Simulated annealing (SA) is a probabilistic technique for approximating the global optimum of a given function. Specifically, it is a metaheuristic to approximate global optimization in a large search space for an optimization problem.

The SA mimics the Physical Annealing process but is used for optimizing parameters in a model. This process is very useful for situations where there are a lot of local minima such that algorithms like Gradient Descent would fail [9] in the determination of a global response. For example, in Figure 171, if Gradient Descent started at the starting point indicated, it would be trapped at the local minima and not be able to reach the global minima.

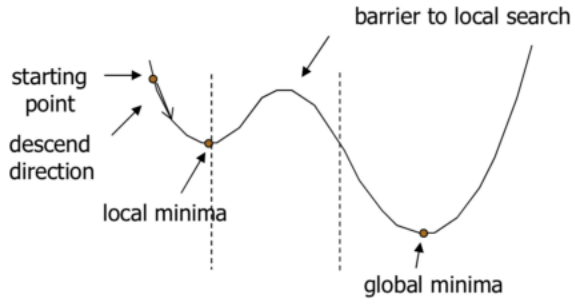

Figure 171 – Example [9] Objective function with local minima.

The SA annealing algorithm can be summarized with the following steps:

1) The algorithm first starts with an initial solution $s = S_0$, which can be any solution that fits the criteria for an acceptable solution, and an initial temperature $t = t_0$
2) Setup a temperature reduction parameter α, to be used in one of the available cooling rules. In RAVEN, the following rules have been deployed:
    a. Exponential: $t_k = t_0 * \alpha^k$
    b. Boltzmann: $t_k = \frac{t_0}{\log(k+d)}$
    c. Cauchy: $t_k = \frac{t_0}{k+d}$
    d. Veryfast: $t_k = t_0 * \exp\left(-\gamma k^{\frac{1}{D}}\right)$

    Where: - k, is the iteration counter
    - D, is the dimensionality of the problem
    - γ, is the decay constant
    - d, bias (offset) constant
3) Starting at the initial temperature, loop through ***n*** iterations of step (4) and then decrease the temperature according to the cooling rule. Stop the iterations once the termination conditions (convergence) are met
4) Given the neighborhood of solutions $N(s)$, pick one of the solutions and calculate the difference in cost between the old solution and the new neighbor solution. The neighborhood of a solution are all solutions that are close to the solution. For example, the neighborhood of a set of 5 parameters might be if we were to change one of the five parameters but kept the remaining four the same.
5) If the difference in cost between the old and new solution is greater than 0 (the new solution is better), then accept the new solution. If the difference in cost is less than 0 (the old solution is better), then generate a random number between 0 and 1 and accept it if it's under the value calculated from the Energy Magnitude equation (Δc is the change in cost of the objective function):

$$P = \begin{cases} 1 & if\ \Delta c \leq 0 \\ e^{-\Delta c / t_k} & if\ \Delta c > 0 \end{cases}$$

5.2 Genetic Algorithms

A genetic algorithm is a heuristic search that is inspired by the theory of natural evolution. This algorithm reflects the process of natural selection where the fittest individuals are selected for reproduction in order to produce offspring of the next generation.

The process of natural selection starts with the selection of fittest individuals from a population. The population produces offspring which inherit the characteristics of the parents and will be added to the next generation. If parents have better fitness, their

offspring will be better than parents and have a better chance at surviving. This process keeps on iterating and at the end, a generation with the fittest individuals will be found.

This idea can be applied for a search/optimization problem. A set of solutions for a problem is considered and the set of best ones out of them are selected.

5.2.1 Terminology

In the following brief explanation of the GA methods, the following terms and definitions will be used [10]:

- **Phenotype space** – The actual real problem solution space, comprising of solutions in the raw (non-computational) representations.
- **Genotype Space** – The computational space comprising of all candidate solutions after encoding to a computational representation.
- **Population** – A subset of all candidate solutions in the Genotype (encoded) space.
- **Chromosomes (Individual)** – A single possible solution of the problem at hand taken from that population.
- **Gene** – A single element in the chromosome.
- **Allele** – The value in the Gene.
- **Mating (Reproduction) Pool** – a collection of parents used to create a new generation.
- **Fitness Function –** The function used to rank the solutions (**Elitism**). It might or might not be the same as the objective function.
- **Decoding and Encoding** – are the optional processes to convert Phenotype representation (real variables) into Genotype representation (Computational representation).
- **Reproduction Operations** – operations that alter the composition of a certain chromosome, i.e., **crossover, mutation, selection.**

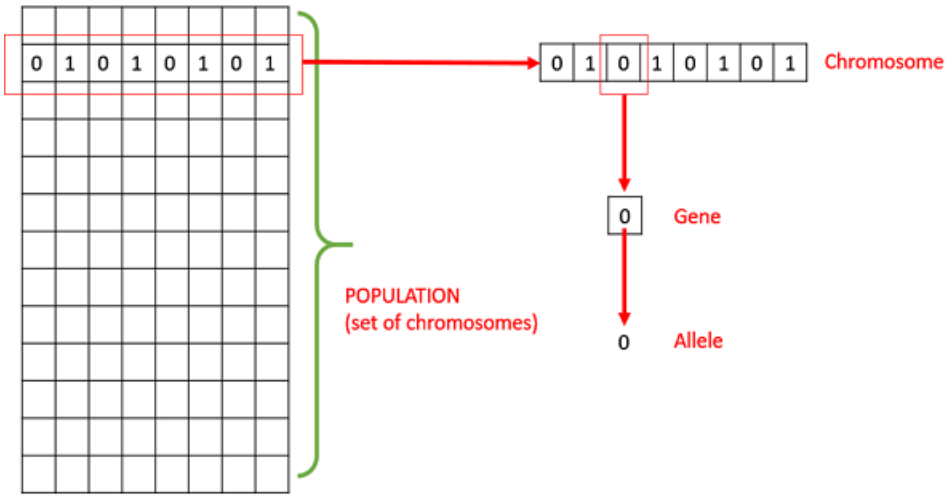

Figure 172 - Genetic Algorithm Population, Chromosome and Gene concepts [10].

5.2.2 GA workflow

The GA algorithm workflow can be summarized by the following steps (see Figure 173):

1. Perform a Genotype variable representation according to the problem under investigation. (**binary**, integer, **permutation**, or real representation).
2. Create initial population
   - Perform uniform sampling of the region of interest:
   - Monte-Carlo sampling of *N* samples $(\boldsymbol{x}, f(\boldsymbol{x}))_n \quad , n = 1, \dots, N$
3. Reproduction: creation of a new population
   - Random sample *N* samples with replacement from the population of Step 1 based on their fitness
4. Parent selection (selecting parents that mate and recombine to create off-springs for the next generation)
5. Crossover: creation of children population
   - Create *N/2* pairs without replacement (parents)
   - Create 2 elements from each pair (children)
6. Mutation
   - Random change a bit of the gene from a subset of the population of Step (4)
7. Replacement of parents
   - Consider only children and remove parents
8. Repeat Steps 2 through 6 (each iteration is a generation) till convergence criteria are met.

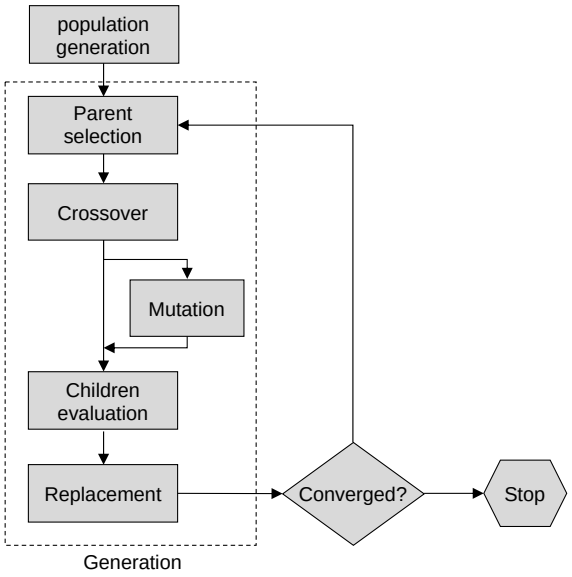

Figure 173 - GA workflow.

Based on the previous pseudo algorithm, the GA optimization methods have been deployed in the RAVEN framework following the philosophy of highly modularity and reusability of the methods, objects and classes. Figure 174 schematically shows how the algorithms have been implemented in RAVEN, providing a parallelism to the schematic workflow reported in Figure 173.

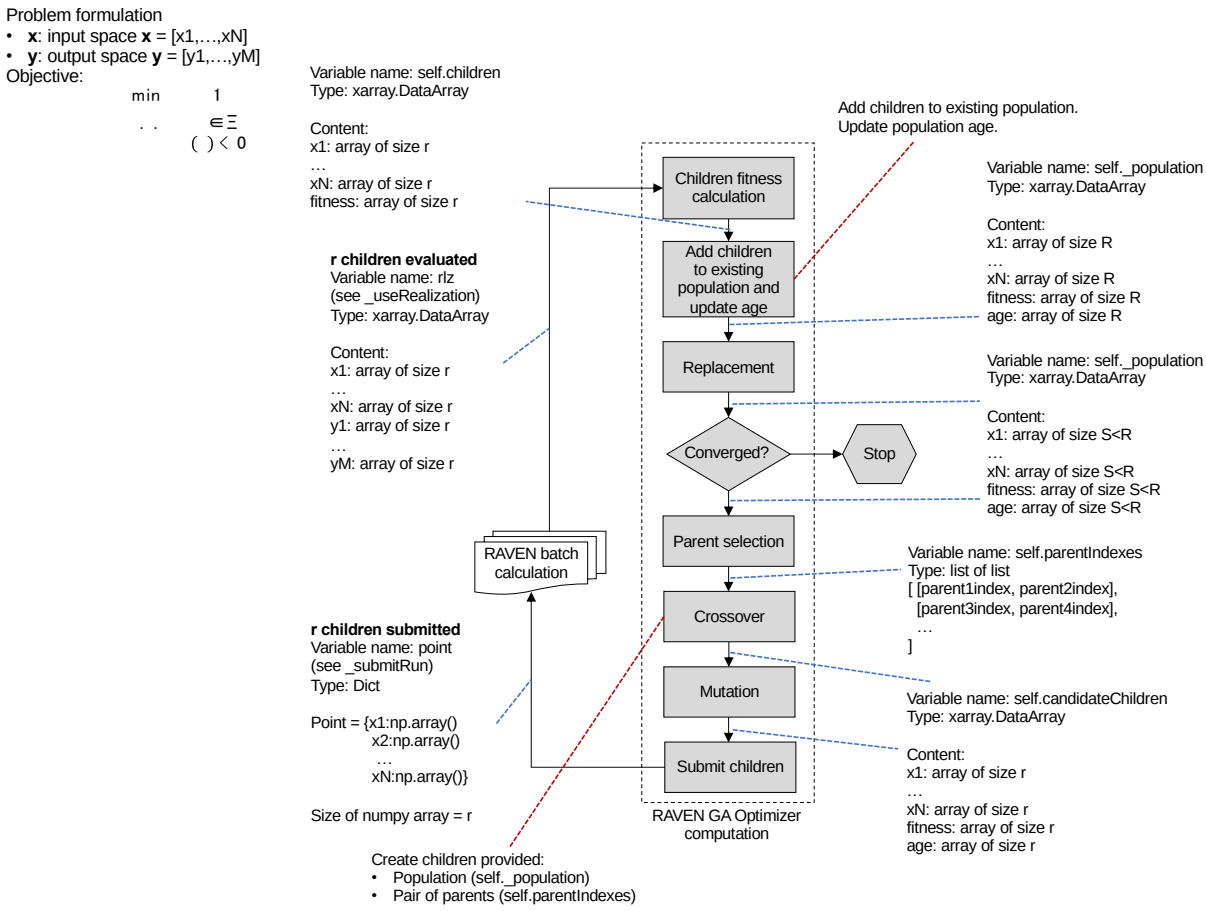

Figure 174 - RAVEN GA workflow.

6. CONCLUSIONS AND FUTURE WORK

The Phase I of the "Plant Reload Process Optimization" has been focused on the deployment of the modeling, simulation and analysis of the 10 identified Chapter 15 limiting events (DBAs) for a prototypical PWR. In addition, the initial development of the heuristic optimization framework within the RAVEN software has been initiated, delivering two of the main algorithms in such category: 1) Simulating Annealing optimization, and 2) Genetic Algorithm search.

In the following sections, findings and proposed future work about both main activities are reported and discussed.

6.1 Future work on plant and DBA modeling

The 10 identified limiting transients have been simulated and the results have been discussed in section 4. In general, the RELAP simulations are good or acceptable approximations of the FSAR analyses. Through this Phase I, the following modeling upgrades have been determined to be of critical importance:

- The vessel model used for the Phase I is insufficient to handle the complicated phenomena in the downcomer experienced during a LBLOCA blowdown. In addition, the core modeling is too coarse, both axially and radially. The vessel model should be remade using

a MULTID RELAP component (or with 1D components utilizing crossflow), with special consideration given as follows:

  - The lower plenum nodalization should be studied for effects on fluid retention during LBLOCA blowdown.
  - The downcomer noding should be studied for effects on ECCS bypass.
  - The core and upper plenum modeling should be redesigned considering both the upper plenum structures above each fuel assembly and for handling power variation in assemblies.
  - Components should be added or modified to properly model core bypass flow and tune the model to obtain an appropriate value.

- The calculation of power distribution inputs for the core based on peaking factor inputs and power shape definition should be performed using coupled reactor physics modules (e.g. PHISICS [11] [12])
- The kinetics model should be updated consistent with the increased detail in the vessel model. In addition, control logic should be assembled that allows the analyst to enter coefficients of reactivity exactly consistently with the FSAR inputs. As of now, approximations are made which fit into the existing RELAP input structure.
- The material properties for the fuel rods and pellets should be examined for suitability. The existing inputs have extremely erratic and nonphysical dependence on temperature.
- Additional work should be done to determine the actual conditions experienced during HZP operation at the plant, and the model should be updated to appropriately model HZP. Most of the HZP transients herein never actually reach a fully converged SS.
- Studies of the choked flow models should be performed, as the break flow in the RELAP runs herein generally differs significantly from the FSAR analyses they are emulating.
- The broken loop SG noding should be re-visited with SGTR events in mind. Currently, all tubes being part of one pipe component likely overestimates break flow.

The following model updates are considered of lower importance, but should be considered nonetheless:

- Either the optimizer which obtains acceptable RCS loop DPs should be finished or run-specific loss coefficient multiplier inputs should be added. As it is, some RCS loop DPs are very close, while others are fairly far off from the desired value.
- A containment model should be constructed to obtain a better run-specific backpressure curve for LBLOCA and possibly to be able to assess containment response criteria.
- Model changes due to steam generator tube plugging level should be implemented to automatically calculate based on an assumed percentage of tube plugging.
- Additional reactor trip and SI signal setpoints may be implemented, if sufficient information to perform the modeling is found.

6.2 Future work on optimization framework.

In FY20, two classes of heuristic approaches have been developed: 1) Simulating Annealing Optimization Methods, and 2) Genetic Algorithms. Some prototypical calculations and simulations have been executed to demonstrate the functionality and mechanics of the algorithms within the RAVEN framework.

Through this Phase I, the following upgrades of the heuristic optimizations have been identified and determined to be of critical importance:

- Generic heuristic methods:
    1) Development of a methodology for the treatment of implicit and explicit constraints, both for discrete and continuous problems
    2) Methodology development for the assessment and usage of the concept of risk (coming from the scenario evaluation) in the fuel pattern and thermal limit optimization
- Simulating Annealing:
    3) Extension of the algorithm for discrete and hybrid discrete/continuous parameter optimization
    4) Adaptive tuning of the cooling rule for accelerating the optimization convergence
    5) Implementation of a robust method to assess the convergence of the objective function
- Genetic Algorithms:
    6) Extension of the algorithm for continuous and hybrid discrete/continuous parameter optimization
    7) Improvement of the performance of the population collection from the RAVEN data structures
    8) Implementation of a robust method to assess the convergence of the objective function, since the current method is solely based on the number of performed iteration
    9) Augmentation of the algorithm with some of the characteristics of the particle swarm methodologies, particularly indicated for fuel pattern optimizations

6.3 Phase II plan.

Among the different activities that will be carried in FY21, in the following sections the key tasks to be deployed are reported.

6.3.1 Optimization

Improvement and upgrade of the optimization algorithms tackling (at minimum) bullets (1), (2), (3), (6), (7) and (9) explained in section 6.2

6.3.2 Plant Model Enhancements

Update of the RELAP5-3D model (with the addition of the neutronics model PHISICS) for addressing the discrepancies and issues discussed in section 6.1.

6.3.3 Identification of uncertainty contributors

Identification of the uncertainty contributors for the modeled scenarios, in order to introduce the concept of risk in the optimization analysis:

- System response uncertainties: uncertainties that relate to the Thermal-Hydraulic modeling
- Fuel rod uncertainties: uncertainties in the simulation of fuel performance used as input to the DBA simulations, as well as any needed post-processing of fuel rods results based on the T/H simulations
- Core design uncertainties: uncertainties in the core design process, such as power distributions, burnups, enrichment, etc.
-

6.3.4 Define Scenarios to Migrate to RISA

This activity will focus on the deliverables that will define what scenarios from Chapter 15 will be migrated to Risk Informed Chapter 19 criteria. Deliverables will include a list of scenarios, justification for those scenarios being handled in risk informed space and impacts on removing these scenarios from classical Chapter 15 analysis.

6.3.5 Modify the Framework for RISA Cases

This activity will focus on the needed upgrades (grounded on the Phase I conclusions) of the methodological and software framework (based on RAVEN) needed to finalize and enhance the analyses.

6.3.6 RISA Simulation

This activity is mostly about the simulation of the selected RISA scenarios. This task represents the summary of all the methodological, selection and software upgrades curried out in Phase I and II.

6.3.7 Phase II Finalization

This activity focuses on the formal documentation and finalization of Phase II. This includes the generation of the documentation requested by the project (e.g. Final Technical Report, etc.).

REFERENCES

[1] U.S. Department of Energy, "Light Water Reactor Sustainability Research and Development Program Plan," 2009.

[2] R. Slizard, H. Zhang, S. Hess, J. Gaertner, D. Mandelli, S. Prescott and M. Farmer, "RISA Industry Use Case Analysis," Idaho National Laboratory, Idaho Falls, 2018.

[3] A. Alfonsi, C. Frepoli and C. Smith, "Risk-Informed Systems Analysis (RISA) Plant Reload Process Optimization Technical Plan," *Idaho National Laboratory,* Vols. INL/EXT-19-55784, 2019.

[4] The RELAP5-3D Code Development Team, "RELAP5-3D Code Manual Volume V: User's Guidelines," IDAHO NATIONAL LABORATORY, IDAHO FALLS, 2014.

[5] U.S. Nuclear Regulatory Commision, "Standard Review Plan for the Review of Safety Analysis Reports for Nuclear Power Plants: LWR Edition (NUREG-0800, Formerly issued as NUREG-75/087)," 2017. [Online]. Available: https://www.nrc.gov/reading-rm/doc-collections/nuregs/staff/sr0800/.

[6] C. Rabiti, A. Alfonsi, J. Cogliati, D. Mandelli, R. Kinoshita and S. Sen, "RAVEN Users Manual," Idaho National Laboratory, INL/EXT-15-34123, 2015.

[7] A. Alfonsi, C. Rabiti, D. Mandelli, J. Cogliati, C. Wang, P. W. Talbot, D. P. Maljovec and C. Smith, "RAVEN Theory Manual," *Idaho National Laboratory,* Vols. INL/EXT-16-38178.

[8] Rabiti, C., et al., "Deployment and Overview of RAVEN Capabilities for a Probabilistic Risk Assessment Demo for a PWR Station Blackout," Idaho National Laboratory, 2013.

[9] F. Liang. [Online]. Available: https://towardsdatascience.com/optimization-techniques-simulated-annealing-d6a4785a1de7.

[10] T. Points, "Tutorial Points," 2020. [Online]. Available: https://www.tutorialspoint.com/genetic_algorithms/index.htm.

[11] C. Rabiti, A. Alfonsi and A. Epiney, "New simulation schemes and capabilities for the PHISICS/RELAP5-3D coupled suite," *Nuclear Science and Engineering,* vol. 182, no. 1, pp. 104-118, 2016.

[12] A. Alfonsi, C. Rabiti, A. S. Epiney, Y. Wang and J. Cogliati, "PHISICS toolkit: Multi-reactor transmutation analysis utility-MRTAU," in *PHYSOR 2012 – Advances in Reactor Physics – Linking Research, Industry, and Education*, Knoxville, Tennessee, USA, 2012.

[13] C. Smith, D. Mandelli, S. Prescott, A. Alfonsi, C. Rabiti, J. Cogliati and R. Kinoshita, "Analysis of Pressurized Water Reactor Station Blackout Caused by External Flooding Using the RISMC Toolkit," Idaho National Laboratory, INL/EXT-14-32906, 2014.

[14] R. Szilard, R. Youngblood, C. Frepoli, J. Yurko, G. Swindlehurst, H. Zhang, H. Zhao, P. Bayless, C. Rabiti, A. Alfonsi and C. Smith, "Industry Application Emergency Core Cooling System Cladding Acceptance Criteria Problem Statment," Idaho National Laboratory, INL-EXT-15-35073.

[15] R. Boring, D. Mandelli, M. Rasmussen, S. Herberger, T. Ulrich, K. Groth and C. Smith, "Integration of Human Reliability Analysis Models into the Simulation-Based Framework for the Risk-Informed Safety Margin Characterization Toolkit," INL, INL/EXT-16-39015, 2016.

[16] "Vogtle Electric Generating Plant, Units 1 and 2 - Redaction of UFSAR Revision 20," [Online]. Available: https://www.nrc.gov/docs/ML1703/ML17032A132.html.

[17] ML16357A264, "Byron 1/2 and Braidwood 1/2 UFSAR," [Online]. Available: https://www.nrc.gov/docs/ML1635/ML16357A264.html.

[18] Commonwealth Edison Company, "Zion Station Updated Final Safety Analysis Report, UFSAR," ML081370019.

[19] Nuclear Energy Agency, "Nuclear Fuel Safety Criteria Technical Review," OECD 2012, NEA No. 7072 .

[20] R. L. Williamson, J. D. Hales, S. R. Novascone, M. R. Tonks, D. R. Gaston, C. J. Permann, D. Andrs and a. R. C. Martineau, "Multidimensional multiphysics simulation of nuclear fuel behavior," *Journal of Nuclear Materials,* vol. 423, pp. 149-163, 149â€“163.